Title
PHENOMENOLOGY OF RESONANCES AND PARTICLE SUPERMULTIPLETS

Author
Barbaro-Galtieri, Angela.

Publication Date
1966-09-30

UCRL-17054

University of California

Ernest O. Lawrence Radiation Laboratory

PHENOMENOLOGY OF RESONANCES AND PARTICLE SUPERMULTIPLETS

Berkeley, California

DISCLAIMER

Revised from the lectures
at the School Ettore Maiorana
at Erice, Italy (June 19-July 4, 1966)

UCRL-17054
Preprint

UNIVERSITY OF CALIFORNIA

Lawrence Radiation Laboratory
Berkeley, California

AEC Contract No. W-7405-eng-48

PHENOMENOLOGY OF RESONANCES AND PARTICLE SUPERMULTIPLETS

Angela Barbaro-Galtieri

September 30, 1966

PHENOMENOLOGY OF RESONANCES AND PARTICLE SUPERMULTIPLETS

Contents

PHENOMENOLOGY OF RESONANCES AND PARTICLE SUPERMULTIPLETS

Angela Barbaro-Galtieri

Lawrence Radiation Laboratory
University of California
Berkeley, California

September 30, 1966

ABSTRACT

This report is a series of three lectures given at the Ettore Maiorana Summer School on "Strong and Weak Interactions--Present Problems," Erice, Italy. This school was held June 19 through July 5, 1966. The first section deals with baryon resonances with zero strangeness. Phase-shift analyses are discussed as well as partial-wave analysis of $\pi^{\pm}p$ elastic and charge-exchange scattering. Backward scattering at 180° as a means to determine the parity of resonances is discussed also. Section II is a review of present knowledge of hyperon resonances with strangeness (-2, -1, +1). The well-known as well as new possible resonances are discussed. This includes the recent, precise measurements of total cross sections in K^-p, K^-d, K^+p, and K^+d. Section III is a review of the present situation of SU(3) supermultiplets for baryons and mesons as well.

I. BARYON RESONANCES WITH STRANGENESS = 0

1. Introduction

The number of known resonant states has been growing regularly in the past few years. Some resonances or bumps remain mysterious for a few years before their properties are determined; some others, instead, appear suddenly on the scene with their properties completely specified.

The discovery of a resonance can be made in two distinct ways: in formation experiments or in production experiments. A resonance is made in a "formation experiment" when a proton target is bombarded with a meson beam and the total energy in the c. m. corresponds to the mass of the resonance. If, instead, the resonance is produced in association with other particles, it is made in a "production experiment"--this is always the case for meson resonances.

We will discuss here mainly the analysis of formation experiments. In fact, it turned out that formation experiments are the most useful for determination of the quantum numbers of baryon resonances. Professor Fiorini will review the present situation of meson resonances.

It is very hard to compile tables of resonances, and in producing a new version of the wallet cards we conform to the idea that only states well established should be classified.[1] Tables 1 and 2 are the current revised tables of resonances, but some states are missing, mainly $Y_1^*(2260)$ and some new nucleonic resonances with mass larger than 3000 MeV.

In these lectures I will try to review the present situation on baryon resonances, and to classify meson and baryon multiplets into supermultiplets, according to our present experimental knowledge.

Table 1. Baryon resonances.

		Beam π or K (MeV/c)	I(J^P) ⊢ = estab.	Sym-bol	Mass (MeV)	Γ (MeV)	Mass² and [Γ(M²)] (BeV)²	Partial Decay Modes: Mode	Fraction (%)	Q (MeV)	p or p_max (MeV/c)
N	p	See Table S	1/2(1/2⁺)	N^I_α	938.2		0.88		See Table S		
	n				939.6		0.88				
	$N^*_{1/2}(1400)$[a]	T = 426 p = 549	1/2(1/2⁺) p_{11}	N'_α	~1400	≈200	1.96 [0.56]	πN	≈60	322	367
	$N^*_{1/2}(1550)$[a]	T = 663 p = 790	1/2(1/2⁻) s_{11}	N^I_β	≈ 1570	≈130	2.40 [0.40]	πN Nη	≈30 seen	472 62	478 210
	$N^*_{1/2}(1518)$[a]	T = 610 p = 737	1/2(3/2⁻) d_{13}	N_γ	≈1518	≈80	2.30 [0.24]	πN $\Delta_\delta\pi$	≈50 seen	440 142	454 222
	$N^*_{1/2}(1700)$[a]	T = 921 p = 1051	1/2(1/2⁻) s_{11}	N'_β	≈1700	≈240	2.89 [0.82]	πN Nρ	≈90	622 5	580 64
	$N^*_{1/2}(1688)$[a]	T = 900 p = 1030	1/2(5/2⁻) d_{15}	N^{II}_β	≈1688	≈100	2.86 [0.34]	πN ΛK	≈35	610 75	572 231
	$N^*_{1/2}(1688)$[a]	T = 900 p = 1030	1/2(5/2⁺) f_{15}	N^{II}_α	≈1688	≈145	2.87 [0.49]	πN $\Delta_\delta\pi$	≈50 seen	610 342	572 372
	$N^*_{1/2}(2190)$	T = 1937 p = 2072	1/2(7/2⁻)	N^{II}_γ	≈2190	200	4.80 [0.88]	πN ΛK	30	1112 577	888 711
	$N^*_{1/2}(2650)$	T = 3123 p = 3260	1/2(11/2⁻) ⊢ ?	N^{III}_γ	2649 ±10	≈300	7.02 [1.59]	πN ΛK	≈7	1572 1037	1154 1022
Δ	$N^*_{3/2}(1236)$	T = 195 p = 304	3/2(3/2⁺)	$(\Delta^I_\delta)^{++}$	1236.0 ±0.55	120.0 ±2.0	1.53 [0.30]	πN	100	158	231
				$m_0 - m_{++} = 0.45 \pm 0.85$							
				$m_- - m_{++} = 7.9 \pm 6.8$			$\Gamma_- - \Gamma_{++} = 25 \pm 23$				
	$N^*_{3/2}(1670)$[a]	T = 867 p = 997	3/2(1/2⁻)	Δ_β	≈1670	≈180	2.79 [0.60]	πN	≈44	592	560
	$N^*_{3/2}(1920)$	T = 1346 p = 1479	3/2(7/2⁺)	Δ^{II}_δ	≈1920	≈200	3.69 [0.77]	πN ΣK	≈50	842 229	722 435
	$N^*_{3/2}(2420)$	T = 2502 p = 2638	3/2(11/2⁺) ⊢ ?	Δ^{III}_δ	2423 ±10	≈275	5.86 [1.33]	πN ΣK	≈10	1342 729	1023 828
	$N^*_{3/2}(2850)$	T = 3709 p = 3847	3/2(15/2⁺) ⊢ ?	Δ^{IV}_δ	2850 ±12	≈300	8.12 [1.71]	πN	≈3	1772	1266
Z	$Z^*_0(1865)$	T = 761 p = 1153	0(1/2) ⊢ ?	Z_0	1863	150	3.48 [0.56]	KN Δ_δK	≈55	432 135	579 320
Λ	Λ	See Table S	0(1/2⁺)	Λ^I_α	1115.4		1.24		See Table S		
	$Y^*_0(1405)$	<0 K⁻p	0(1/2⁻)	Λ_β	≈1405[b]	≈35[b]	1.97 [0.10]	Σπ	100	68	142
	$Y^*_0(1520)$	T = 138 p = 395	0(3/2⁻)	Λ^I_γ	1518.8 ±1.5	16 ±2	2.31 [0.05]	$\bar{K}N$ Σπ Λππ	29±4 55±7 16±2	83 183 125	237 260 252
	$Y^*_0(1670)$	T = 393 p = 737	0(1/2⁻)	Λ'_β	≈1670	≈18	2.79 [0.06]	$\bar{K}N$ Λη	seen seen	233 6	410 66
			May be s-wave scattering length of either sign.								
	$Y^*_0(1815)$	T = 662 p = 1046	0(5/2⁺)	Λ^{II}_α	1815	≈50	3.29 [0.18]	$\bar{K}N$ Σπ Λη $Y^*_1(1385)\pi$	≈75 ≈9 ≈1 ≈15	378 478 151 290	538 499 344 358
	$Y^*_0(2110)$	T = 1280 p = 1703	0(7/2⁻)	Λ^{II}_γ	2110	155	4.45 [0.65]	$\bar{K}N$ Σπ	≈32	673 773	755 706
Σ	Σ	See Table S	1(1/2⁺)	Σ^I_α	+ 1189.5 0 1192.6 - 1197.4		+ 1.41 0 1.42 - 1.43		See Table S		
	$Y^*_1(1385)$	<0 K⁻p	1(3/2⁺)	Σ^I_δ	+ 1381.0 $s = 1.3^c$ ±1.0 - 1384.0 $s = 1.6^c$ ±1.2	40±4 $s = 2.2^c$ 46±9 $s = 3.4^c$	1.92 [0.12]	Λπ Σπ	91±2 9±2 $s = 1.4^c$	130 48	208 117
	$Y^*_1(1660)$	T = 375 p = 716	1(3/2) ⊢ ?	Σ_γ	≈1660	≈50	2.76 [0.17]	$\bar{K}N$ Λπ Σπ Λππ $Y^*_0(1405)\pi \leftarrow \Sigma\pi\pi$	~15 ~5 ~30 ~20 ~30	223 405 323 265 184	400 439 379 389 316
			Large contradictions among measured branching ratios.								
	$Y^*_1(1765)$	T = 558 p = 928	1(5/2⁻)	Σ_β	1767 ±4 $s = 1.1^c$	84 ±12 $s = 2.0^c$	3.10 [0.30]	$\bar{K}N$ Λπ Σπ $Y^*_1(1385)\pi$ $Y^*_0(1520)\pi$	≈50 14 <3 ≈10 15	323 510 423 235 100	492 514 458 311 182
	$Y^*_1(1915)$	T = 861 p = 1262	1(5/2⁺) ⊢ ?	Σ^{II}_α	≈1915	≈65	3.67 [0.25]	$\bar{K}N$ Λπ	≈10 ≈12	478 660	616 622
	$Y^*_1(2035)$	T = 1114 p = 1530	1(7/2⁺)	Σ^{II}_δ	2035	160	4.14 [0.65]	$\bar{K}N$ Λπ Σπ	≈20 ≈20	598 785 698	703 703 655
Ξ	Ξ	See Table S	1/2(1/2⁺) ⊢ ?	Ξ_α	0 1314 - 1321		0 1.73 - 1.75		See Table S		
	$\Xi^*_{1/2}(1530)$		1/2(3/2⁺)	$(\Xi_\delta)^0$	1528.7 ±1.1	7.3 ±1.7	2.34 [0.02]	Ξπ	100	70	145
			(p wave)	$m_- - m_0 = 4.2 \pm 1.7$							
	$\Xi^*_{1/2}(1820)$		1/2(3/2⁻) ⊢ ?	Ξ_γ	1815 ±3	16 ±8 $s = 2.2^c$	3.31 [0.06]	$\Lambda\bar{K}$ Ξπ $\Xi^*(1530)\pi$ Ξππ	≈65 ~10 ~20 ~5	207 360 150 220	396 413 234 356
			Branching ratios poorly known.								
	$\Xi^*_{1/2}(1933)$		1/2(5/2⁺) ⊢ ?	Ξ^{II}_α	1933 ±16	140 ±35	3.74 [0.54]	Ξπ $\Lambda\bar{K}$		473 320	501 505
Ω	Ω⁻	See Table S	0(3/2⁺)	Ω_δ	1675		2.81		See Table S		

See listings for other states for which there is evidence, but which are omitted from this table: $N^*_{1/2}(3030)$, $N^*_?(3245)$, $N^*_{3/2}(3230)$, $N^*_{5/2}(1570)$, $Z^*_1(1910)$, $Y^*_0(2340)$, $Y^*_1(2260)$, $\Xi^*_{1/2}(1705)$.

a. Resonance parameters are dependent on difficult and uncertain readings of Argand diagrams from phase-shift analyses. See baryon notes following data listings.

b. Effective-range fits give M = 1409.4 ± 1.1 ($s = 1.5^c$) and Γ = 36 ± 2. See listings.

c. Quoted error includes s (scale) factor. See footnote to Table S.

MUB-3408-A

Table 2. Meson resonances.

	Mass (MeV)	$I(J^{PG})CA$ ⊢=estab.	Symbol	Γ (MeV)	$(\text{Mass})^2$ $[\Gamma(M^2)]$ $(\text{BeV})^2$	Important decays: Partial modes	Fraction (%)	Q[d] (MeV)	p or p_{max}[d] (MeV/c)
η	548.6 ±0.4	$0(0^{-+})C^+A^-$	η_β	<10 Theo. ~100 eV	0.301 [<0.004]	See Table S			
S_0§ ω	783.4 ±0.9 S = 2.0*	$0(1^{--})C^-A^-$	η'_γ	12.0 ±1.5	0.613 [0.02]	$\pi^+\pi^-\pi^0$	~90	369	327
						$\pi^+\pi^-$	seen†	504	366
						neutral($\pi^0\gamma$)	9±.4	648	380
						η+neutral	<1.7	234	199
						$\pi^+\pi^-\gamma$	<5	504	366
						e^+e^-	≈0.015	782	391
						$\mu^+\mu^-$	<0.10	572	377
η'	958.0 ±0.9	$0(0^{-+})C^+A^-$	η'_β	<4	0.918 [<0.008]	$\eta 2\pi$	77±4	131	232
η						$\rho\gamma$	23±4	203	182
$K\bar{K}_0$	1068 ±10	$0(0^{++})C^+A^+$	η_α	80 ±15	1.14 [0.17]	$\pi\pi$	<70	798	516
	May be large scattering length					$K\bar{K}$	>30	73	194
ϕ	1018.6 ±0.5	$0(1^{--})C^-A^+$	η_γ	3.6 ±0.8	1.039 [0.007]	K_1K_2	38±4	23	109
						K^+K^-	47±4	32	126
						$\pi\rho+3\pi$	15±5	117	188
						$\pi^0\gamma$	?	885	501
						η+neutral	<12	471	362
						$\mu^+\mu^-$	<0.5	808	499
						e^+e^-	<0.3	1018	510
f	1254 ±12	$0(2^{++})C^+A^+$	η''_α	112 ±8	1.57 [0.28]	$\pi\pi$	large	974	611
						4π	<4	695	547
						$\bar{K}K$	<4	265	386
D	1286 ±6	$0(1^{++})C^+A^-$	η_δ	40 ±10	1.65 [0.10]	$K\bar{K}\pi$		154	303
						K^*K		-100	<0
E (a)	1418 ±8	$0(1^{++})CA^-$	η_δ	63 ±8	2.01 [0.17]	$K^*\bar{K}$ + $K\bar{K}\pi$ overlap	large	35 293	151 430
f'	1500	$0(2^{++})C^+A^+$	η''_α	80	2.25 [0.24]	$\pi\pi$ small by SU 3		1221	739
						$\bar{K}K$	~60	505	561
						$K\bar{K}^*(890)$	~40	111	274
$\pi^\pm$	139.6	$1(0^{--})C_n^+A^-$	π_β		0.019 [0.018]	See Table S			
π^0	135.0								
$\rho^\pm$	758.3 ±2.8 S=2.8*	$1(1^{+-})C_n^-A^+$	π_γ	128.7 ±7.7	0.58 [0.20]	2π	100	486	357
				S=2.1*		4π	<5	207	243
ρ^0	756.4 ±3.2, S=1.6*			115.5 ±8.2 S=2.1*		$\pi\gamma$	<2	626	370
						e^+e^-	≈0.005	764	382
						$\mu^+\mu^-$	≈0.003	558	370
$K\bar{K}_1$ (a)	1003	$1(0^{+-})C_n^+A^+$	π_α	57	1.006 [.104]	$K^\pm K^0$	large	11	75
						$\eta\pi$	see note	315	333
A1 (b)	1080 ±9	$1(1^{+-})C_n^+A^-$	π_δ	125	1.17 [0.27]	$\rho\pi$	≈100	167	231
						$\bar{K}K$	<1 C forbidden for odd J		
						$\eta\pi$	<1.5	384	380
B (c)	1220	$1(\geq 1^{?+})C_n^-A^+$	π	125 ±37 S=2.2*	1.48 [0.31]	$\omega\pi$	≈100	298	339
						$\pi\pi$	<30 Permitted only for 1^-		
						$\bar{K}K$	<10 assignment, if J<3		
						4π	<50	662	528
A2	1300±9 S = 2.5*	$1(2^{+-})C_n^+$	π''_α	84 ±7 S=1.1*	1.69 [0.22]	$\rho\pi$	≈90	419	426
						$\bar{K}K$	4.6±1.5	333	439
						$\eta\pi$ S= 1.3*	4±4	636	537
Other I=1 bumps excluded.§									
$K^\pm$	493.8	$1/2(0^-)A^-$	K_β		0.244	See Table S			
K^0	497.7				0.248				
κ (a)	725	$1/2(0^+)A^+$	K	<12	0.53 [<0.02]	$K\pi$	≈100	92	154
K^*	891.7 ±0.7	$1/2(1^-)A^+$	K_γ	50 ±1.4	0.80 [0.08]	$K\pi$	≈100	258	288
						$K\pi\pi$	<0.2	118	215
						$\kappa\pi$	<0.2	27	82
K_C (a)	1215 ±15	≤3/2( )A^- ⊢⊣ ??	K	60 ±10	1.476 [0.145]	$K\rho$	~75	-44	<0
						$K^*\pi$	~25	184	253
$K\pi\pi$	1313 ±8	$1/2(1^+)A^-$	K_δ S=1.6*	54 ±20	1.72 .14	$K^*\pi$ + $K\rho$ overlap	large	290 53	340 182
						$K\pi$	?	687	558
K^*	1415 ±6	$1/2(2^+)A^+$	K_α	96 ±7	1.99 [0.27]	$K\pi$	50±10	767	604
						$K^*\pi$	50±10	369	400
						$K\rho$	<10	137	296
						$K\omega$ S=1.5*	1±1	124	281
						$K\eta$	2±1	358	467
$K\pi\pi$	1827 ±31, S=4.9*	$1/2(\ )A^-$	K	83 ±13	3.34 [0.30]	$K\pi\pi$	large	1032	808
						$K\omega$	seen	520	625
						$K\pi$	<5	1167	825
$K^*_{3/2}$ etc. excluded§									

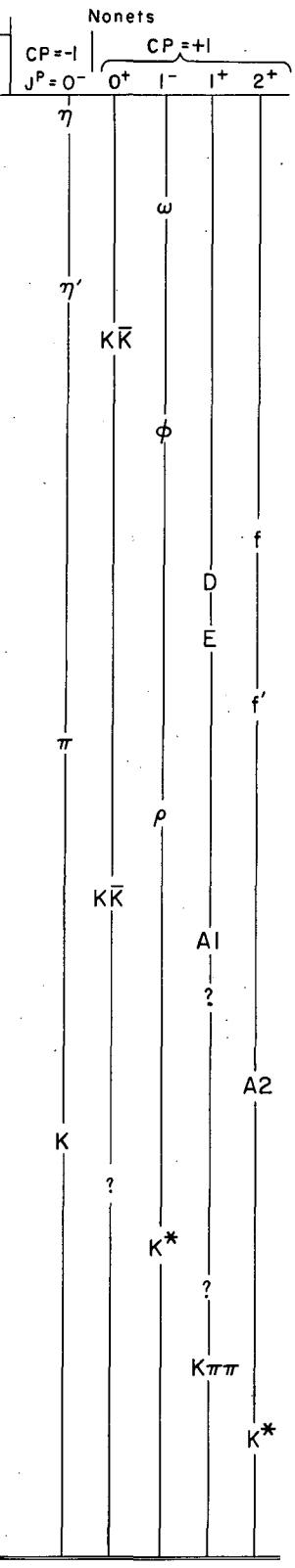

§The following bumps, excluded above, are listed among the data cards: S_0(720), 3π(1630), ππ(1670), H(975), S(1930), T(2200), U(2390), $K^*_{3/2}$(1175), $K^*_{3/2}$(1270), K^+K^+(1055 and 1280).

†Reported values range between <0.5% and 11%, and depend on assumptions on ρ-ω interference.

*Quoted error includes S (scale) factor. See footnote to Table S.

(a) It has not been shown that this entry corresponds to a state with well defined quantum numbers. The Kappa may well disappear after the 1966 Berkeley Conference.
(b) Bump is an unresolved mixture of resonance and "Deck Effect."
(c) Maybe entirely "Deck Effect."
(d) Q and p are calculated from nominal values which may differ slightly from the latest averages.

2. Elementary Theory for Phase-Shift Analysis

Baryon resonances are usually studied in "formation experiments"; it is useful, therefore, to begin by introducing the formalism we are going to use.[2] I will then try to summarize the analysis necessary to extract the resonances and their properties from the experimental results.

2.1 Elastic Scattering

A particle travelling along the z axis is described by a plane wave $\psi = e^{ikz}$, where ik is the momentum of the incoming particle. After scattering, the final wave function will be

$$\psi = e^{ikz} + \frac{F(\theta)}{r} e^{ikr}.$$

The $F(\theta)$ contains all the angular dependence of the scattered wave and can be written as

$$F(\theta) = \frac{1}{k} \sum_{\ell} (2\ell + 1) \frac{\eta_\ell e^{2i\delta_\ell} - 1}{2i} P_\ell(\cos\theta), \qquad (1)$$

where $P_\ell(\cos\theta)$ are Legendre polynomials of order ℓ, η_ℓ (a real number between 0 and 1) represents the attenuation suffered by the ℓth outgoing wave, and $2\delta_\ell$ is the phase shift of the ℓth wave.

The differential cross section for elastic scattering is then

$$\frac{d\sigma}{d\Omega} = |F(\theta)|^2 = \frac{1}{k^2} \left| \sum_{\ell} (2\ell + 1) \frac{\eta_\ell e^{2i\delta_\ell} - 1}{2i} P_\ell(\cos\theta) \right|^2. \qquad (2)$$

In Eq. (2) the scattering amplitude is written as

$$T_e = \frac{\eta e^{2i\delta} - 1}{2i}, \qquad (3)$$

and we will follow this notation from now on. The scattering usually takes place on a target with spin $\pm 1/2$, so it is necessary to introduce the total angular momentum $J = \ell \pm 1/2$. Equation (1) will then become

$$f(\theta) = \frac{1}{k} \sum_{\ell} [(\ell + 1)T_{\ell}^{+} + \ell\, T_{\ell}^{-}]\, P_{\ell}, \tag{4}$$

where $T_{\ell}^{\pm}$ corresponds to the scattering amplitude for $J = \ell \pm 1/2$. It is also necessary to introduce a spin-flip amplitude

$$g(\theta) = \frac{i}{k} \sin\theta \sum_{\ell} [T_{\ell}^{+} - T_{\ell}^{-}] \frac{dP_{\ell}}{d\cos\theta}. \tag{5}$$

Finally, we can write the differential cross section and the polarization in terms of f and g:

$$\begin{aligned} \frac{d\sigma}{d\Omega} &= I = |f|^2 + |g|^2 \\ \vec{P}\,\frac{d\sigma}{d\Omega} &= I\vec{P} = 2\,\mathrm{Re}(f^{*}g)\vec{n}. \end{aligned} \tag{6}$$

If one plots T_e on the complex plane, it will be a vector that lies on (or inside for $\eta < 1$) a circle of radius $1/2$ $(\eta/2)$ and center $i/2$, which is called the unitary circle (see Fig. 1). As the energy of the incident particle is changed, the point representing T_e will move in the plane.

2.2 Resonant Amplitude

The interaction between two particles is said to be resonant when the scattering amplitude for a particular set of quantum numbers (spin, parity, isotropic spin) is a maximum. In addition, the vector T_e has to move in the complex plane in a characteristic manner, according to the Breit-Wigner formula

$$T_e = \frac{x}{\epsilon - i} \quad \text{with} \quad \epsilon = (E - E_r)\frac{2}{\Gamma_{\text{total}}}, \tag{7}$$

$$\mathrm{Re}\ T_e = \frac{\epsilon x}{\epsilon^2 + 1}$$

$$\mathrm{Im}\ T_e = \frac{x}{\epsilon^2 + 1}.$$

A resonant amplitude describes a circle of diameter x, if x is the elasticity of the resonance, i.e., $x = \Gamma(\text{elastic})/\Gamma(\text{total})$. The top of

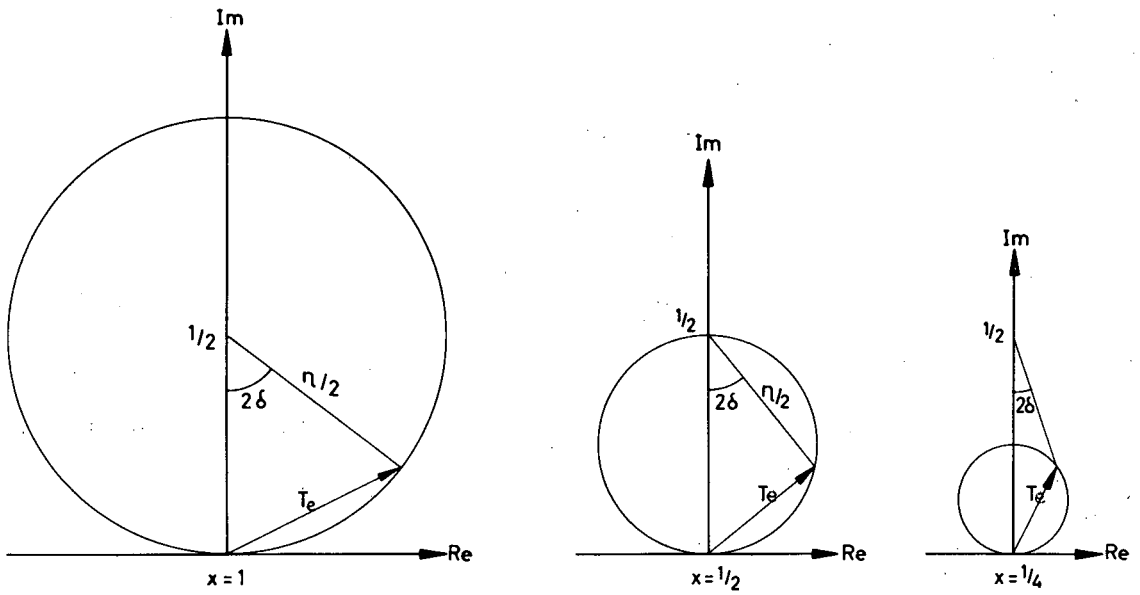

MUB-14064

Fig. 1. The elastic-scattering amplitude T_e in the complex plane (a) For pure elastic scattering ($\eta = 1$), T_e lies on the unitary circle. If the amplitude is resonant, the circle represents a resonance with elasticity $x = 1$. (b) Resonant amplitude for $x = 0.5$. (c) Resonant amplitude for $x < 0.5$. Notice that at resonance $\delta = 0°$.

the circle is the resonant energy, where the amplitude is pure imaginary. In Fig. 1 we can see that at resonance $\delta = 90°$. For elasticity $x < 0.5$, δ does not go to 90° at resonance, but goes instead to 0°. Notice that regardless of x, the resonant amplitude always passes through 90°. The relation between x and η, at the resonant energy, is

$$\eta = |2x - 1|.$$

The parameter η varies with energy; x instead is nearly a constant. The elasticity x will be energy dependent only if Γ(elastic) and Γ(total) have different energy dependence. (See Ref. 2 for a discussion of this point.)

2.3 Effect of Non-Resonant Background

The scattering amplitude assumes a peculiar behavior if, in addition to a resonance, a non-resonant background is present with the same spin, parity (J^P), and isotopic spin (I) as the resonance. This problem has been treated by Dalitz using the K-matrix formalism,[3] and more recently by Michael.[4] Figure 2 illustrates the situation. The circular trajectory is displaced and the center of it is no longer on the imaginary axis but is instead at a point c'. If the vector OR represents the background amplitude, the resonance energy is no longer at the top of the circle (E^*) but is displaced by an angle $2\delta_B$, which is the background phase in the resonant eigenstate. The total amplitude will then assume trajectories as in Fig. 2(b), that depend on the sign of the background. In Sec. 2.4 we will see that experiments show the presence of such trajectories.

2.4 Practical Considerations

The experimental measurement of I and $I\vec{P}$ should provide information on the scattering amplitudes (3), that is, on the nature of the interaction that has taken place. From a practical point of view, Eqs. (6) are usually written as

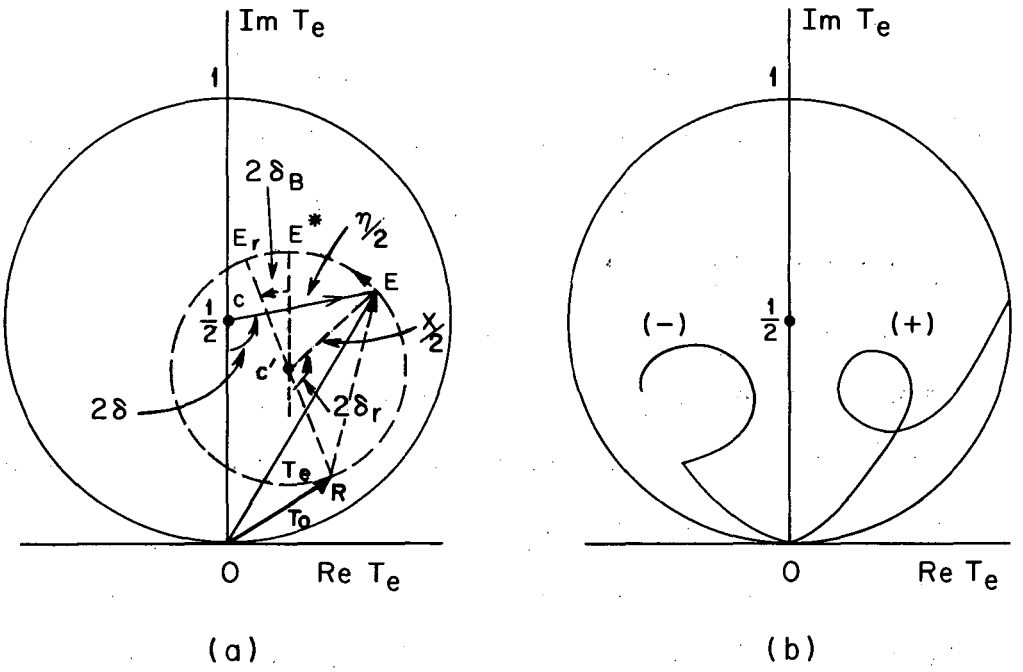

Fig. 2. Plot of T_e for the case in which a non-resonant background, with same quantum numbers as the resonance, is present. (a) The vector OE represents the total amplitude T_e with parameters η, δ. The vector OR represents the total background amplitude. The vector RE is the resonant amplitude with elasticity x and phase $2\delta_r$. $2\delta_B$ is the background phase in the resonant eigenstate and represents the displacement of the resonant energy from the top of the circle. (b) Trajectory of resonances with attractive background (+) and repulsive background (-).

$$I = \lambda^2 \sum_\ell A_\ell P_\ell$$

$$\vec{IP} = \vec{n}\, \lambda^2 \sum_\ell B_\ell P'_\ell, \tag{8}$$

where $\lambda = 1/k$, P_ℓ are Legendre polynomials, and P'_ℓ are the first associated Legendre polynomials. Tables 3 and 4 contain the coefficients of the partial-wave expansions of I and IP in function of the scattering amplitudes (S, P, $\cdots$ H) through J = 9/2. These tables are taken from Ref. 2, to which the reader is referred for further details on the properties of these coefficients.

I now want to point out a few of the difficulties encountered in analyzing the data in order to get the scattering amplitudes (3).

(i) First of all, we do not know at what point we have to stop the summation in Eq. (8). As a first approximation, angular momentum states with $\ell > kr$ [r of the order of 1 Fermi = (197 MeV/c^{-1})] can be neglected, but this condition gives only an upper limit.

(ii) For scattering of a 0-spin particle on a spin-1/2 target, the Minami ambiguity is present. From the coefficients of Tables 3 and 4, one sees that under interchange of parity for the same J, for example, $S_1 \rightarrow P_1$, I remains invariant but IP changes sign. This means that measurement of angular distributions alone cannot determine the parity of the states present in the scattering.

(iii) Even if the polarization has been measured, the solution is still not unique, since the operation of "complex conjugation" on all amplitudes will also leave I unchanged, and change the sign of IP. Thus, a further dynamical argument must be used to determine the angular momentum states. For a resonance, this is the Wigner condition, for which the amplitude has to move across the complex plane counterclockwise.

Table 3. $I = \lambda^2 \sum_m A_m P_m(\cos\theta)$.

	A_0	A_1	A_2	A_3	A_4	A_5	A_6	A_7	A_8	A_9
$S_1S_1 + P_1P_1$	1									
S_1P_1		2								
$S_1P_3 + P_1D_3$		4								
$S_1D_3 + P_1P_3$	0		4							
$S_1D_5 + P_1F_5$	0		6							
$S_1F_5 + P_1D_5$		0		6						
$S_1F_7 + P_1G_7$		0		8						
$S_1G_7 + P_1F_7$	0		0		8					
$S_1G_9 + P_1H_9$	0		0		10					
$S_1H_9 + P_1G_9$		0		0		10				
$P_3P_3 + D_3D_3$	2		2							
P_3D_3		4/5		36/5						
$P_3D_5 + D_3F_5$		36/5		24/5						
$P_3F_5 + D_3D_5$	0		12/7		72/7					
$P_3F_7 + D_3G_7$	0		72/7		40/7					
$P_3G_7 + D_3F_7$		0		8/3		40/3				
$P_3G_9 + D_3H_9$		0		40/3		20/3				
$P_3H_9 + D_3G_9$	0		0		40/11		180/11			
$D_5D_5 + F_5F_5$	3		24/7		18/7					
D_5F_5		18/35		16/5		100/7				
$D_5F_7 + F_5G_7$		72/7		8		40/7				
$D_5G_7 + F_5F_7$	0		8/7		360/77		200/11			
$D_5G_9 + F_5H_9$	0		100/7		720/77		70/11			
$D_5H_9 + F_5G_9$		0		20/11		80/13		3150/143		
$F_7F_7 + G_7G_7$	4		100/21		324/77		100/33			
F_7G_7		8/21		24/11		600/91		9800/429		
$F_7G_9 + G_7H_9$		40/3		120/11		120/13		2800/429		
$F_7H_9 + G_7G_9$	0		200/231		3240/1001		280/33		3920/143	
$G_9G_9 + H_9H_9$	5		200/33		810/143		160/33		490/143	
G_9H_9		10/33		240/143		60/13		78400/7293		79380/2431

$$S_1P_2 + P_1D_3 = \mathrm{Re}(S_1^* P_3 + P_1^* D_3)$$

Table 4. $I\vec{P} = \hat{n}\lambda^2 \sum_m B_m P^1_m(\cos\theta)$.

	B_1	B_2	B_3	B_4	B_5	B_6	B_7	B_8	B_9
S_1P_1	2								
$S_1P_3 - P_1D_3$	-2								
$S_1D_3 - P_1P_3$		2							
$S_1D_5 - P_1F_5$		-2							
$S_1F_5 - P_1D_5$	0		2						
$S_1F_7 - P_1G_7$	0		-2						
$S_1G_7 - P_1F_7$		0		2					
$S_1G_9 - P_1H_9$		0		-2					
$S_1H_9 - P_1G_9$	0		0		2				
P_3D_3	8/5		12/5						
$P_3D_5 - D_3F_5$	-18/5		-2/5						
$P_3F_5 - D_3D_5$		10/7		18/7					
$P_3F_7 - D_3G_7$		-24/7		-4/7					
$P_3G_7 - D_3F_7$	0		4/3		8/3				
$P_3G_9 - D_3H_9$	0		-10/3		-2/3				
$P_3H_9 - D_3G_9$		0		14/11		30/11			
D_5F_5	54/35		8/5		20/7				
$D_5F_7 - F_5G_7$	-36/7		-2/3		-4/21				
$D_5G_7 - F_5F_7$		4/3		18/11		100/33			
$D_5G_9 - F_5H_9$		-100/21		-72/77		-10/33			
$D_5H_9 - F_5G_9$	0		40/33		64/39		450/143		
F_7G_7	32/21		16/11		160/91		1400/429		
$F_7G_9 - G_7H_9$	-20/3		-10/11		-12/39		-50/429		
$F_7H_9 - G_7G_9$		100/77		1458/1001		20/11		490/143	
G_9H_9	50/33		200/143		20/13		14000/7293		8820/2431

$$S_1P_3 - P_1D_3 = \mathrm{Im}(S_1^*P_3 - P_1^*D_3)$$

In practice, solving Eqs. (8) for phase shifts and absorption parameters requires a large amount of experimental data. Since the relations between I and IP, and η_{2J}, δ_{2J} are so complex and the above-mentioned ambiguities are present, it has been impossible until now to find a unique set of phase shifts and absorption parameters without the introduction of some hypothesis of another nature or some theoretical prediction.

3. Total Cross Sections

The optical theorem relates the elastic forward amplitude to the total cross section by

$$\sigma_{total} = \frac{4\pi}{k} \text{Im } f(0).$$

The contribution of a resonant state, from Eqs. (4) and (7), is

$$(\sigma_{total})_r = 4\pi \lambda^2 (J + 1/2) \frac{x_e}{\epsilon^2 + 1} \tag{9}$$

where $\lambda = 1/k$. For x_e small and J small, it is not likely that a resonance produces any peak in the total cross section.

Notice that from Eqs. (4) through (7), the contribution of a resonance to the elastic cross section is

$$(\sigma_{elastic})_r = 4\pi \lambda^2 (J + 1/2) \frac{x_e^2}{\epsilon^2 + 1} \tag{10}$$

i.e., proportional to x_e^2, smaller than to the total cross section.

Historically the bump hunting began in studying pion-nucleon scattering. Since the discovery of $\Delta(1238)$ as a bump in the $\pi^+ p$ total cross section, 12 more sure resonances and 3 possible ones have been added to the family of pion-nucleon resonances.

The total cross sections for $\pi^- p$ and $\pi^+ p$ as functions of pion kinetic energy are shown in Fig. 3. They present a very interesting profile, with

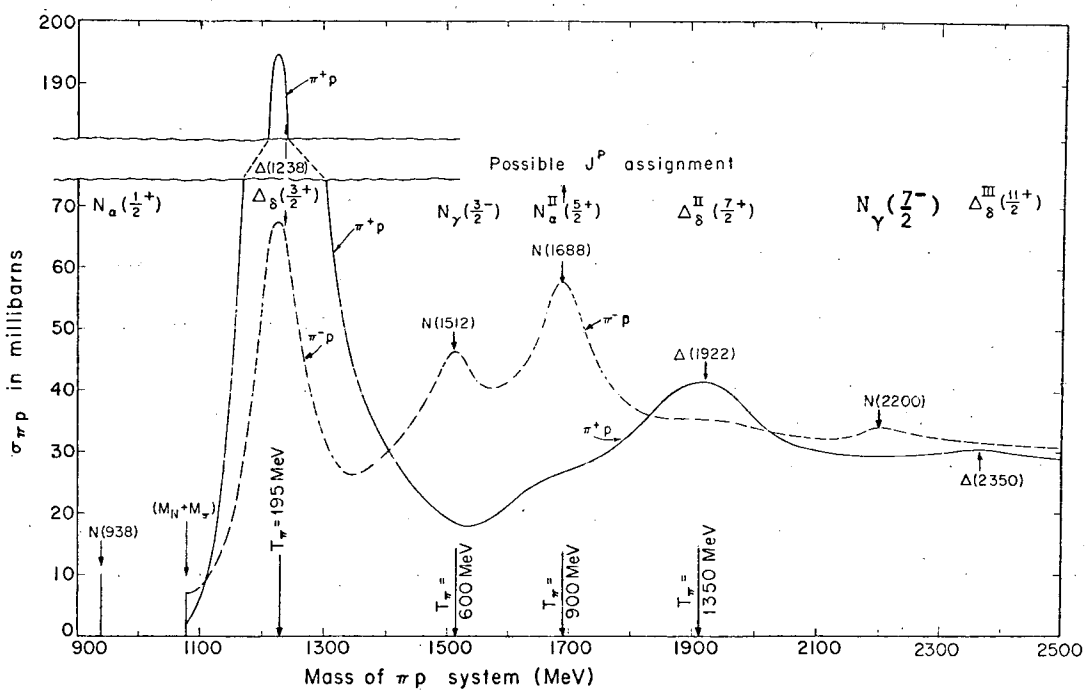

MUB-13728

Fig. 3. The $\pi^{\pm}$ total cross sections versus π laboratory kinetic energy. Vertical lines indicate energies where resonant states are present.

bumps and valleys. Figure 4 shows the two isospin states, separated according to the relations

$$\sigma(\pi^- p) = 1/3\ \sigma(I = 3/2) + 2/3\ \sigma(I = 1/2);$$

$$\sigma(\pi^+ p) = \sigma(I = 3/2).$$

The bumps and shoulders which turned out to contain resonances are indicated by arrows. (This plot is taken from Diddens et al.[5])

4. Nucleon Resonances with Measured Quantum Numbers

4.1 Generalities

All the baryon resonances with strangeness of 0 have been discovered in formation experiments. They appeared first as bumps in total cross-section experiments. Subsequent analysis of elastic and charge-exchange differential cross section and polarization were necessary in order to determine their properties. Phase-shift and partial-wave analyses have been done, which, together with theoretical calculations, have provided quantum number assignment for the resonances with mass below 2.2 GeV.

4.2 Results of Phase-Shift Analysis

In various laboratories many experiments have been done on $\pi^{\pm} p$ elastic scattering and charge exchange. As good polarization measurements have not been made until recently, only part of the structure shown in the total cross-section data has been understood.

Many groups are working on the analysis of the experimental data. The assumptions that each group has made are different, and I will try to summarize them here.

(a) Roper,[6] at Livermore, has analyzed the data up to $T_\pi = 700$ MeV, using an energy-dependent form for the phase shifts of the type

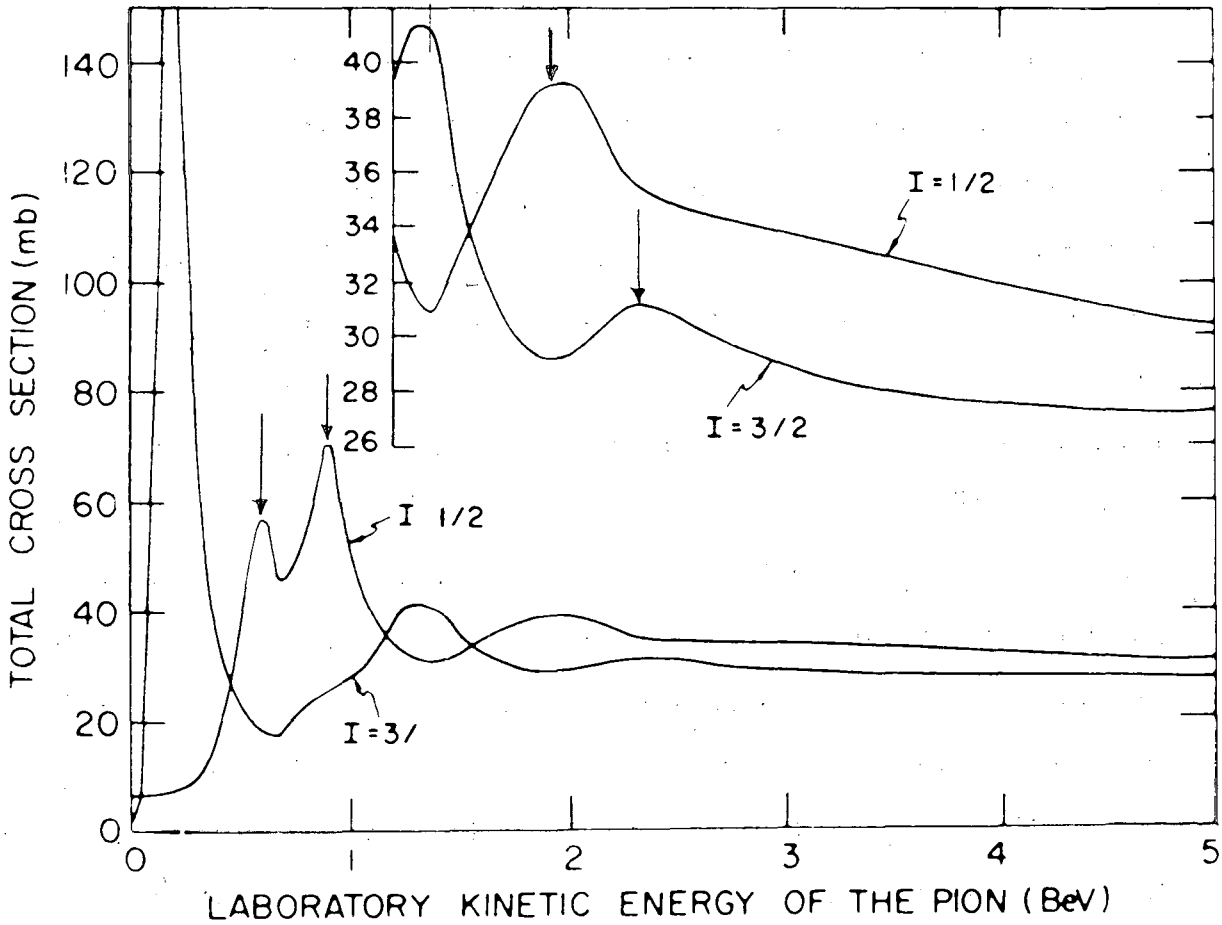

Fig. 4. The πN total cross section in the two isotopic spin states. For pion energy greater than 1.2 GeV, the cross sections are also shown magnified. The arrows indicate bumps and shoulders which turned out to be resonances. (Plot taken from Ref. 5.)

$$\delta_\ell = k^{2\ell+1} \sum_{n=0}^{\ell_{max}-\ell} a_n k^n, \qquad (11)$$

where ℓ_{max} is the maximum ℓ used in the fit. This form was used for the non-resonant amplitudes, whereas for the resonances, Breit-Wigner amplitudes were used. In this way he found that the phase shift of the P_{11} amplitude, which had the energy dependence (11), went through 90° at M = 1500 MeV. This is known as the Roper resonance, and subsequent analyses confirmed its existence.

(b) Collaborators at Imperial College and the University College of London have analyzed experimental data up to T_π = 1300 MeV.[7] In various articles, Auvil, Lovelace, Donnachie, and Lea (ALDL) have developed a semiphenomenological technique which uses fits to partial-wave dispersion relations in addition to phase-shift analysis at separate energies. In this way they get from theory the energy dependence of the amplitudes. The theoretical predictions use the dispersion-relations calculations of Donnachie and Hamilton.[8] Figures 5 and 6 show their results for the amplitude of the S_{31} state, i.e., isospin = 3/2, $J^P = 1/2^-$. It has quite a peculiar behavior. It indicates that a repulsive background is superimposed on a resonant state in the same state of isotopic spin, angular momentum, and parity. The resonance S_{31} is at about M = 1690 MeV.

(c) Brandsen, Moorhouse, and O'Donnell use a similar method because they make use of the predictions of dispersion relations to decide among the various solutions of the fit.[9] However, the parameterization they use is different from that of ALDL, as it is based on dispersion relations for the inverse amplitudes. They reach solutions which are in qualitative agreement with ALDL's.

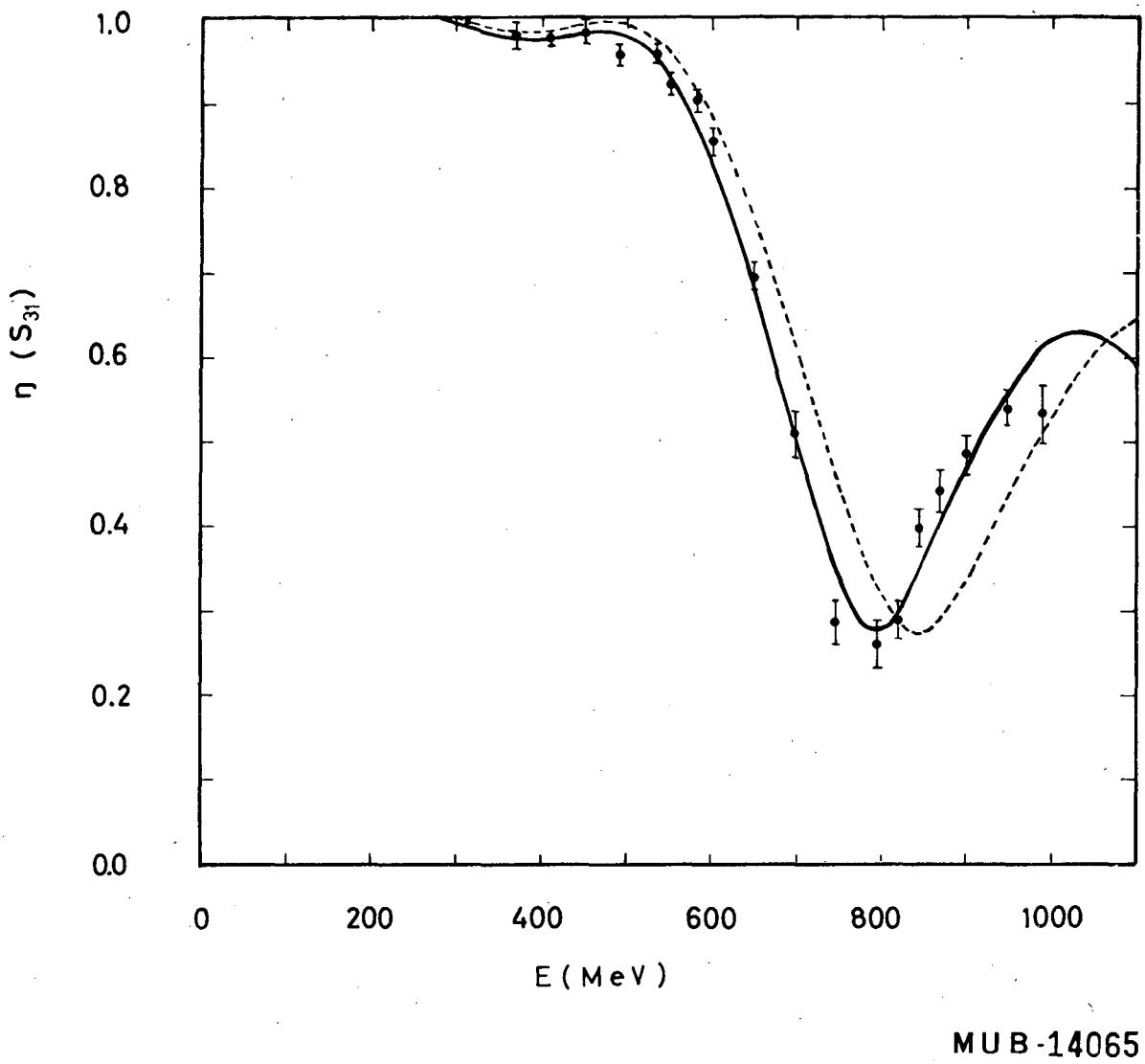

Fig. 5. The solutions of Donnachie et al.[7] for the absorption parameter η of the S_{31} state. The solid line is a dispersion-relation fit, the dashed line a dispersion-relation prediction.

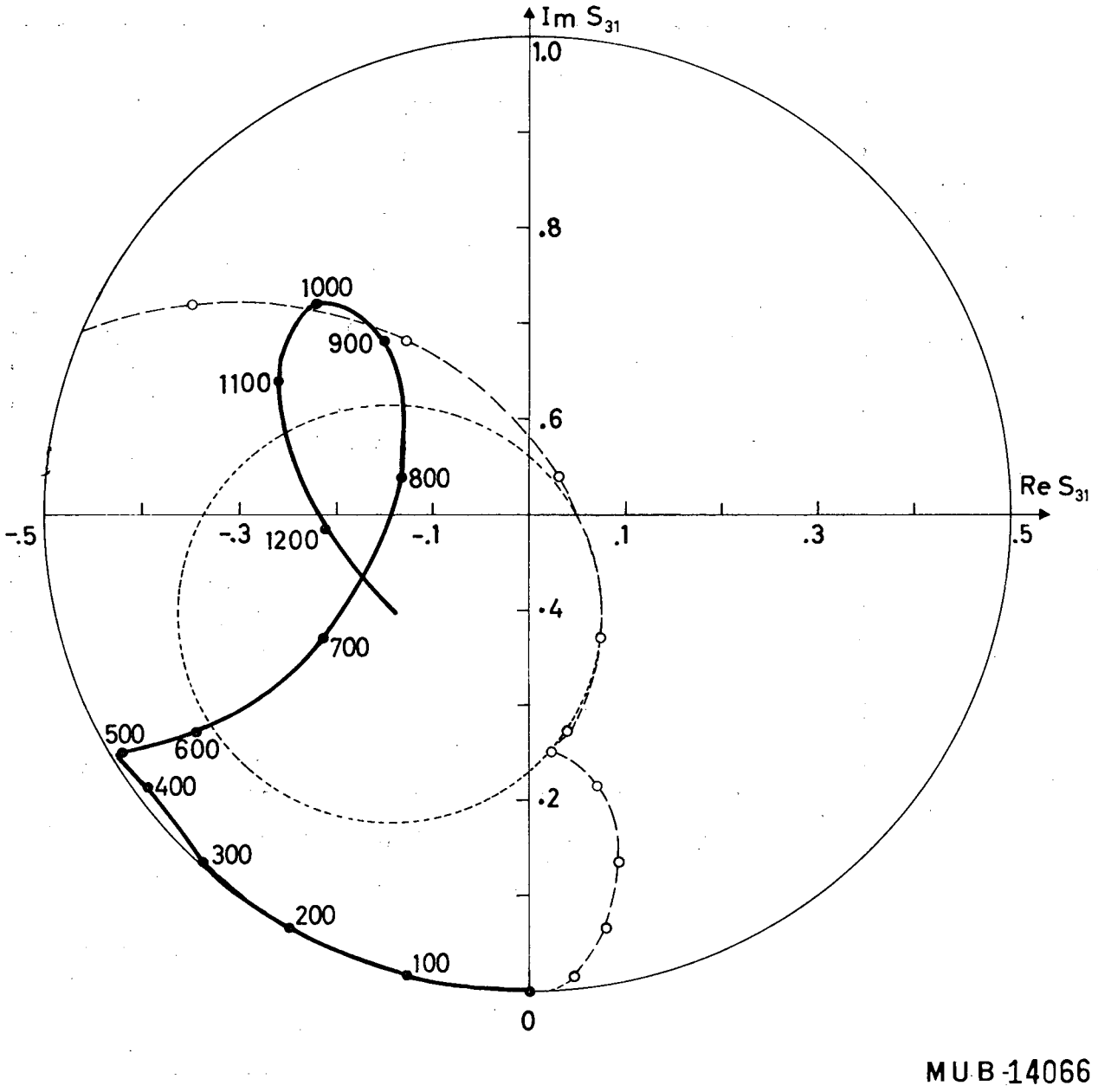

Fig. 6. Behavior of S_{31} of Donnachie et al.[7] in the complex plane.

(d) Bareyre et al., of Saclay, have used a completely different approach.[10] For each energy, starting from a random set of phase shifts, they fit Eqs. (6) to the data, searching for the minimum χ^2. They find that the solution is not unique, but if they require continuity of the solutions with energy, then the ambiguity is completely removed. The analysis, done at 13 different kinetic energies between 310 and 990 MeV, was made up to F wave (except for the two highest energies, at which G wave was introduced). At each energy there are 28 parameters to fit, and the average number of points used is 62. Their results are really astonishing; they are shown in Figs. 7 and 8 as amplitudes in the complex plane and as functions of total c.m. energy. Figure 7 shows their solutions for I = 3/2 πp scattering, and Fig. 8 the I = 1/2 solutions. The P_{33} [Δ(1238)] phase shift goes through 90°, and so do the D_{13} [N^*(1530)], the P_{11} [N^*(1510)], and the F_{15} [N^*(1688)]. As the D_{15} [N^*(1690)] phase shift goes through 0°, a resonance with $x < 0.5$ is indicated. The S_{31}, S_{11} also show some cusp behavior at ≈1690 MeV and 1560 MeV, respectively.

Figure 9 summarizes the amplitudes of Bareyre et al. as plotted by Rosenfeld.[11] To exhibit the velocity, he put hatch marks every 10 MeV across all the trajectories. Note that most of them are not circular, which is an indication that background amplitudes are present and displace the resonant energy from the $\delta = 90°$ point. Figure 10 shows the S_{11} amplitude of these same authors as fitted by Michael.[4] At 1550-MeV total energy, it shows a first resonant behavior above a large background in the same state of IJP. At 1700 MeV it crosses the imaginary axis where $\delta = 90°$, which is an indication of a second resonance at this energy.

The S_{11} resonance at 1550 MeV seems to be associated with the threshold for the reaction $\pi^- p \to \eta n$. Bulos et al.[12] studied this reaction

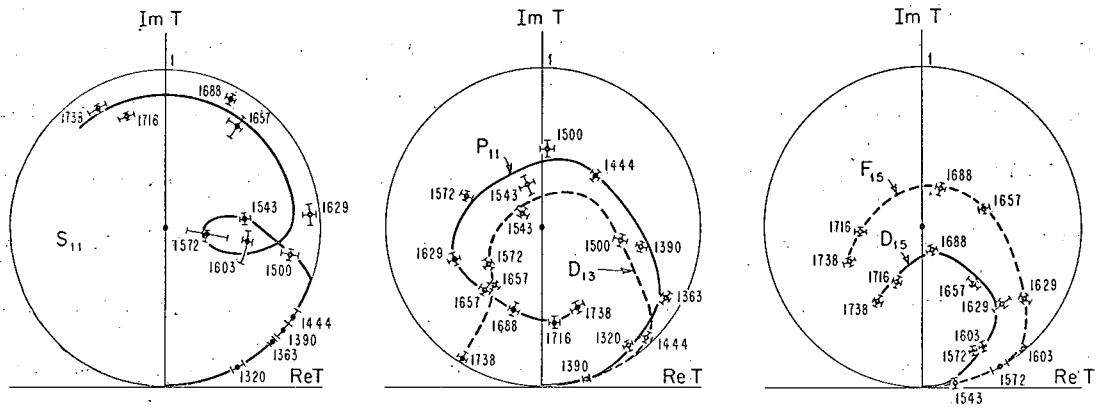

MUB-14067

Fig. 7. Amplitudes for the I = 1/2 state of the πp system plotted in the complex plane, according to the solutions of Bareyre et al.[10]

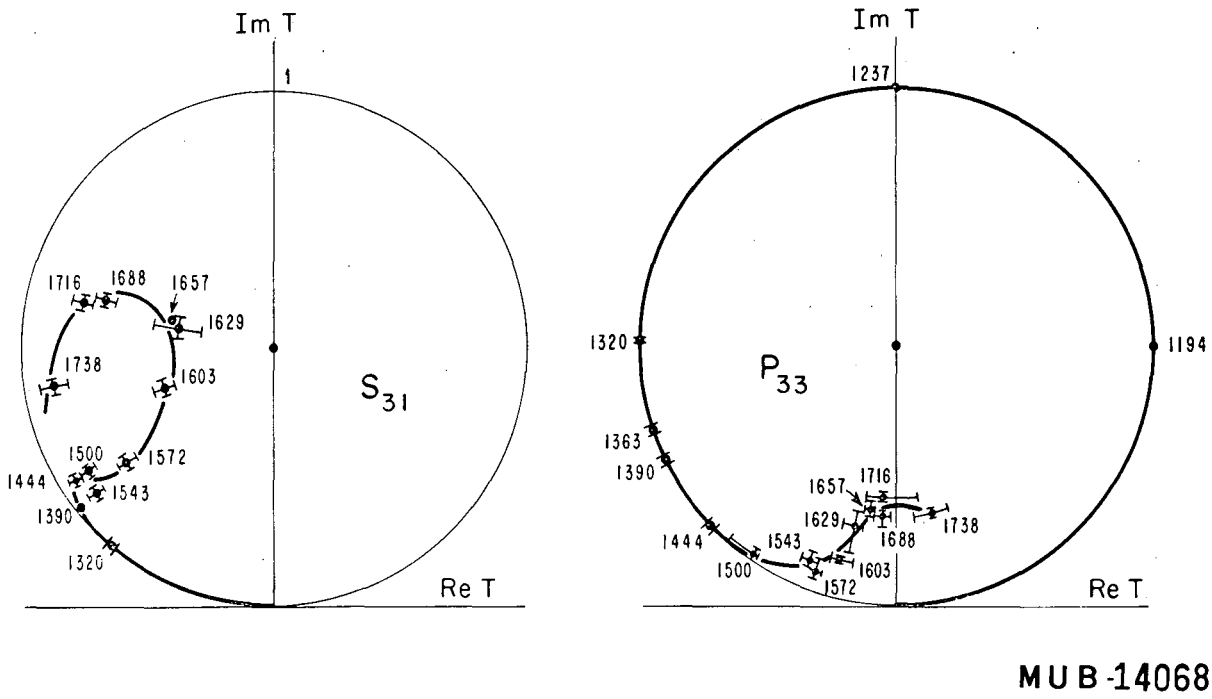

Fig. 8. Amplitudes for the I = 3/2 state of the πp system plotted in the complex plane, according to the solutions of Bareyre et al.[10]

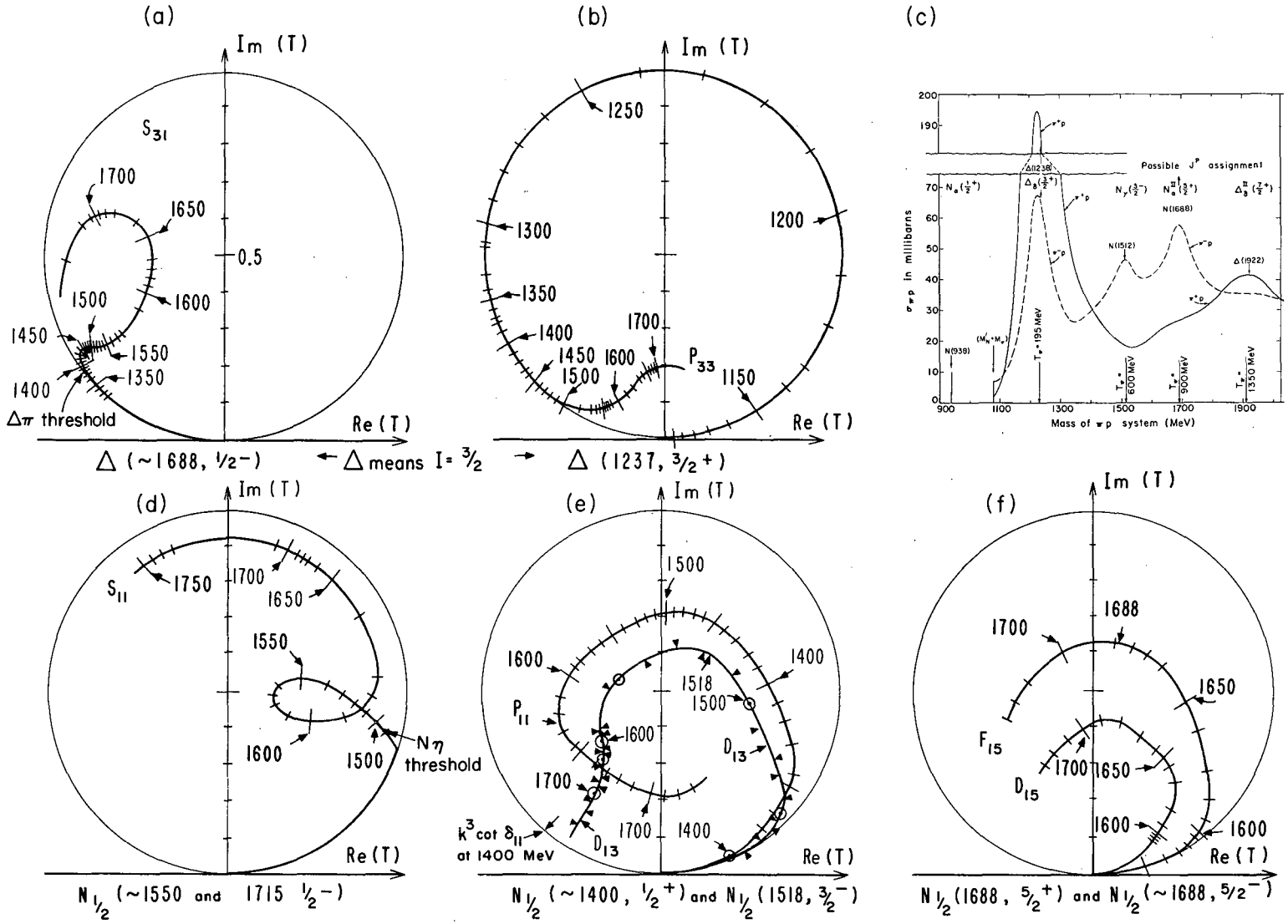

Fig. 9. Amplitudes for I = 3/2 and I = 1/2 states according to the solution of Bareyre et al.[10] Smooth curves are guessed from the experimental points of Figs. 7 and 8. To exhibit the velocity, hatch marks are placed every 10 MeV across all the trajectories. Most of the trajectories are not circular because some background amplitude is present, thus displacing the resonant energy from the 90° point.

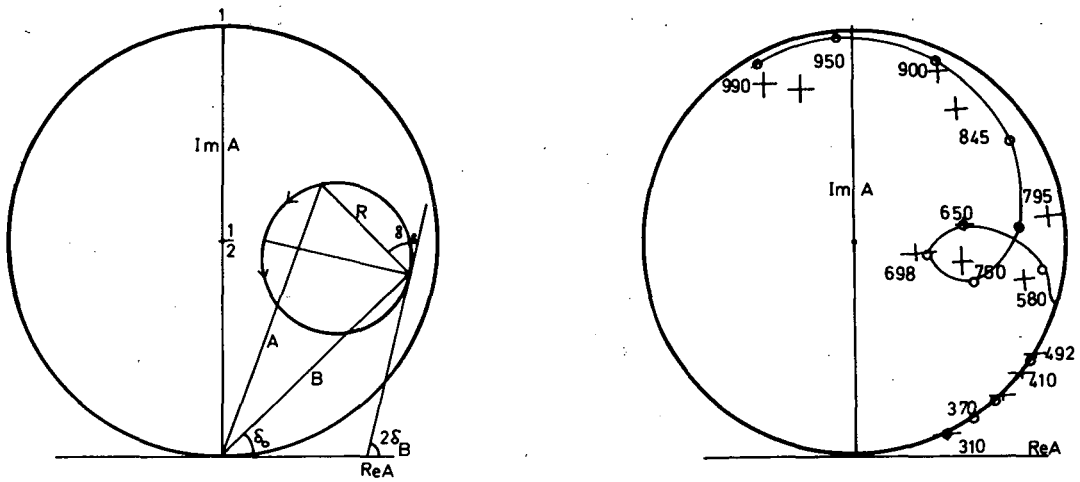

MUB-14069

Fig. 10. S_{11} amplitude of Bareyre et al.[10] as fitted by Michael,[4] using two resonances in the S_{11} state. (a) The Argand diagram for $A = \rho_1 a_{11}$ shows the addition of a background $B = \epsilon_0 \exp(i\delta_0) \sin\delta_0$ in the same partial wave to a resonant amplitude $R = \epsilon_R \exp(i\delta_R) \sin\delta_R$ after the latter has been rotated by twice the phase δ_B of v_1, coupling of the resonance to channel 1. This coupling is a function of the energy and of the couplings to the other channels. The circular path shown corresponds to increasing energy through the resonance at $\delta_R = 1/2\pi$ with B constant in energy. (b) The S_{11} πN phase shift amplitude A from the analysis of Bareyre et al.[10] is shown by the crosses at each laboratory pion kinetic energy in MeV. The smooth curve represents the amplitude A calculated assuming that each resonance is the only background to the other resonance. The circles are the values of A calculated at each energy where a phase shift determination exists.

and found a rapid rise of the cross section, which has reached 2.5 mb at T_π = 600 MeV. Hendry and Moorhouse[13] studied the energy dependence of this reaction and conclude that only a resonance can satisfactorily explain the observed behavior. Figure 11(a) shows their fit to the data of Bulos et al.[12] The photoproduction data of Bacci et al.[14] and Prepost et al.[15] show the same behavior as the πn data; they are shown in Fig. 11(b), together with higher energy points.[16]

The spectroscopy of the nucleonic resonances, resulting from the phase-shift analyses a, b, c, d, is shown in the following table:

2I, 2J	J^P	M (MeV)	Γ (MeV)	x	Groups
S_{11}	$1^-/2$	1530	100	0.5	b, c, d
S_{11}	$1^-/2$	1700	200	?	c, d
P_{11}	$1^+/2$	≈1450	200	0.6	a, b, c, d
D_{13}	$3/2^-$	1527	100	0.5	a, b, c, d
D_{15}	$5/2^-$	1690	100	0.35	b, c, d
F_{15}	$5/2^+$	1688	120	0.8	a, b, c, d
S_{31}	$1/2^-$	1690	120	0.5	b, d
P_{33}	$3/2^+$	1236	125	1.0	a, b, c, d
F_{37}	$7/2^+$	1920	200	0.6	b

Since Roper has not worked on this problem recently, his results do not appear often in the table. The other authors agree in the general behavior of the phase shifts, although they do not agree on the values of the resonant parameters. However, the discrepancy is not large.

From the above table it is clear that the bump in π^-p total cross section of ≈600 MeV turned out to contain three resonant states, whereas the one around 900 MeV is explained by the existence of four resonances!

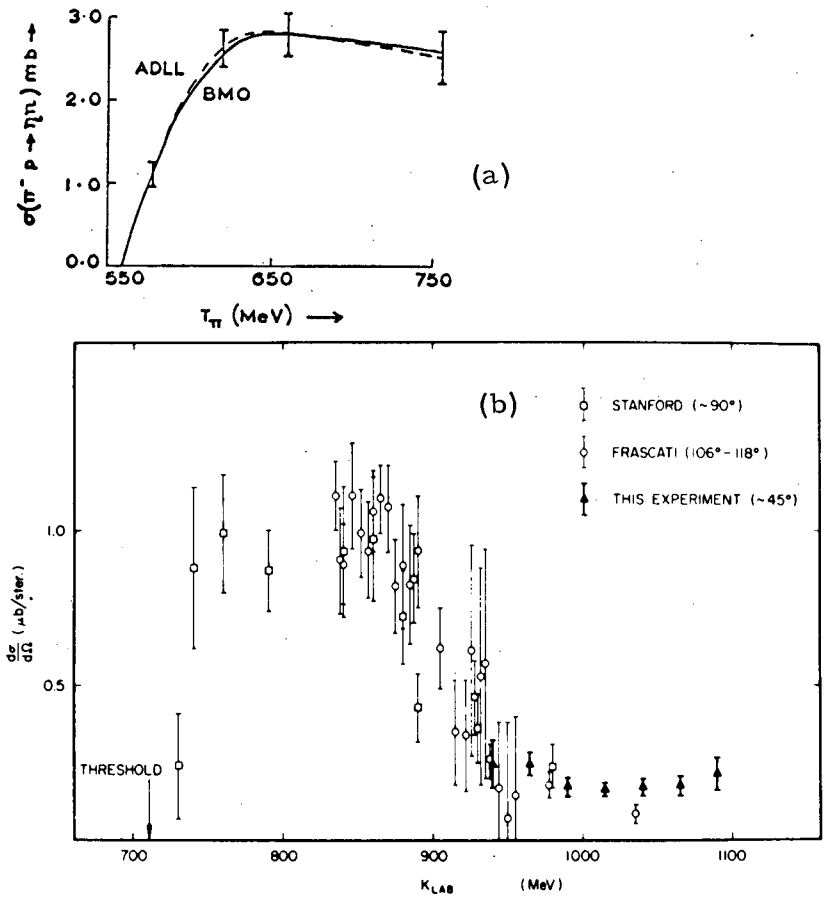

MUB-13729

Fig. 11. (a) (above) Cross section for $\pi^- p \to \eta n$ from Bulos et al.[12] The curves correspond to simultaneous fitting of the production and phase-shift analyses data of Refs. 7, done by Hendry and Moorhouse.[13] (b) (below) Differential cross section for $\gamma p \to p + \eta$. The lower energy data are from Frascati[14] and Stanford.[15] The data above 940 MeV/c are from Heusch et al.[16]

In conclusion, the phase-shift analysis has resolved two bumps which contain seven resonances in the total cross section. However, it should be emphasized that this multitude of resonances should be looked upon with some caution. There is still need of new improved data before we can accept this present situation without reservation. Perhaps I should mention that Cence,[17] from the University of Hawaii, has published a set of phase shifts in the region of T_π between 300 and 700 MeV; this region does not show any resonance at all, except for the well-known P_{33}.

Draxler and Hüper[18] have checked the consistency of the phase-shift analysis of Bareyre et al., Cence, and Auvil, and Lovelace et al. with dispersion relations for πN-scattering amplitude in the forward direction. They find that the agreement of the Saclay group analysis with prediction is good, but the analysis of Cence is clearly in disagreement with the prediction. The set of δ, η of Auvil, Lovelace et al. was obtained by using dispersion relations and is clearly in agreement with the predictions. Höhler et al.[19] have done calculations of the same type for the forward-scattering amplitude in charge exchange. They found good agreement with experimental data in charge exchange, and also with the phase-shift analysis of Bareyre et al. Figure 12 shows the comparison of their calculations with experimental values.

Finally, some of these resonances have also been detected in production experiments. The reader can find these references in Rosenfeld et al.[1]

4.3 Use of Polarized Targets

A new technique recently introduced will help considerably in the analysis of nucleon resonances. To measure the polarization of the recoil proton is very hard, and this fact has delayed the understanding of πp

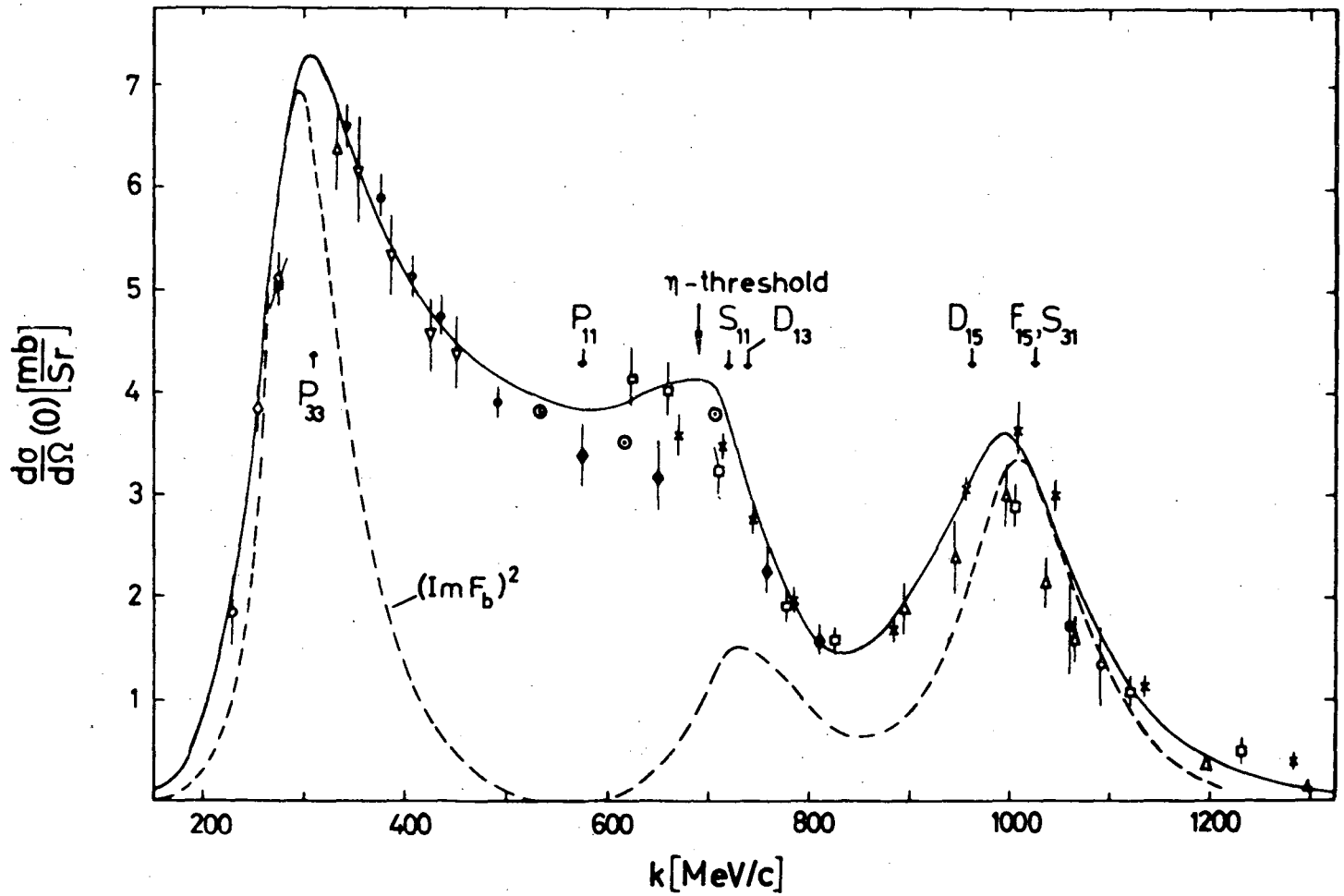

Fig. 12. Charge-exchange forward cross section. Plot from Höler et al.[19] Solid line is prediction of dispersion relation, dashed line is contribution of imaginary part. Data from various experiments listed in Ref. 19. ⊙ values calculated from the phase-shift analysis of Bareyre et al.[10]

UCRL-17054

scattering for a long time. This new technique involves the use of a polarized target. If it is bombarded with pions, the angular distribution of the scattered pions and the differential cross section will be

$$I(\theta) = I_0(\theta)\,(1 + \vec{P}_0 \cdot \vec{P}_T),$$

where $I_0(\theta)$ and $\vec{P}_0$ are the differential cross section and the polarization, respectively, of the recoil proton for an unpolarized target, and P_T is the polarization of the target. By measuring a left-right asymmetry, we can obtain P_0 if P_T is known:

$$\frac{IL - IR}{IL + IR} = P_0 P_T.$$

Δ(1920): An experiment performed at Nimrod by Duke et al.[20] supplied the first surprising results of this technique. They measured both angular distributions and polarization in the region between 1.56 and 2.02 GeV total c.m. energy (0.8 to 1.7 GeV/c incident momentum of π^- and π^+). Their analysis supplies a $7/2^+$ assignment for this resonance. They use the following Legendre polynomial expansion:

$$\frac{d\sigma}{d\Omega} = \sum_n C_n^{\pm} P_n(\cos\theta)$$

$$\frac{1}{\sin\theta} P_0 \frac{d\sigma}{d\Omega} = \sum_n D_n^{\pm} P_n(\cos\theta).$$

Figure 13 shows their C_n^+ coefficients for $\pi^+ p$ elastic scattering. The behavior of C_5 and C_6 suggests spin 7/2 for Δ(1920). Figure 14 shows the coefficients D_n^- for scattering of π^- from the polarized target. The sign of the coefficient D_5^- is enough to solve the ambiguity between the two possible parity assignments. Another result of this experiment has been the suggestion

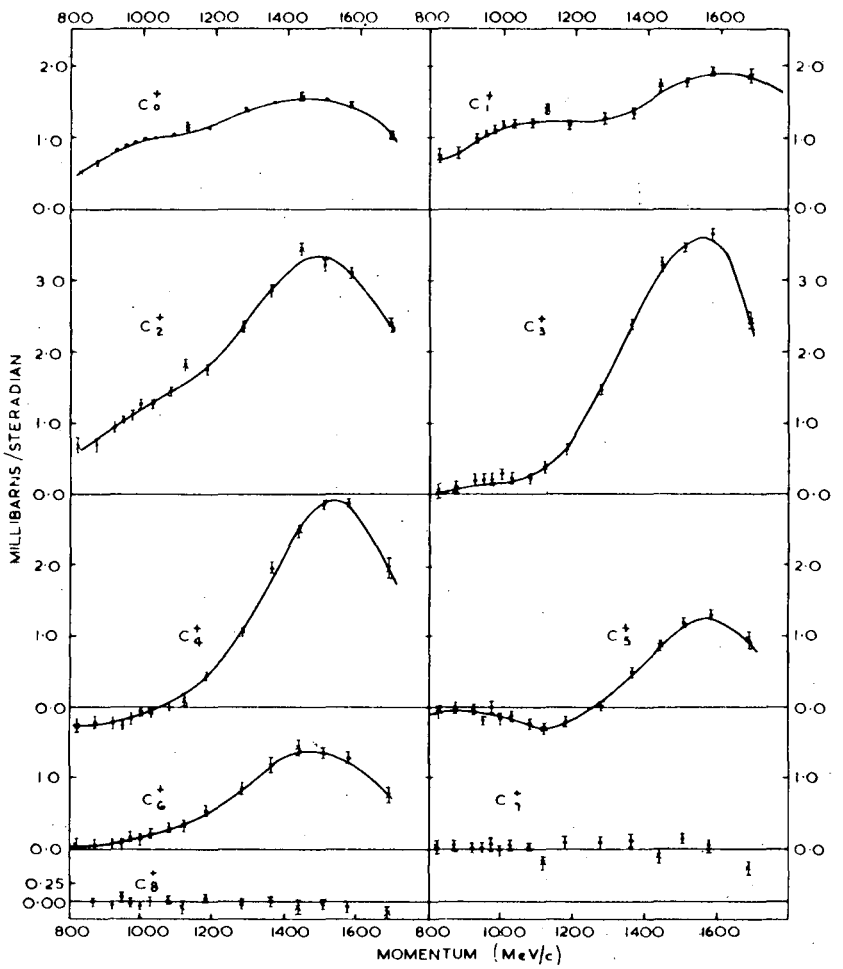

MUB-14070

Fig. 13. The coefficients C_n^+ for $\pi^+ p$ elastic scattering:[20]

$C_5 = 14.3\,(F_5^* D_5) + 5.7\,(F_7^* D_5 + G_7^* F_5) + 6.6\,(G_7^* F_7)$

$C_6 = 18.2\,(F_7^* F_5 + G_7^* D_5) + 3.0\,(|F_7|^2 + |G_7|^2)$

$C_7 = 22.8\,(F_7^* G_7)$.

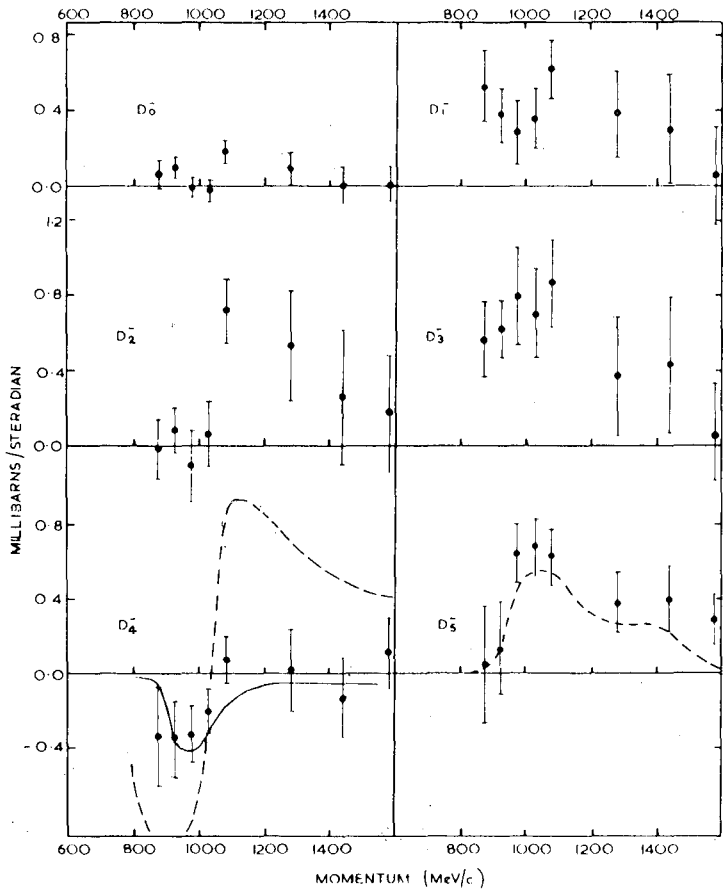

MUB-14071

Fig. 14. The coefficients D_n^- of the Legendre polynomials expansion of $(\frac{1}{\sin\theta}\,\mathrm{IP})$ for π^-p scattering.[20]

$D_4 = -12.9\,(F_5^*D_5) + 0.86\,(F_7^*D_5 - G_7^*F_5) - 22.6\,(G_7^*F_7)$

$D_5 = 16.7\,(F_7^*F_5 - G_7^*D_5)$.

that the bump at M = 1688 MeV is really due to two resonant states, one $F_{5/2}$, the other $D_{5/2}$. Their coefficient C_5^- shows a large peak due to $D_{5/2}$ $F_{5/2}$ interference. The full curve on the D_4^- coefficient is calculated with the assumption of these two resonances, in addition to $\Delta(1920)$. The subsequent phase-shift analysis of Bareyre et al.[10] confirmed this hypothesis.

$N^*(2190)$: Yokosawa et al.[21] at the ZGS in Argonne have also used the polarized-target technique to determine the quantum numbers of $N^*(2190)$. Their analysis gives a $7/2^-$ assignment for this resonance. The technique is similar to the previous one, i.e., they study the behavior of the coefficients of a Legendre polynomial expansion of IP. Figure 15 shows their experimental distribution of $IP(\theta)/\lambda^2$. Figure 16 shows the coefficients of IP/λ^2. What they observe here is the interference between $\Delta(1920)$ and $N^*(2130)$. The coefficient b_7 is, in fact, $b_7 = +3.3\ G_7^* F_7$.

The results of these two experiments are very promising, and in the future this technique will really help the understanding of many resonant phenomena.

Independent evidence on parity of $N^*(2130)$ from the experiment of Kormanyos et al.[25] will be shown in Sec. 6.

5. Resonances with Mass Greater than 2.2 GeV

In Fig. 4 we have seen an indication of an enhancement in the total $\pi^+ p$ total cross section, corresponding to a mass of ≈2360 MeV. Since then, other evidence has been added to the existence of this and other possible resonances in photoproduction by Alvarez et al.,[22] and in charge-exchange cross section by Wahlig et al.[22] The total cross sections have been measured with large accuracy by Citron et al.,[22] and more structure has appeared. Figure 17 shows the I = 3/2 and I = 1/2 total cross sections, as reported by Citron et al.[22] They show some structure, and recently Galbraith[23] suggested

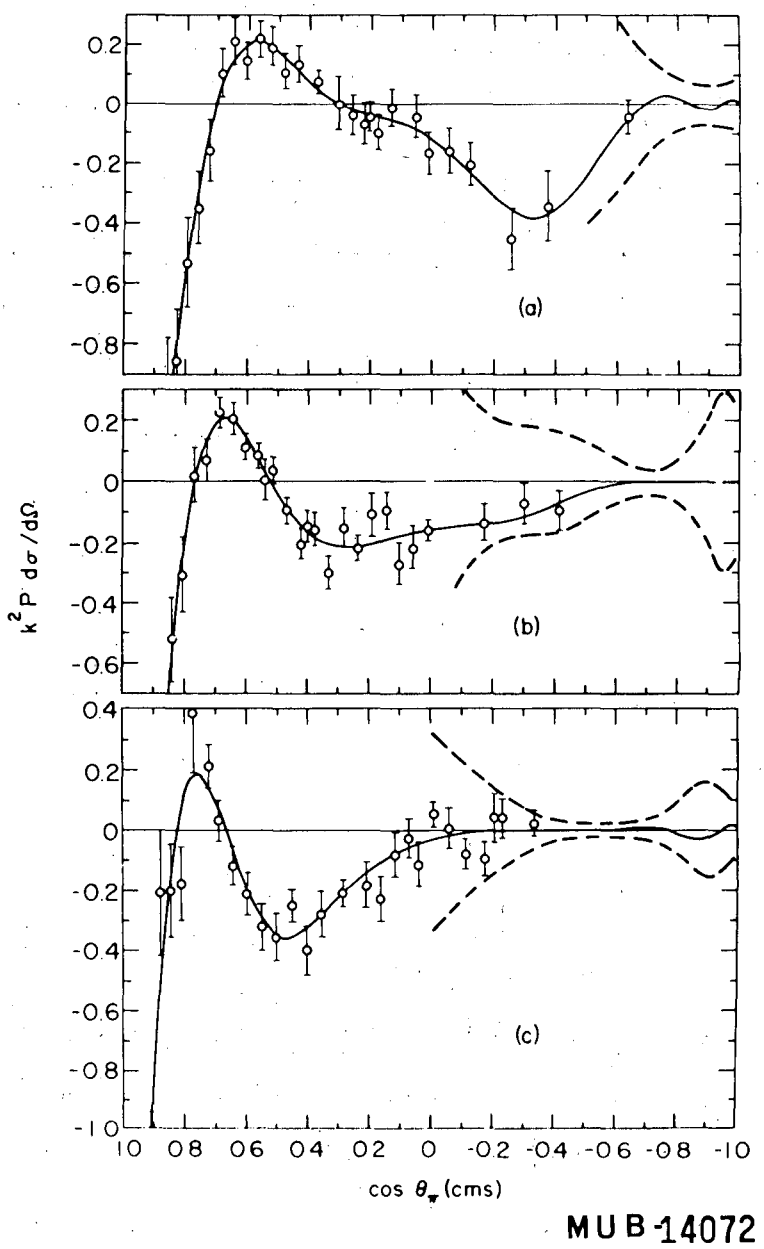

Fig. 15. The IP/λ^2 distribution of Yokosawa et al.[21] at (a) 1.7 GeV/c, (b) 2.07 GeV/c, (c) 2.5 GeV/c π^-.

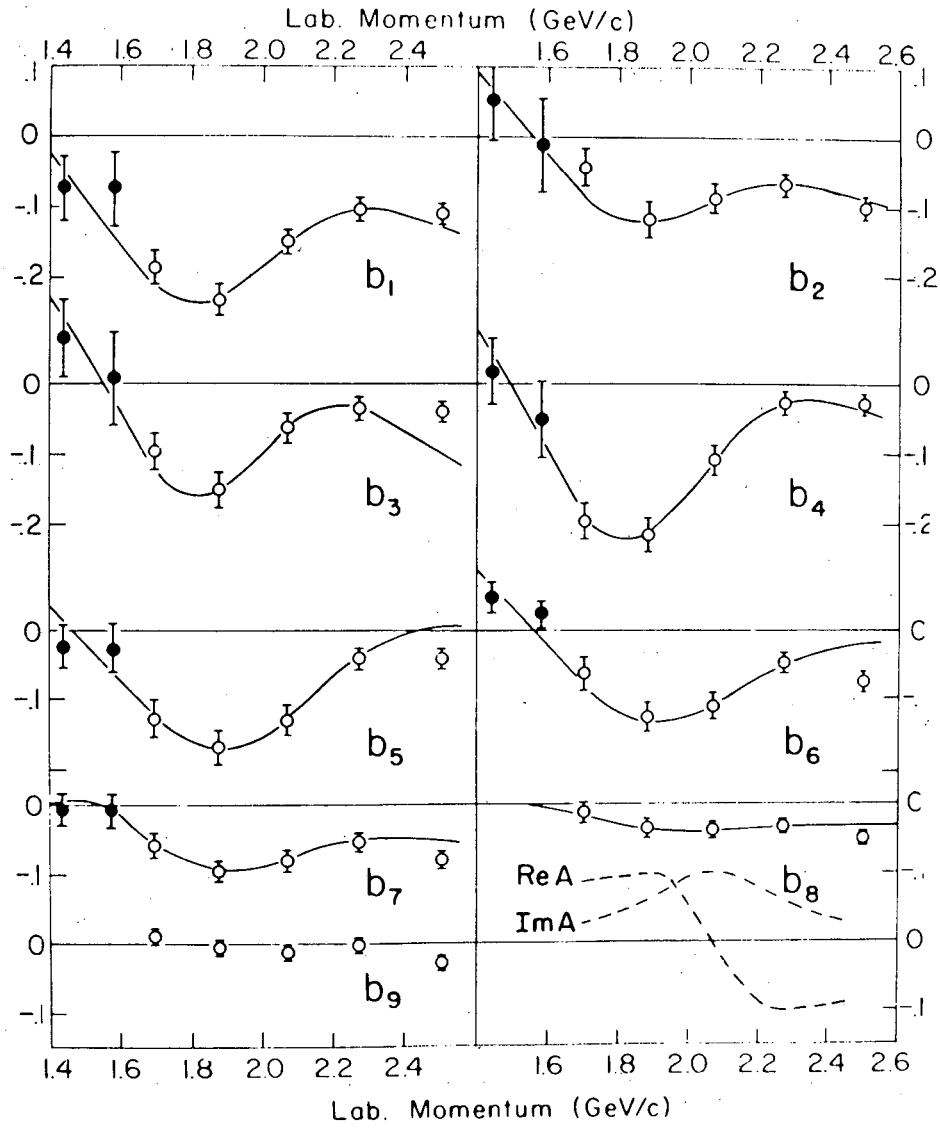

Fig. 16. The coefficients of the Legendre polynomials expansion of IP/λ^2 from Yokosawa et al.[21] The curves are calculated assuming $\Delta(1920)$ as a $F_{7/2}$ and $N^*(2150)$ as a $G_{7/2}$ resonance. $B_6 = 3.03\ (D_5^* G_7 - F_5^* F_7)$, $B_7 = 3.26\ (F_7^* G_7)$.

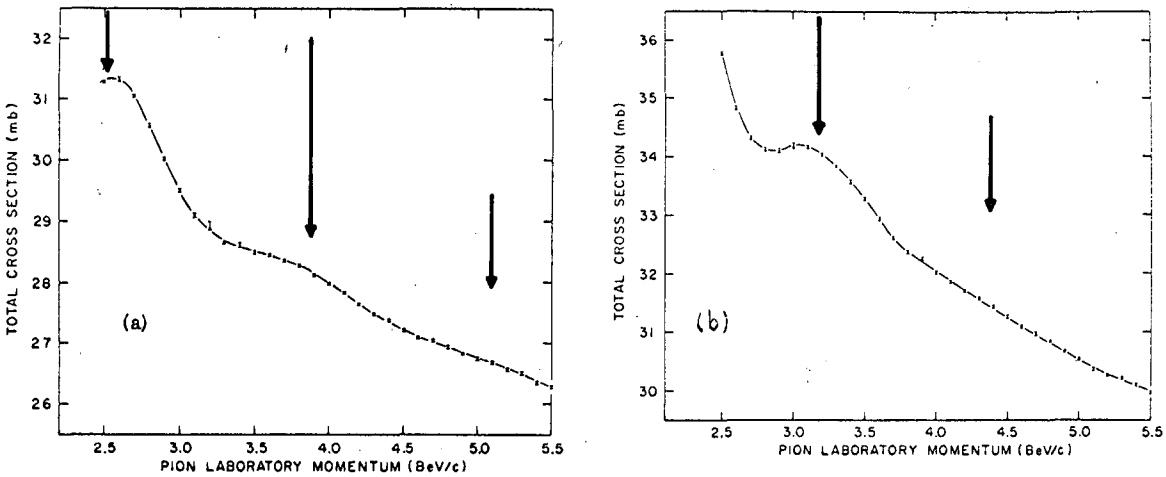

MUB-13303

Fig. 17. The pion-proton total cross sections above 2.4 BeV/c.[23]
(a) The I = 3/2 cross section; (b) The I = 1/2 cross section.

that the following resonances are present in this data.

	Mass (MeV)	Width (MeV)	$(J + 1/2)x$
N^*	2640	360	≈0.41
	3020	400	≈0.055
Δ	2420	310	≈0.68
	2840	400	≈0.25
	3220	440	≈0.063

The contribution of a resonant state to the total cross section at the resonant energy, according to (9), is

$$\sigma_T = 4\pi\lambda^2(J + 1/2)x.$$

The column on the right gives the product of spin factors and elasticities.

The charge-exchange data agree with this situation. Figure 18 shows the charge-exchange forward cross section from 1.5 to 1.8 GeV/c. This plot is taken from Höler et al.[19] The arrows 2 through 5 refer to the position of the five higher mass resonances of the above table. Resonances $N^*(3020)$ and $\Delta(3220)$ are not evident in either Fig. 17 or 18, and it is hoped a different kind of experiment will be used to ascertain their existence.

6. Elastic Scattering at 180°

The experimental differential cross section in the backward direction shows a sharp peak at 180°; this is true for π^-p and π^+p around 2 GeV/c or higher energy. Heinz and Ross[24] suggested using this behavior to determine spin and parity of resonances. When the presence of only one resonance is assumed, the spin-flip and non-spin-flip amplitudes at 180° will be [see Eqs. (4) and (5)]:

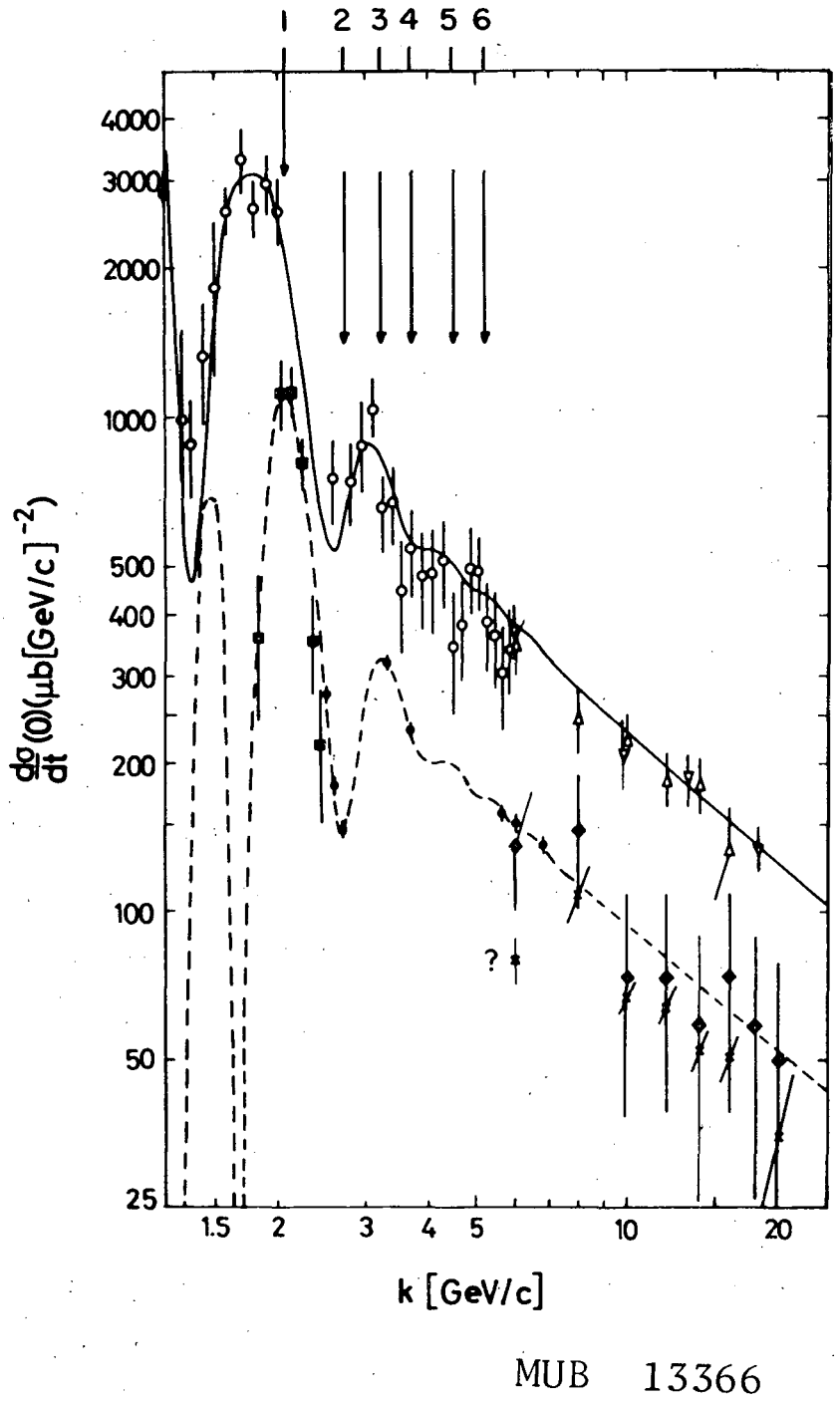

Fig. 18. Charge-exchange forward cross section (1.5 to 18 GeV/c). Plot from Höler et al.[19] Solid line is prediction of dispersion relation, dashed line is contribution of imaginary part. Data from various experiments listed in Ref. 19. ● ◆ calculated from Citron et al.[22] and Galbraith.[23]

$$f(180°) = \frac{1}{k}(J + 1/2)\, T_R P_\ell(-1) = \frac{1}{k}(J + 1/2)\, \frac{x}{\epsilon - i}(-1)^\ell$$

$$g(180°) = 0,$$

where we have used the relation $P_\ell(-1)^\ell = (-1)^\ell$, and for the resonant amplitude the Breit-Wigner amplitude of Eq. (7). This amplitude has the same sign as ℓ up to the resonance energy, and changes sign for $E > E$ (resonance).

The idea is to study the interference of this amplitude with only one other smaller amplitude slowly varying with the energy. Heinz and Ross[24] suggested that at 180°, the background can be described by only one amplitude, i.e., the one representing baryon exchange. For $\pi^- p$ and $\pi^+ p$, the situation is illustrated in the following diagrams.

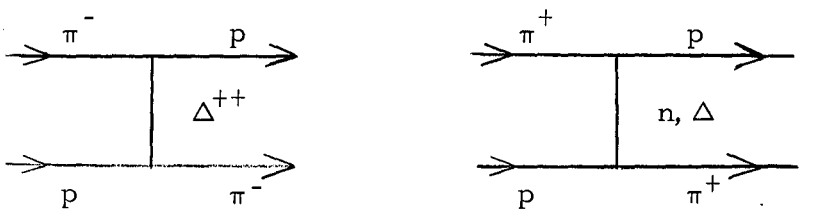

Only $\Delta(1238)$ exchange is possible for $\pi^- p$, whereas n or Δ is exchanged in $\pi^+ p$ scattering. Of course, here we assume that the contribution from the exchange of higher mass baryon systems is negligible.

Kormanyos et al.[25] at the ZGS measured the cross section for $\pi^- p$ elastic scattering at 180° over the momentum range 1.6 to 5.3 GeV/c. Their data showed the behavior predicted by Heinz and Ross.

Barger and Cline[26] have made some calculations to reproduce the behavior the data of Kormanyos et al., and have obtained very good agreement with the experimental results. They assume the exchange in the u channel of the $\Delta(1238)$ Regge trajectory, and add to this amplitude a resonant amplitude, which is the sum over all the resonant states known in this region.

Of course, they had to make some assumptions about quantum numbers, elasticities, and widths of these resonances, of which properties very little is known, but the agreement is remarkable. Figure 19 shows the results. The quantum numbers and the elasticities they used are shown in the following table.

Mass (MeV)	J^P	x	Γ (MeV)
$N^*(2190)$	$7/2^-$	0.15	200
$N^*(2640)$	$11/2^-$	0.07	360
$N^*(3020)$	$15/2^-$	0.01	400
$\Delta(1924)$	$7/2^+$	0.35	170
$\Delta(2420)$	$11/2^+$	0.15	310
$\Delta(2840)$	$15/2^+$	0.06	400
$\Delta(3220)$	$19/2^+$	0.01	440

The J^P assignment of the resonances was made on the assumption that they are recurrences of the Regge trajectories for $N^*(1512)$ and $\Delta(1238)$. In the Chew-Low plot so constructed, the resonances lie in approximately straight-line trajectories [Fig. 9(c)].

It should be pointed out that only the quantum numbers of $\Delta(1920)$ and $N^*(2190)$ are known from more direct measurements, and they seem to fit the data very well. For the other quantum numbers and elasticities [perhaps with the exception of the parity of $\Delta(2420)$], my personal feeling is that we should wait for more data before confirming them. From these first results this technique seems to be very promising, and eventually may provide accurate determinations of resonance parameters.

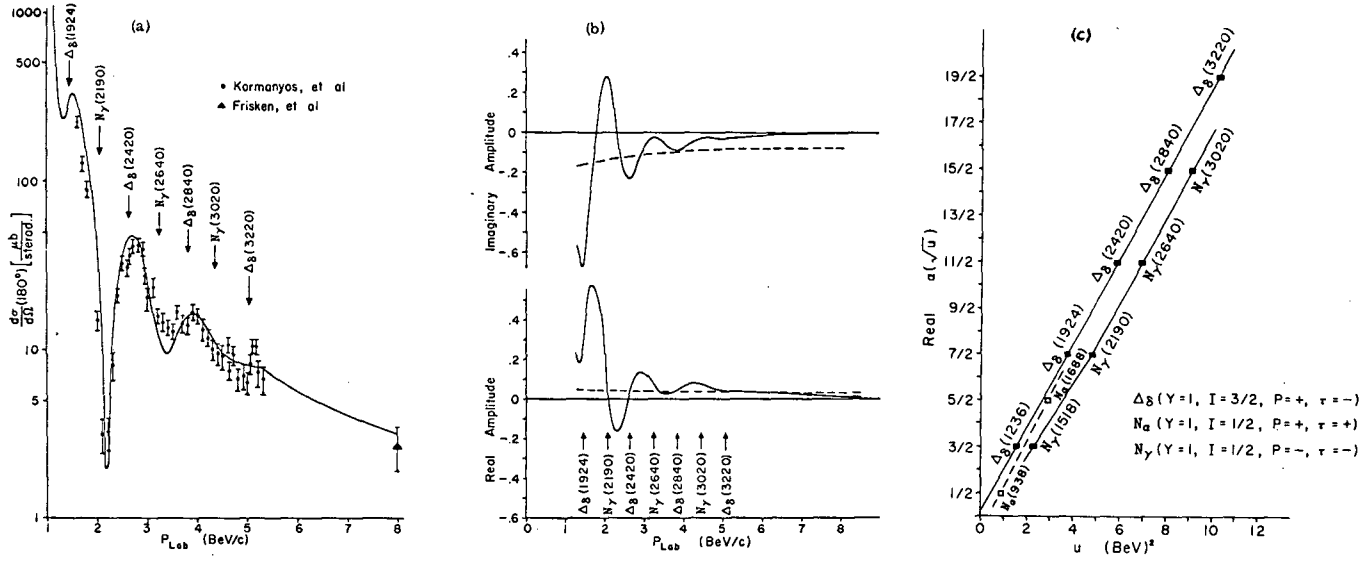

MUB-13490

Fig. 19. Calculations of Barger and Cline[26] to fit the backward scattering experiments. (a) Theoretical curve for the 180° $\pi^- p$ elastic scattering differential cross section as a function of laboratory momentum (the theoretical curve involves one free parameter, the residue of the Δ_δ, N_α, and N_γ Regge recurrences. Experimental data are taken from Ref. 25 and from Frisken et al. [Phys. Rev. Letters 15, 313 (1965). (b) Real and imaginary parts of f^{Regge} and f^{Res}. The Δ_δ, N_α, N_γ resonance amplitude (f^{Res}) is represented by the solid curves and the Δ_δ exchange amplitude (f^{Regge}) is represented by the dashed curves. Relative units are used on the ordinate. (c) Chew-Frautchi plot for the hypercharge Y = 1 Regge recurrences used for the curve in (a). Here P indicates the parity and τ the signature [$\tau = (-1)^{J-1/2}$].

7. Conclusions on S = 0 Baryon Resonances

Figure 20 shows the present situation on nucleonic resonances in a plot made by Tripp.[2] It has only those resonances with a mass of <3 GeV. There are 10 states for which we know the quantum numbers, and 3 more for which further study is necessary.

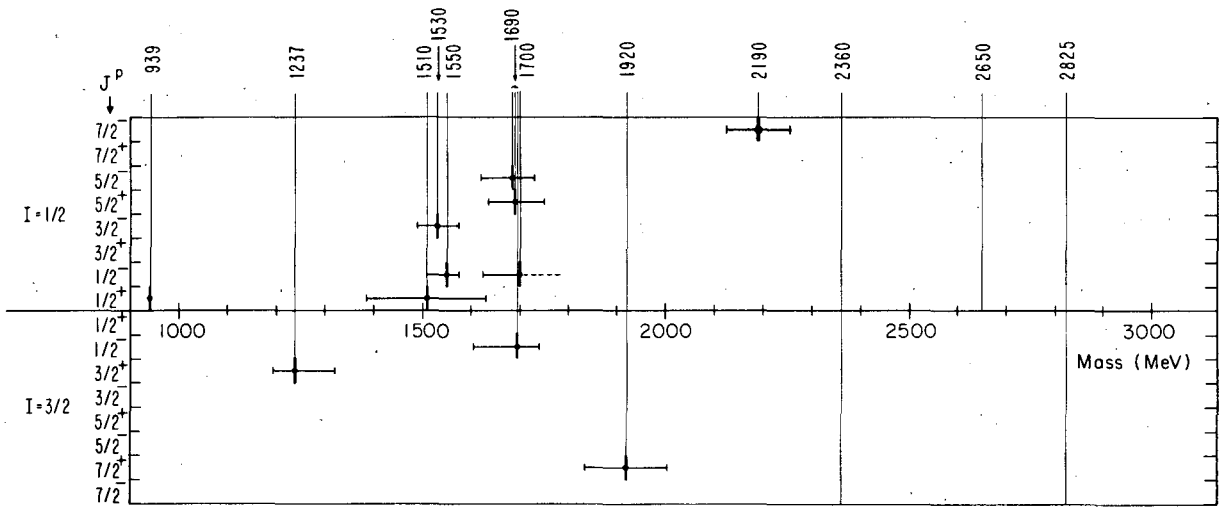

Fig. 20. Present nucleonic resonances. Taken from Ref. 2.

II. BARYON RESONANCES WITH STRANGENESS $\neq 0$

1. Introduction

This section is a review of resonances with baryon number B = +1, and negative strangeness S = -1, -2. At the end I discuss the possibility of S = +1 resonances.

Most of these resonances have been discovered in production experiments and, in general, the analysis of the experimental data is different from that of nucleon resonances. However, it turns out that it is very hard to determine quantum numbers of resonant states in production experiments because the presence of very little background (as little as 5%) can produce difficulties in the uniqueness of the determination; therefore, accurate formation experiments are necessary. Of course for S = -2 resonances this is not possible.

Generally, for S = -1 resonances, many channels are open ($\bar{K}N$, $\Lambda\pi$, $\Sigma\pi$, $\Lambda\eta$, etc.), and each channel provides information about its quantum numbers.

2. Scattering Amplitudes for Inelastic Channels

In Part I, the elastic-scattering amplitude was written as a function of η, δ--i.e.

$$T_e = \frac{\eta e^{2i\delta} - 1}{2i} .$$

For an inelastic channel, the expression is

$$T_i = \frac{\eta' e^{2i\delta'}}{2i} . \qquad (12)$$

The term $-(1/2i)$ is not present, because there is no inelastic channel in the incident wave. Figure 21 schematically shows elastic and inelastic amplitudes in the complex plane.[27] For inelastic scattering, the center of the

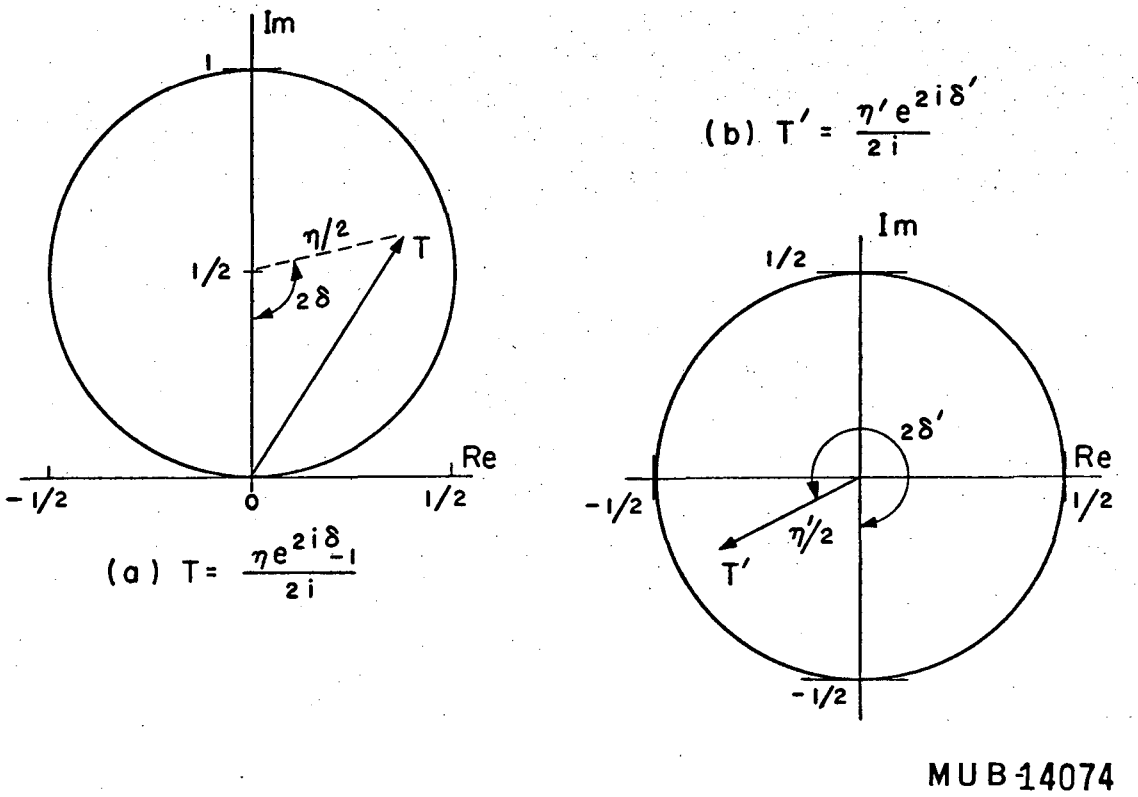

Fig. 21. Unitarity bounds each partial-wave amplitude to a circle of unit diameter. (a) For elastic scattering, the center of the circle is at i/2. (b) For scattering to an inelastic channel, the center is at the origin. An amplitude is specified by two real numbers, conveniently η and δ. From Ref. 27.

circle is at the origin, and the maximum length of the amplitude is 1/2. Unitarity requires that η be smaller than unity, and if many channels are open in a single partial wave, it requires also that

$$\eta^2 + \eta'^2 + \eta''^2 + \cdots = 1.$$

A resonance produced in a channel a and decaying in β is described by a Breit-Wigner amplitude

$$T_{a\beta} = \frac{\sqrt{x_a x_\beta}}{\epsilon - i} \qquad \epsilon = (E - E_r)\frac{2}{\Gamma}, \tag{13}$$

where $x_a = \Gamma_a/\Gamma_{total}$, $x_\beta = \Gamma_\beta/\Gamma_{total}$. For $a = \beta$--i.e., for the elastic channel--Eq. (13) is the same as Eq. (7) of Section I. Figure 22 shows the behavior of the resonant amplitudes for elastic and inelastic channels. Notice that for an inelastic channel the diameter of the circle is $\sqrt{x_a x_\beta}$.

It is important in formation experiments that the elasticity x_a should not be too small. The cross section in any channel is proportional to $x_a x_\beta$, whereas the elastic is proportional to x_a^2. If many channels are open and no single x_i is large, this makes the identification and study of the resonance difficult.

3. Total Cross-Section Data

The measurements of total cross sections give an idea of the resonant states present in a reaction. Figures 23 and 24 show the total cross-section data available for K^- interacting with hydrogen and deuterium. Cool et al.[28] have recently measured both cross sections with great accuracy in the momentum range 1.0 to 2.45 GeV/c. The large peak in the 1-GeV/c region, known for a long time as the "Kerth bump," contains, as we know now, at least two resonances--$Y_1^*(1765)$ and $Y_0^*(1820)$. A second smaller bump appears at $\approx$1.6 GeV/c and this has been resolved into resonances also, as will be seen in Sec. 8.

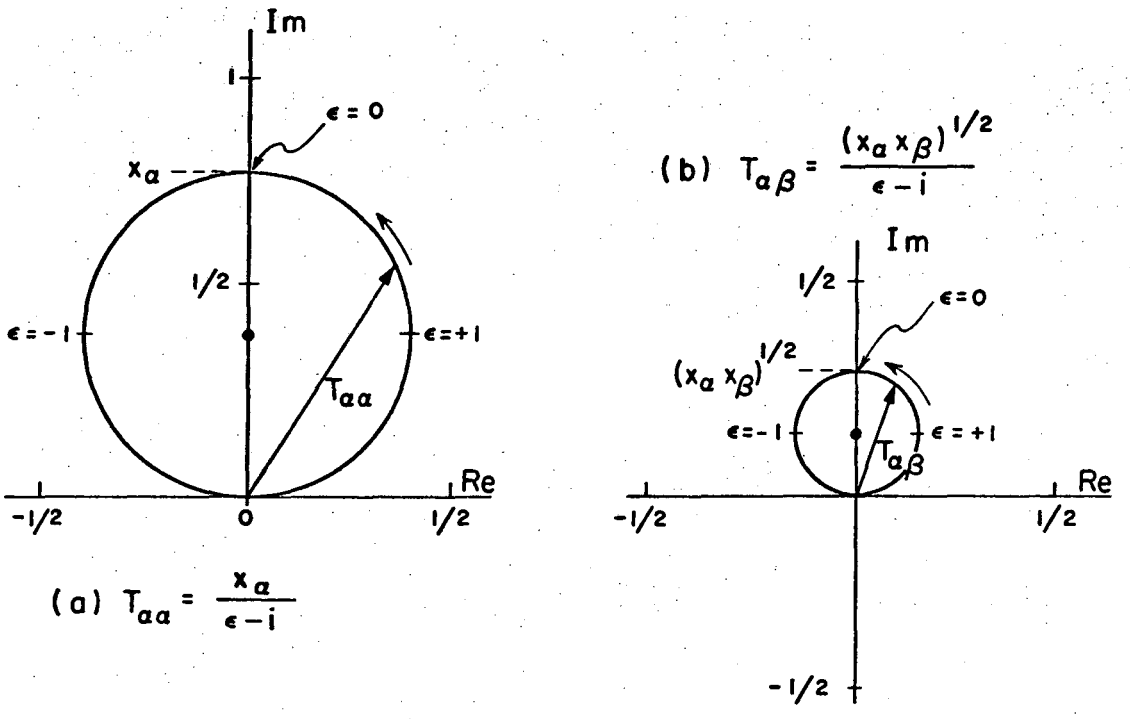

Fig. 22. The energy dependence of resonant amplitudes is given by the Breit-Wigner form: with increasing energy, the amplitudes trace circles in the counterclockwise direction. (a) For elastic scattering, the diameter of the circle is x_a. (b) For scattering to an inelastic channel, the diameter is $(x_a x_\beta)^{1/2}$. From Ref. 27.

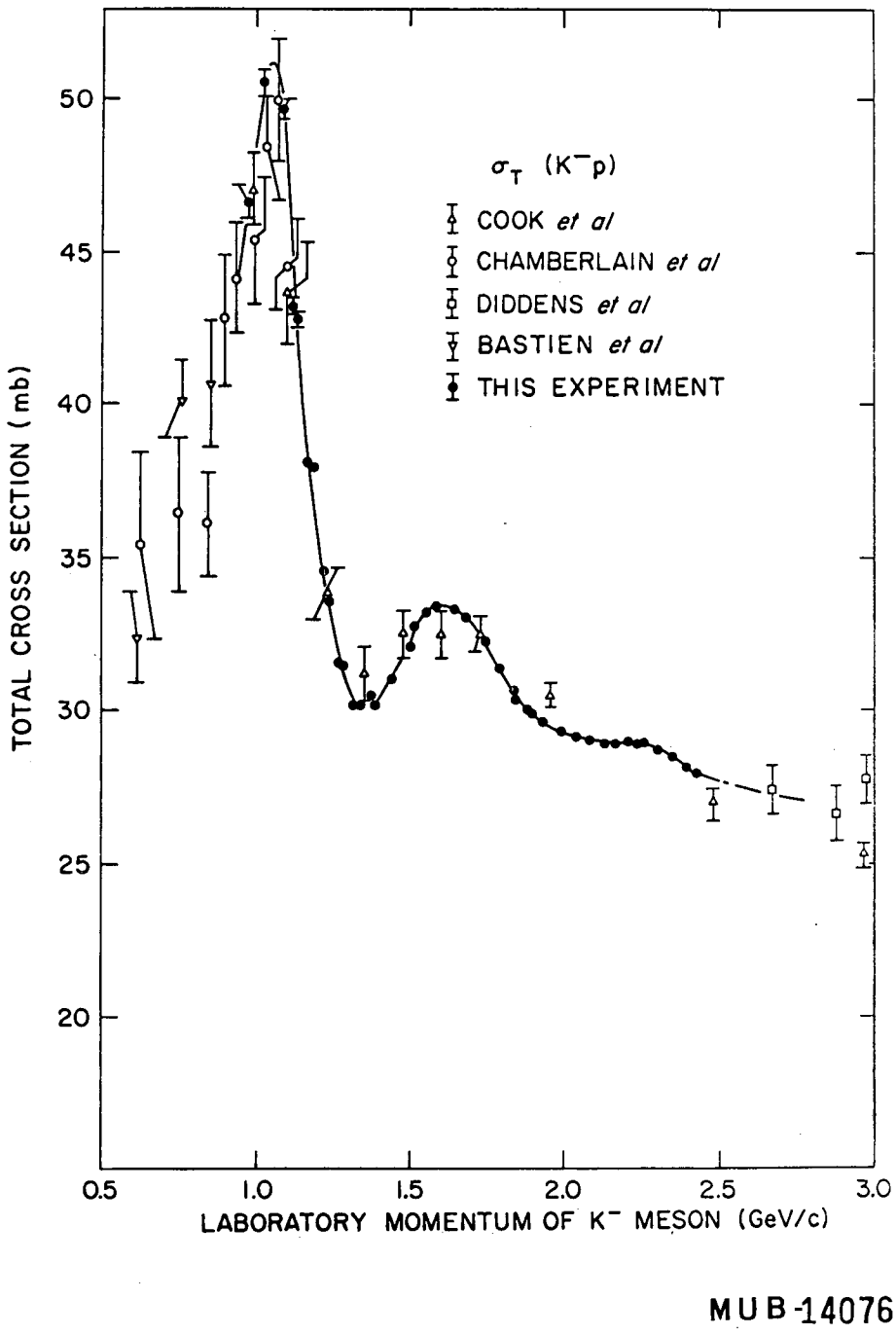

Fig. 23. K^-p total cross section. New data are from Cool et al.[28]

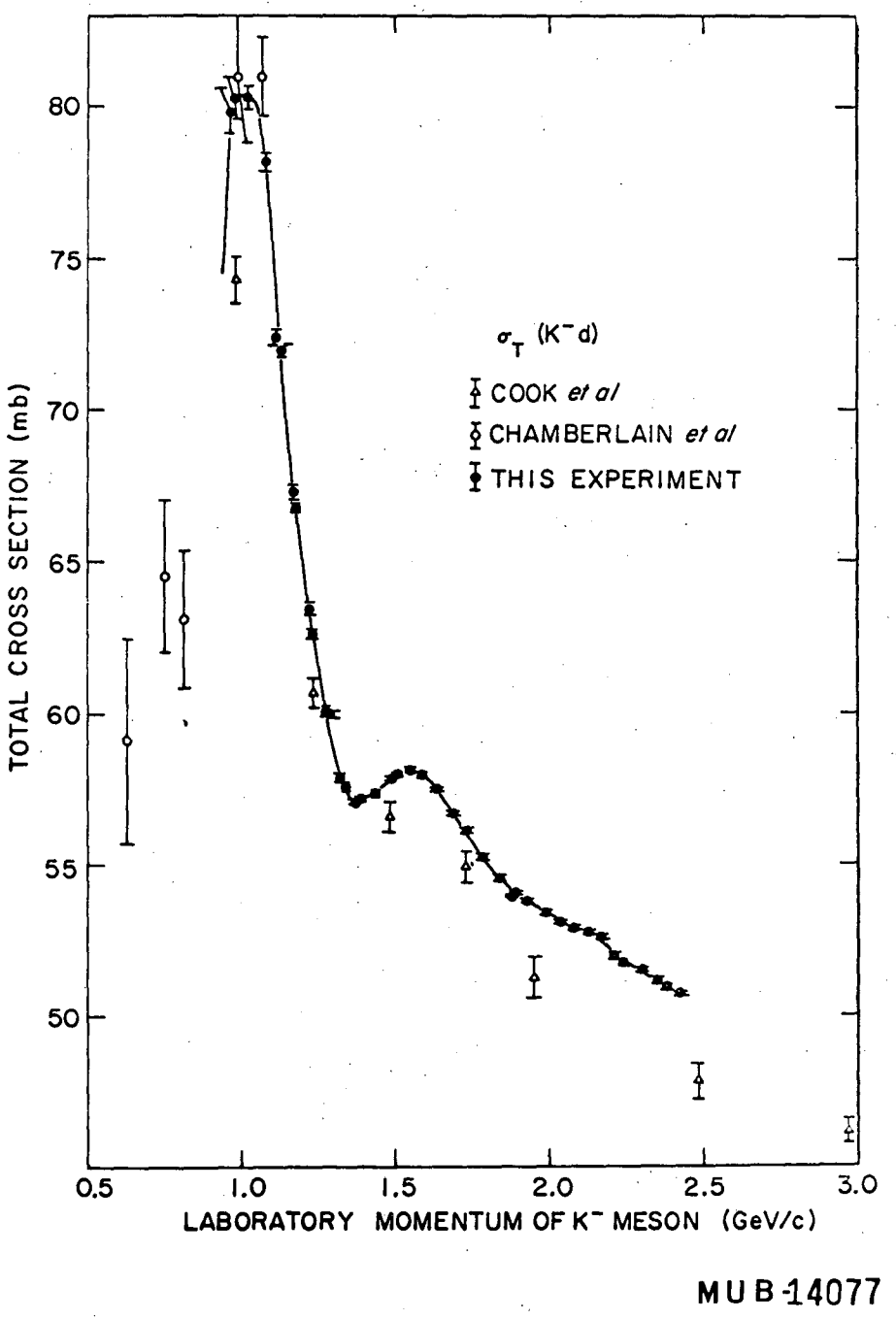

Fig. 24. K^-d total cross section. New data are from Cool et al.[28]

As stated before, the elasticity of a resonance is very important for its identification. The maximum contribution of a resonant state to σ_{total} from Eq. (9) is proportional to $(J + 1/2)x_e$. For x_e small and J small, it is not likely that a resonance produces any peak in the total cross section. In fact, $Y^*(1660)$, whose elasticity is now estimated to be $x \approx 0.15$, is only slightly visible in this data.

4. Well-Known Resonances

4.1 $Y_1^*(1385) \cdot P_{13}$

This state has been known for a long time. The spin-parity assignment $J^P = 3/2^+$ is open to very little doubt (see UCRL-8030 for references[1]). Its main decay mode is $\Lambda\pi$ (90%). Its branching ratio to $\Sigma\pi$ is $(10 \pm 2)\%$.

4.2 $Y_0^*(1405) \cdot S_{01}$

This resonance was discovered in a production experiment, and its only decay mode is $\Sigma\pi$. The most likely J^P assignment is $1/2^-$, which is an s-wave bound state of the K^-p system. The investigation of low-energy K^-p scattering has indicated that the low-energy scattering length in the I = 0 state is consistent with a bound state of mass and width of $Y_0^*(1405)$. Both the Columbia[29] and Maryland experiments[30] indicate that their most likely solution requires this interpretation of $Y_0^*(1405)$.

4.3 $Y_0^*(1520) \cdot D_{03}$

This resonance has been studied in all channels by Watson, Ferro-Luzzi, and Tripp.[31] Figure 25 shows the cross sections of various channels over the 200 to 500 MeV/c incident K-momentum region. The elasticity of this resonance is small (x = 0.29), as can be seen from Fig. 25(a). The assignment $J^P = 3/2^-$ is certain.

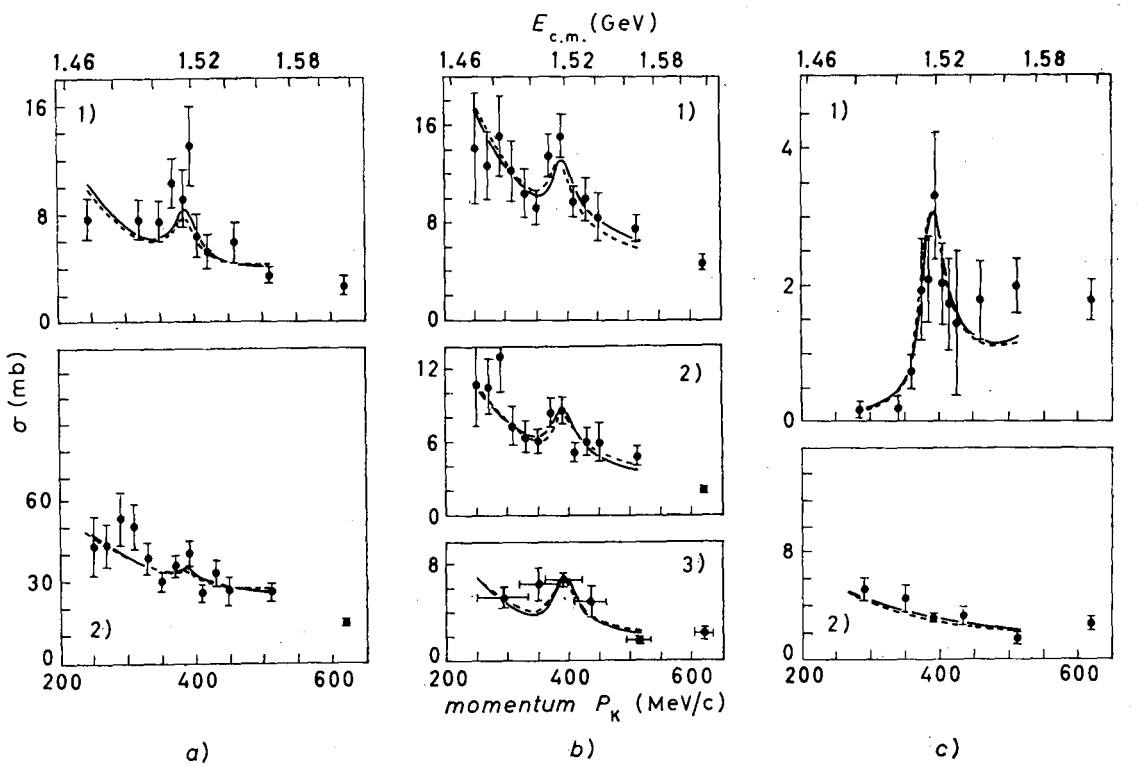

MUB-14078

Fig. 25. Data on the $Y_0^*(1520)$ from Ref. 31. Cross sections as a function of momentum for (a) K^-p charge exchange 1) and elastic scatterings 2); (b) $\Sigma^+\pi^-$, $\Sigma^-\pi^+$, and $\Sigma^0\pi^0$ productions in the order; (c) $\Lambda\pi^+\pi^-$ 1) and $\Lambda\pi^0$ production 2). The solid line corresponds to the best fit of all cross sections, angular distributions, and polarizations to negative KNΣ parity; the dashed lines correspond to the best fit for positive KNΣ parity. Cross sections are not sensitive to the parity.

5. Resonances in the 1660- to 1700-MeV Region

A resonance in this region has been discovered in various production experiments and in a formation experiment at Berkeley in 1962 (Ref. 22). Since then, enhancements in this energy region have been detected and studied in both formation and production experiments. The fine structure of these enhancements and the quantum-number assignments are not clear yet, but it is certain that at least three states are present. The branching ratios reported in the Table of Baryons (Table 1) for the $Y_1^*(1660)$ are the most reasonable estimate, from the contradictory data published until now, if only one I = 1 resonance is assumed for this region.

5.1 Total Cross-Section Data [$Y_0^*(1700)$]

Very precise measurements of K^-p and K^-d total cross sections between 600 and 1400 MeV/c (1610 to 1980 MeV in the c.m.) have been made recently at Nimrod by a British collaboration, Davies et al.[32] Figure 26(a) shows the cross section for K^-d from both Refs. 32 and 28. There are no experimental errors on the line representing the "raw data," since it is a smooth curve drawn through the data. Figure 26 was made by Lynch[33] who did all the corrections to the data necessary to obtain the pure I = 0, 1 spin states, shown in Fig. 26(b). The presence of a new resonant state Y_0^* at M = 1700 MeV (Davies et al.[32] quote 1698 ± 5 MeV) is clear. The $Y_1^*(1660)$ is also present in this data at a mass M = 1655 ± 5 MeV.

5.2 $\Lambda\eta$ Production near Threshold [$Y_0^*(1675)$, $S_{01}(?)$]

Berley et al.[34] at Brookhaven have measured the cross section for the reaction $K^-p \to \Lambda\eta$ from threshold to 200 MeV/c relative momentum in the $\Lambda\eta$ c.m. Their results are shown in Fig. 27. They have analyzed the data in terms of a constant s-wave scattering length or p-wave scattering

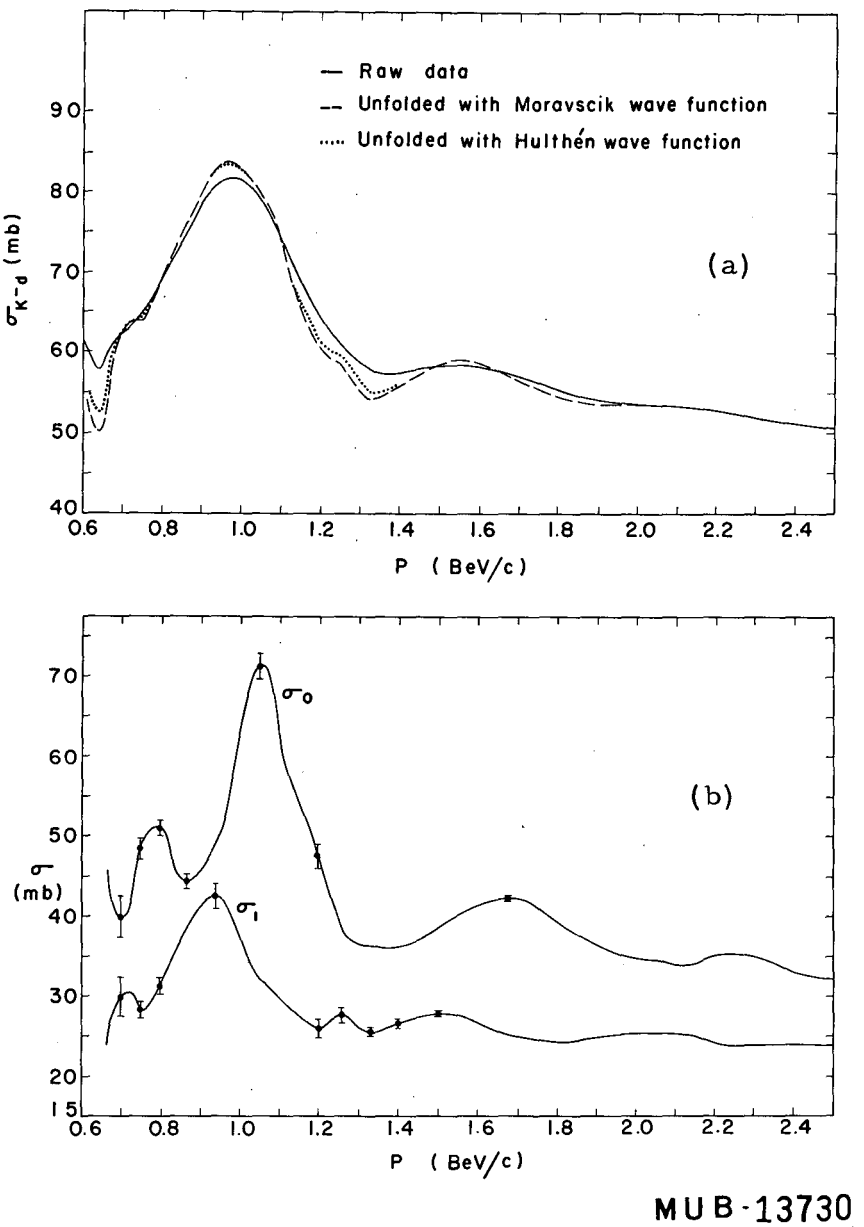

Fig. 26. (a) The K^-d total cross section of Davies et al.[32] and Cool et al.[28]. No experimental errors are given; the smooth line has been drawn by G. Lynch.[33] (b) The cross sections for the pure isospin states I = 0, 1.[33]

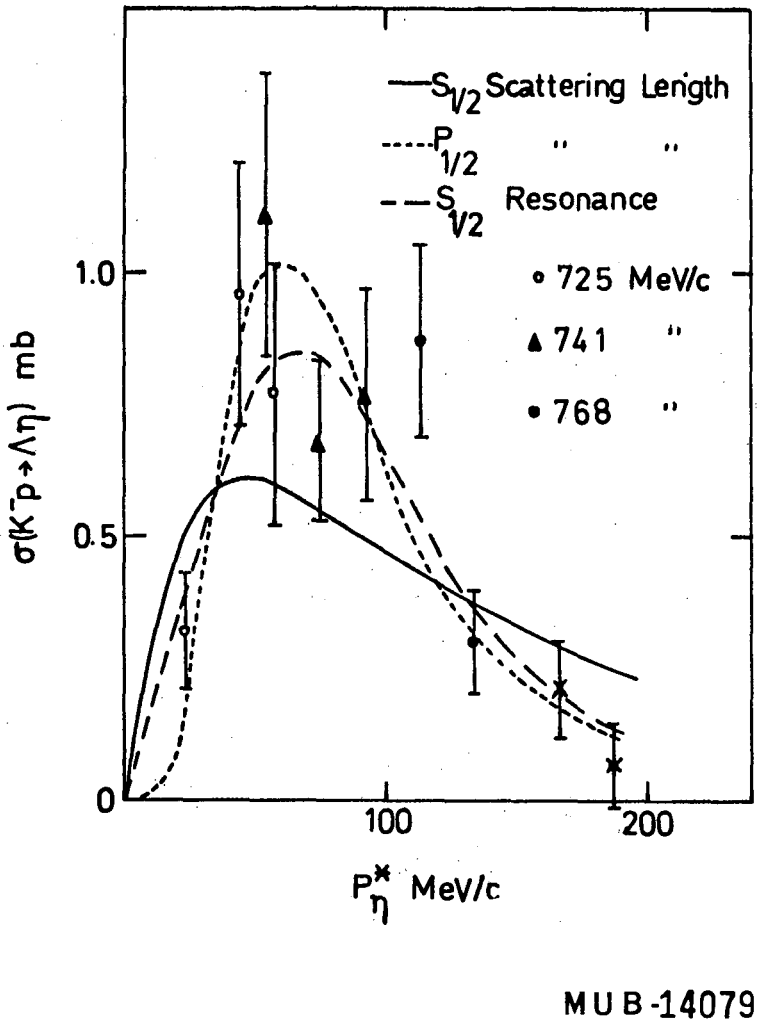

Fig. 27. Cross section of $Kp \rightarrow \Lambda\eta$ as function of the η c.m.'s momentum (Berley et al.[34]).

length.[35] The latter possibility provides a good fit to the cross-section data of Fig. 27; however, the angular distributions observed are isotropic, in contradiction with the p-wave hypothesis, and the scattering length necessary to fit the data is very large $(9.5 + i\ 30.4)\ (F)^3$.

The best fit to the data is obtained with an s-wave resonance of mass M = 1675 MeV, Γ = 15 MeV, and $x_{\bar{K}N} x_{\Lambda\eta} = 0.053$.

The fits of Fig. 27, however, were obtained with a zero-effective-range approximation. More generally the complex phase shift $\delta_c = \delta + i\gamma$ [$\eta' = e^{-2\gamma}$, $\delta' = \delta$ in the notation of Eq. (12)] can be expanded as follows:

$$k^{2\ell+1} \cot \delta_c = \frac{1}{a} + \frac{1}{2} r k^2 + \cdots,$$

where a and r are constants. The zero-effective-range approximation consists in neglecting the second term of the expansion. At this energy perhaps it is more appropriate to introduce the second term in the expansion; this term might improve the fit. Whether this effect has to be considered a resonance or not might just be a matter of semantics. Since it behaves like a resonance (follows the Breit-Wigner resonant-amplitude shape), it should be considered a resonance. Before drawing this conclusion, however, one must improve the statistics and study other channels.[36]

Note that this situation appears also at threshold of $n\eta$ production and $\Sigma\eta$ production; both cases are not completely understood yet. For

$$K^- p \rightarrow Y_0^*(1520) + \pi,$$

the same rapid rise at threshold is present and, as we will see in Sec. 7, it is produced by a resonance $[Y_1^*(1765) \rightarrow Y_0^*(1520) + \pi]$, whose final state is in a p wave.

5.3 Other Formation Experiments

For the I = 1 state, the only channel thoroughly studied is the $\Lambda\pi$ channel, which seems to have a very small enhancement in this region. Consequently the treatment of the background is very critical for the J^P assignment of the resonant amplitude. Fig. 28 shows the results of the two experiments performed in this channel. The data of Berley et al.[37] suggest a $3/2^-$ assignment, after certain assumptions on the background are made. Taher-Zadeh et al.[38] have studied $K^- n \to \Lambda\pi^-$ and suggested the opposite parity. Recently the UCLA group has reanalyzed the data of this experiment, introducing in the D_{15} state an additional background amplitude due to the presence of $Y_1^*(1765)$, which they have not included in their first paper. With this different treatment of the background they seem to agree with the $3/2^-$ assignment.[39]

The $\Sigma^\pm \pi^\mp$ channel is being investigated in various laboratories. Two groups have presented data on this channel at the Berkeley Conference.[40,41] The situation here is more complicated by the presence of the two isospin states. No definite conclusions have been reached by the study of this channel, the analysis being still in progress, but the data of Armenteros et al.[41] definitely require the presence of a $Y_0^*(1700)$ as a D_{03} state.

5.4 Production Experiments

Resonance $Y_1^*(1660)$ seems to be produced copiously in the $\Sigma\pi$ channel (Fig. 29). This data is from the Alvarez Group[42]; the reaction is $K^- p \to \Sigma^+ \pi^- \pi^0$. However, the background present is too large to make a spin analysis possible. The data in Fig. 29 was taken at 1.5 GeV/c incident K^- momentum. At higher momentum the $Y_1^*(1660)$ is produced preferably through K^* exchange, and it is possible to reduce the background by imposing a production-angle cutoff. For the $\Sigma\pi$ channel the very small production at 2.2 GeV/c indicates

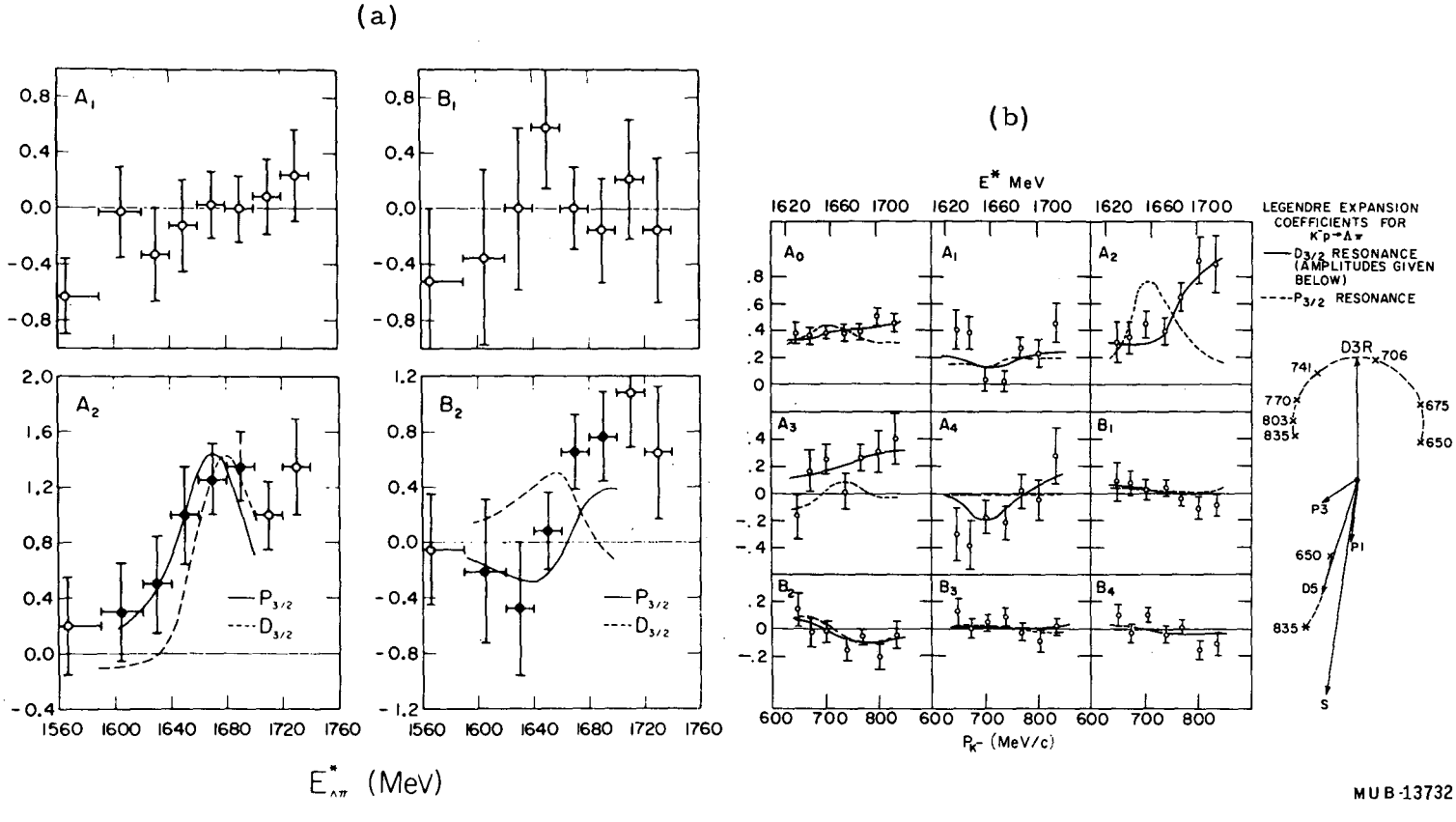

Fig. 28. Study of the $\Lambda\pi$ channel in the 1660 MeV region. (a) Data of Berley et al. (BNL).[37] Coefficients of the $I(\theta)$ (A_i) and $I(\theta)$ $P(\theta)$ (B_i) expansions as function of momentum. Diagram at right shows the assumption made on the background. The $D_{3/2}$ assignment is favored for $Y_1^*(1660)$. (b) Data of the UCLA group (Taher-Zadeh et al.[38]). New analysis of this data prefers $D_{3/2}$ assignment (see text).

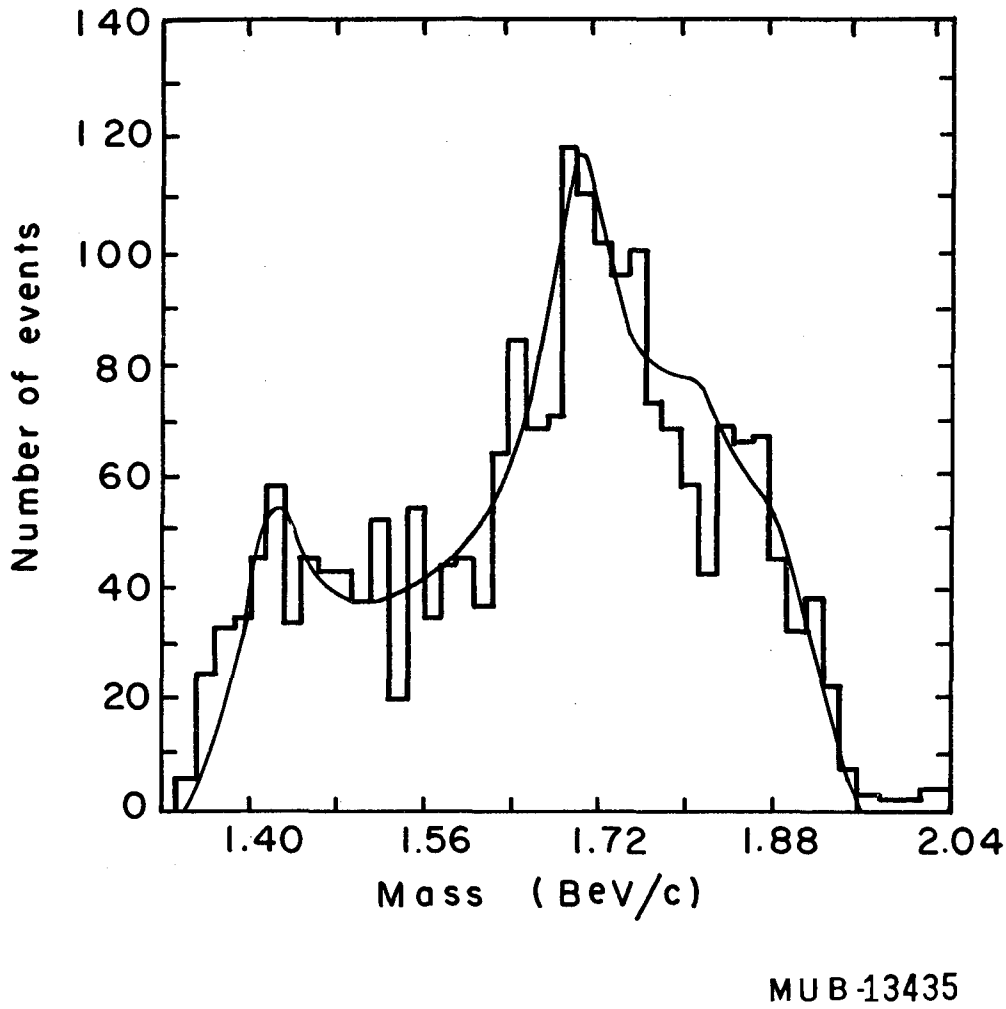

Fig. 29. Invariant mass of $\Sigma^{+}\pi^{0}$ system. Total number of events is 2056. Data at 1.5 BeV/c incident K^{-} momentum.[42]

presence of interference effects.[43] Various groups looked at $Y_1^*(1660) \to \Sigma^{\pm}\pi^{\mp}\pi^+$, which turned out to be $Y_1^*(1660) \to Y_0^*(1405) + \pi$, with very little background in the three-body final state.

In this reaction it is possible for one to study the parity of $Y_1^*(1660)$, using some properties of the Dalitz plot for its three-body decay. For the $\Sigma^-\pi^+\pi^+$ decay of $Y_1^*(1660)$, the $\pi^+\pi^+$ system has to obey Bose statistics, so the system of two identical pions has over-all parity +. This fact has some implications at point A of the Dalitz plot in Fig. 30. In fact, at this point the Σ^- is at rest in the c.m. so its angular momentum state, with respect to the $\pi^+\pi^+$ system, can only be in an s wave, which implies a positive parity for $Y_1^*(1660)$. If the parity of $Y_1^*(1660)$ is negative, there will be a depletion at point A of the Dalitz plot (due to centrifugal barrier).

In practice, the situation is more complicated by the presence of the decay through $Y_0^*(1405) + \pi$ and the presence of background. Furthermore, the statistics required for one to look at only a very small region of the Dalitz plot are very large. Although four different groups have studied this reaction, no conclusive answer has yet been reached. A European group[44] has reached the conclusion of a positive parity, based on very small statistics [see Fig. 31(a)]. Eberhard et al.[45] (Berkeley-Illinois collaboration) favor $3/2^-$ assignment [see Fig. 31(b)]. Slater et al.[46] of the UCLA group favor the $3/2^-$ assignment. And finally, the BNL-Syracuse group excludes the $3/2^+$ assignment.[43] The situation does not seem to be very clear in this decay mode of the I = 1 $Y^*(1660)$. My personal feeling is that the most-probable assignment is $3/2^-$, but we should wait until all the problems related to the background are understood before making up our minds definitely.

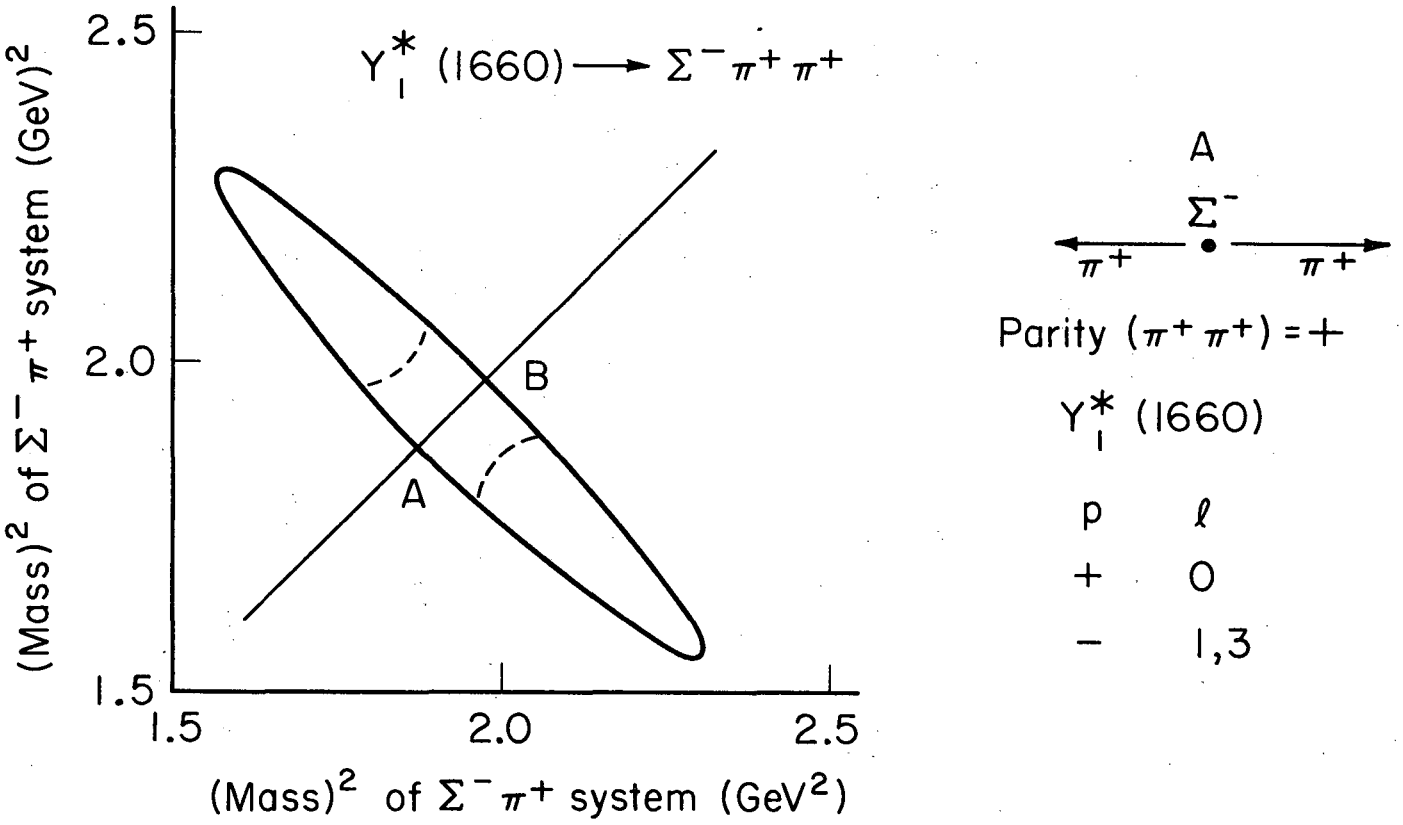

MUB-14080

Fig. 30. Dalitz plot for $\Sigma^- \pi^+ \pi^+$ of a total mass of 1660 MeV. Properties of the Dalitz plot in a region close to A can be used to study the parity of $Y_1^*(1660)$. A depletion is expected in A for negative parity.

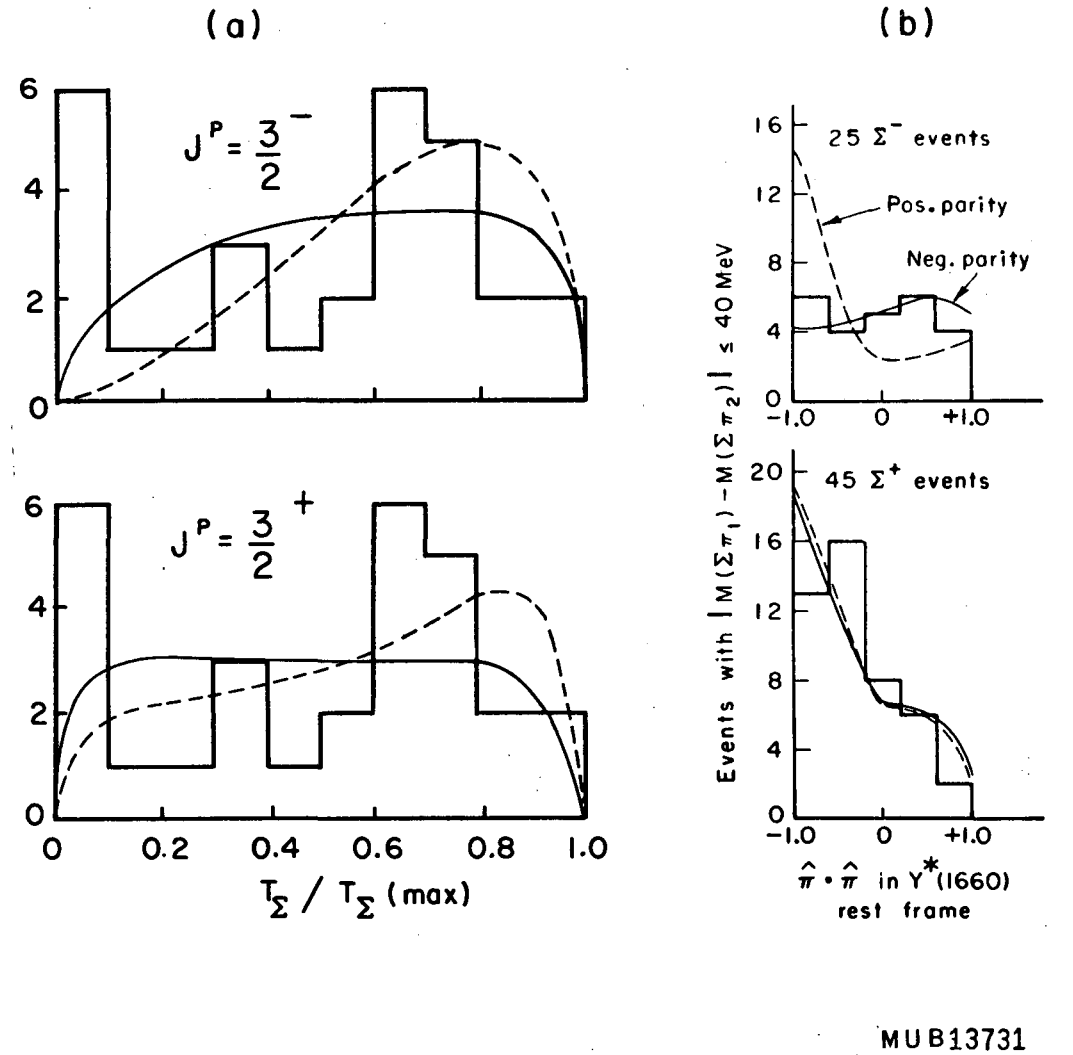

Fig. 31. (a) Distribution of the Σ^- energy in the decay of $Y_1^*(1660) \rightarrow \Sigma^-\pi^+\pi^+$ (Leveque et al.[44]). The curves above are calculated for the negative-parity hypothesis, below for positive parity. The dashed and solid lines are calculated predictions for three-body decay and decay through $Y_0^*(1405)$, respectively. (b) Distribution of the angle between the two pions in the decay of $Y_1^*(1660)$ into $\Sigma^- + \pi^+ + \pi^+$. Data are from Eberhard et al.[45]; it prefers $J^P = 3/2^-$.

5.5 Conclusions

The situation in this energy region is not clear yet, but it is possible that the original enhancement[22] will eventually be split in n resonances, with $n \geq 3$.

The I = 0 state seems to contain two resonances, and the I = 1 state at least one resonance.

The following table summarizes the situation as it looked at the Berkeley Conference, and as summarized by rapporteur Ferro-Luzzi.

I spin	Mass (MeV)	Width (MeV)	Main decay	J^P
1	1660	40	$Y_1^*(1405) + \pi$	$3/2^-$
0	1670	20	$\Lambda\eta$	$1/2^-$
0	1700	30	$\bar{K}n, \Sigma\pi$	$3/2^-$
0, 1	1660	60	$\Sigma\pi$	?

6. Remarks on J^P Determination of Higher Mass Resonances

At higher energies, it becomes more difficult to determine the quantum numbers of hyperon resonances. The number of background amplitudes increases and the spins of the resonances also increase. Both facts require more statistics in angular distributions and polarizations, since it is necessary to determine a larger number of coefficients in the expansion in Legendre polynomials of I and IP:

$$I = \lambda^2 \sum_\ell A_\ell P_\ell$$

$$IP = \lambda^2 \sum_\ell B_\ell P_\ell .$$

Fortunately, a resonance with large mass has new open channels; specifically it can decay in a lower mass resonance whose J^P is known. The following decays of this type have been observed:

$$Y_1^*(1660) \rightarrow Y_0^*(1405) + \pi$$
$$Y_1^*(1765) \rightarrow Y_0^*(1520) + \pi$$
$$Y_0^*(1820) \rightarrow Y_1^*(1385) + \pi.$$

These processes can be employed to establish the J^P of higher resonances.

As has been pointed out in Section 2.4 of Part I, for the decay of a state of given $J^P \rightarrow 1/2^+0^-$--i.e., into a hyperon and a pseudoscalar meson--the Minami ambiguity is present, and both angular distribution and polarization measurements are needed to determine the parity of the state. The angular distributions, for a pure state, will be

$$3/2^{\pm} \rightarrow 1/2^+0^- \qquad I(\theta) = c(1 + 3\cos^2\theta)$$
$$5/2^{\pm} \rightarrow 1/2^+0^- \qquad I(\theta) = c(1 - 2\cos^2\theta + 5\cos^4\theta).$$

These distributions are shown in Fig. 32(a).

Let us now consider the case of $Y_1^*(1765) \rightarrow Y_0^*(1520) + \pi$--i.e., $5/2^- \rightarrow 3/2^-0^-$. This decay can take place via P or F waves. If the F wave is neglected, for example on the basis of its higher centrifugal barrier, the expected angular distribution for this decay can be calculated. Taking the axis of quantization along the direction of the incident K^-, we see that the final wave function will be

$$\psi^{1/2}_{5/2} = \sqrt{1/10}\, Y_1^{-1}\, \chi^{3/2}_{3/2} + \sqrt{3/5}\, Y_1^0\, \chi^{1/2}_{3/2} + \sqrt{3/10}\, Y_1^1\, \chi^{-1/2}_{3/2}, \qquad (14)$$

where Y_1 is the $\ell = 1$ angular momentum state, and χ is the spin state of the decay product. The angular distribution following from Eq. (14) will be

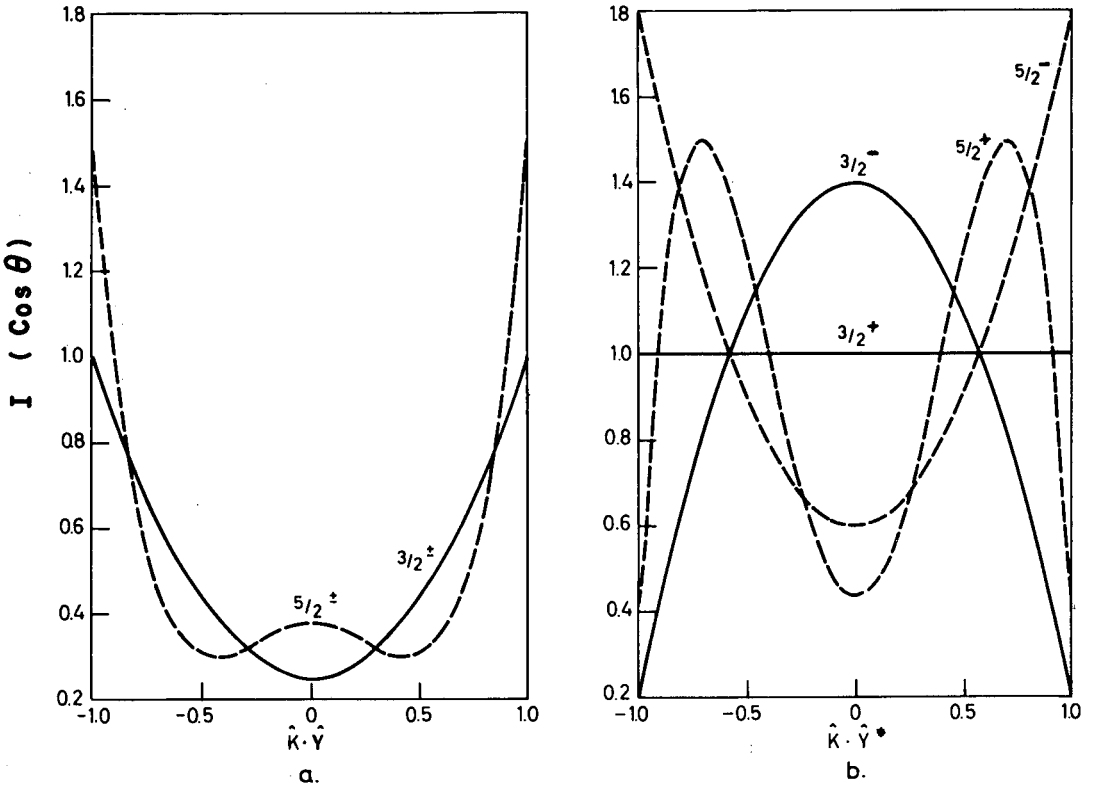

MUB-13434

Fig. 32. (a) The angular distribution of a Y^* of indicated J^P decaying into spin-1/2 and spin-0 particles. (b) The angular distributions for a Y^* of same J^P decaying into another Y^* of spin $3/2^-$ and a 0^- meson.

$$|Y_{5/2}^{1/2}|^2 = c(1 + 2\cos^2\theta).$$

Figure 32(b) shows this angular distribution and all the ones expected for other J^P states decaying via a $3/2^-0^-$ mode. They will be as follows:

$$5/2^+ \propto 1 + 10\cos^2\theta - 10\cos^4\theta$$

$$5/2^- \propto 1 + 2\cos^2\theta$$

$$3/2^+ \propto 1$$

$$3/2^- \propto 7 - 6\cos^2\theta.$$

It is easy to see from Fig. 32 that in this case the angular distribution alone can give information about the spin and parity state of the resonance.

In conclusion, this is a very powerful method for determining the J^P of higher mass resonances. In the case of $Y_1^*(1660) \rightarrow Y^*(1405) + \pi$ it cannot be used, because $Y_0^*(1405)$ has $J^P = 1/2^-$ and the Minami ambiguity is not removed; but the momentum available is small, and it is hoped that the background amplitudes to be taken into account are less numerous than in other channels.

7. $Y_1^*(1765)$, D_{15} and $Y_0^*(1820)$, F_{05}

These two very close resonances have been disentangled in a production experiment,[47] whereas this has been done in formation experiments for nucleonic resonances. In fact, the $Y_1^*(1765)$ was detected in a reaction $K^-n \rightarrow K^-p\pi^-$ at 1.5 GeV/c K^-; at this energy the production of $Y_0^*(1820)$ was very small because the phase space available for it was negligible compared to that of $Y_1^*(1765)$. The data on Kp scattering and $\bar{K}^0n$ had suggested a $J = 5/2$ assignment for both resonances and opposite parity state; the parity remained to be determined. This suggestion was made on the basis of a large A_5 coefficient present in the Legendre-polynomials expansion of Kp

and $\bar{K}^0 n$ differential cross sections. This could be explained only by the $D_{5/2}\ F_{5/2}$ interference term that appears in the A_5 coefficient. The parity assignments have now been established through the study of some particular channels.

The CERN-Heidelberg-Saclay collaboration has studied the decay of $Y_1^*(1765)$ into $Y_0^*(1520) + \pi$, which is a pure I = 1 state.[48] The cross section as a function of momentum is shown in Fig. 33. This is an example of a $5/2^-$ resonance decaying into a $3/2^-$ resonance and a pion. Here, the situation is particularly favorable because the $Y_0^*(1520)$ is very narrow and so stands out clearly over the background. Figure 34 shows the production angular distribution, which clearly favors the $5/2^-$ assignment for this resonance; the decay angular distribution of the $Y_0^*(1520)$ supplies additional information that the J^P assignment is $5/2^-$.

This result automatically assigns a positive parity to the $Y_0^*(1820)$. There is evidence[49] that this resonance decays into $Y_1^*(1385) + \pi$, but the situation is more complicated than in the previous case, because the final state is not in a pure isospin state, and various channels have to be used to eliminate the background.

Another decay mode of $Y_1^*(1765)$ studied is the decay in $\Lambda\pi$. This data has just been published and the evidence for $J^P = 5/2^-$ is quite good. This result is from Kernan et al.[50] of the Powell-Birge group in Berkeley. Figure 35 summarizes the situation. To fit this data, some constant background P_3, D_3, S_1, P_1 is necessary. It is possible to fit the angular distribution coefficients A_2 and A_3 for opposite parity assignment of $Y_1^*(1765)$, just by taking the opposite sign for the background amplitudes. However, in doing so, it is not possible to fit the polarization data at the same time, as can be seen in the B_2 and B_3 coefficients in Fig. 35. This is a very good example of the Minami ambiguity.

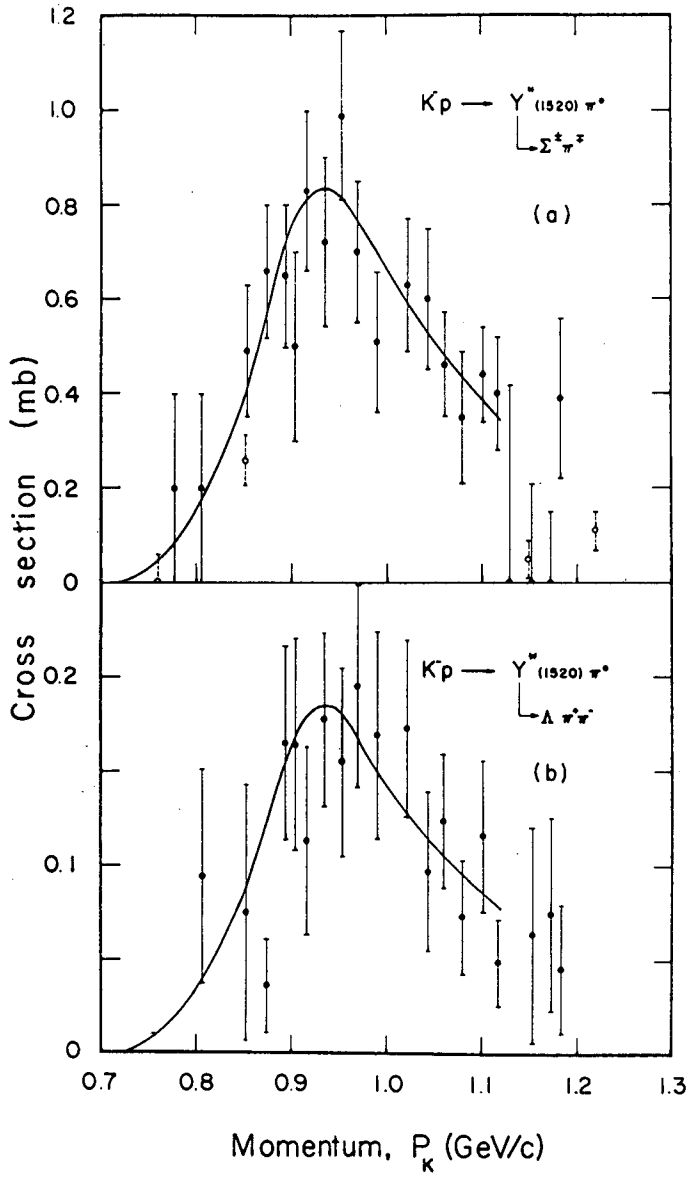

Fig. 33. Cross section as function of K^- laboratory momentum for the reaction $K^-p \rightarrow Y_0^*(1520) + \pi^0$: (a) $Y_0^*(1520) \rightarrow \Sigma^{\pm}\pi^{\mp}$, and (b) $Y_0^*(1520) \rightarrow \Lambda\pi^+\pi^-$. (From Ref. 48.)

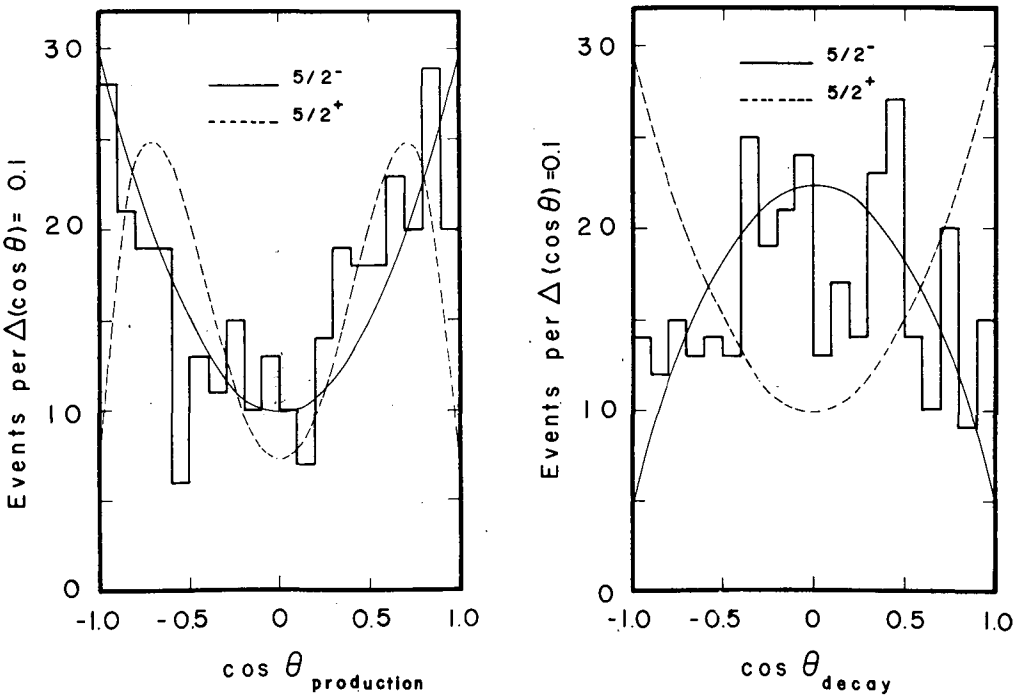

Fig. 34. Production and decay angular distributions of $K^- p \rightarrow Y_0^*(1520) + \pi^0$ for $Y_0^*(1520) \rightarrow \Sigma^{\pm} \pi^{\mp}$ with K^- momentum between 910 and 1070 MeV/c. (From Ref. 48.) $J^P = 3/2^-$ assignment for $Y_1^*(1765)$ is preferred.

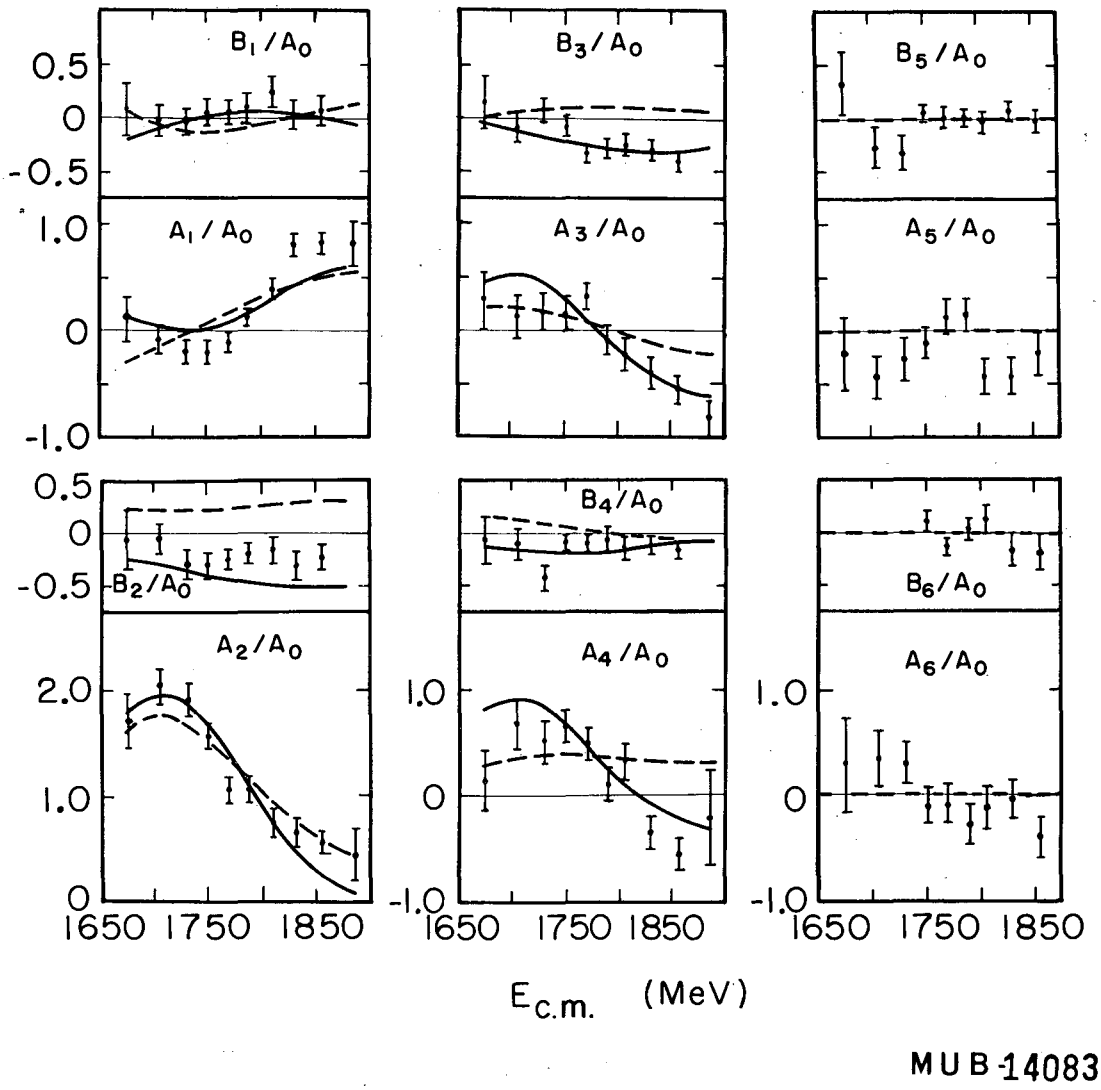

Fig. 35. Coefficients of Legendre polynomials expansion of I and IP of the $\Lambda\pi^-$ data (Ref. 50).

$$A_3 = 4.8\,(P_3^*D_5 + D_3^*F_5) + \cdots$$
$$B_3 = 0.4\,(P_3^*D_5 - D_3^*F_5) + \cdots$$
$$A_2 = 1.71\,(P_3^*F_5 + D_3^*D_5) + 6.0\,(S_1^*D_5 + P_1^*F_5) + \cdots$$
$$B_2 = 1.43\,(P_3^*F_5 - D_3^*D_5) - 2.0\,(S_1^*D_5 - P_1^*F_5) + \cdots$$

The CERN-Heidelberg-Saclay collaboration has also studied this channel with similar results. Figure 36 shows their $\Lambda\pi$ cross sections together with all the other available data at lower and higher momentum.

Because further structure might be present in this energy region, other channels are being studied by the CERN-Heidelberg-Saclay collaboration,[41] and by the Powell-Birge group in Berkeley.

8. $Y_1^*(2030)$, F_{17} and $Y_0^*(2120)$, G_{07}

The existence of some structure in Kp total cross section for incident K^- momenta between 1.4 and 1.8 GeV/c has been detected by Cook et al.[51] in 1961. Since then other groups have detected enhancements in this energy region.[22]

Stevenson and Wohl[22] have studied the reactions $K^-p \to \Lambda\pi^0$ and $K^-p \to \bar{K}^0n$ in this region. Figure 37 shows the K^-p charge-exchange cross section as a function of incident K^- momentum up to 10 GeV/c. This graph is taken from Ref. 41. The data in the 1-GeV region was obtained by these authors, and the data in the 1.5-GeV/c region is from Wohl.[22] Notice that some structure is evident also around 1.2 GeV/c; in this region a new resonance has been detected at M = 1915 MeV as we will see later.

The evidence for the isospin and spin assignment of $Y_1^*(2030)$ is shown in Fig. 38. This is the $\Lambda\pi^0$ channel of the data of Wohl et al.[52] The a_0 coefficient is the cross section divided by $2\pi\lambda^2$. (For the $\bar{K}^0n$ of Fig. 39 this factor is $\pi\lambda^2$, since an isospin factor has been introduced.) All the coefficients are consistent with a J = 7/2 resonance being present at a mass of 2030 MeV. The $\Lambda\pi^0$ is a pure I = 1 state giving this isospin assignment for this resonance. The coefficients of the Legendre polynomials expansion

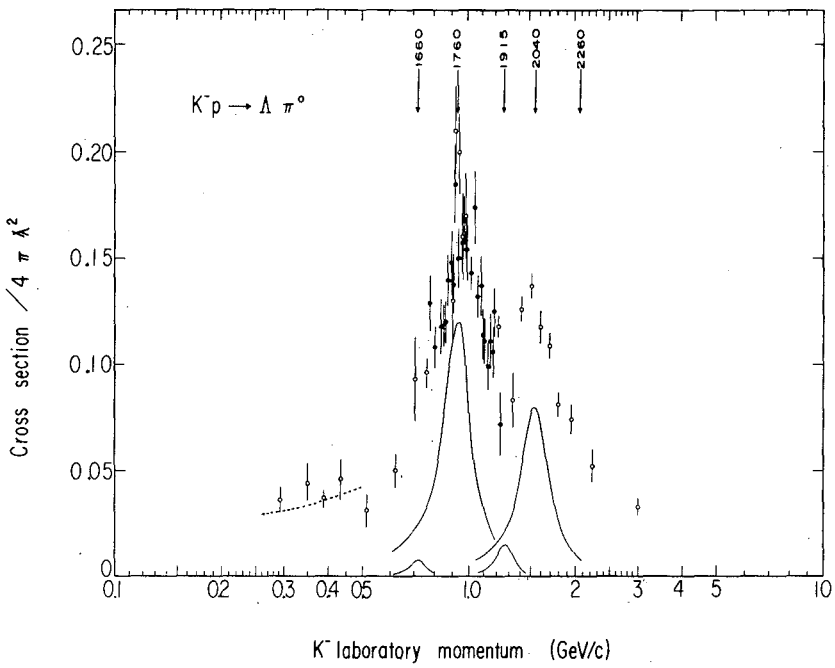

Fig. 36. The $\Lambda\pi$ total cross section as function of K^- momentum.[41]

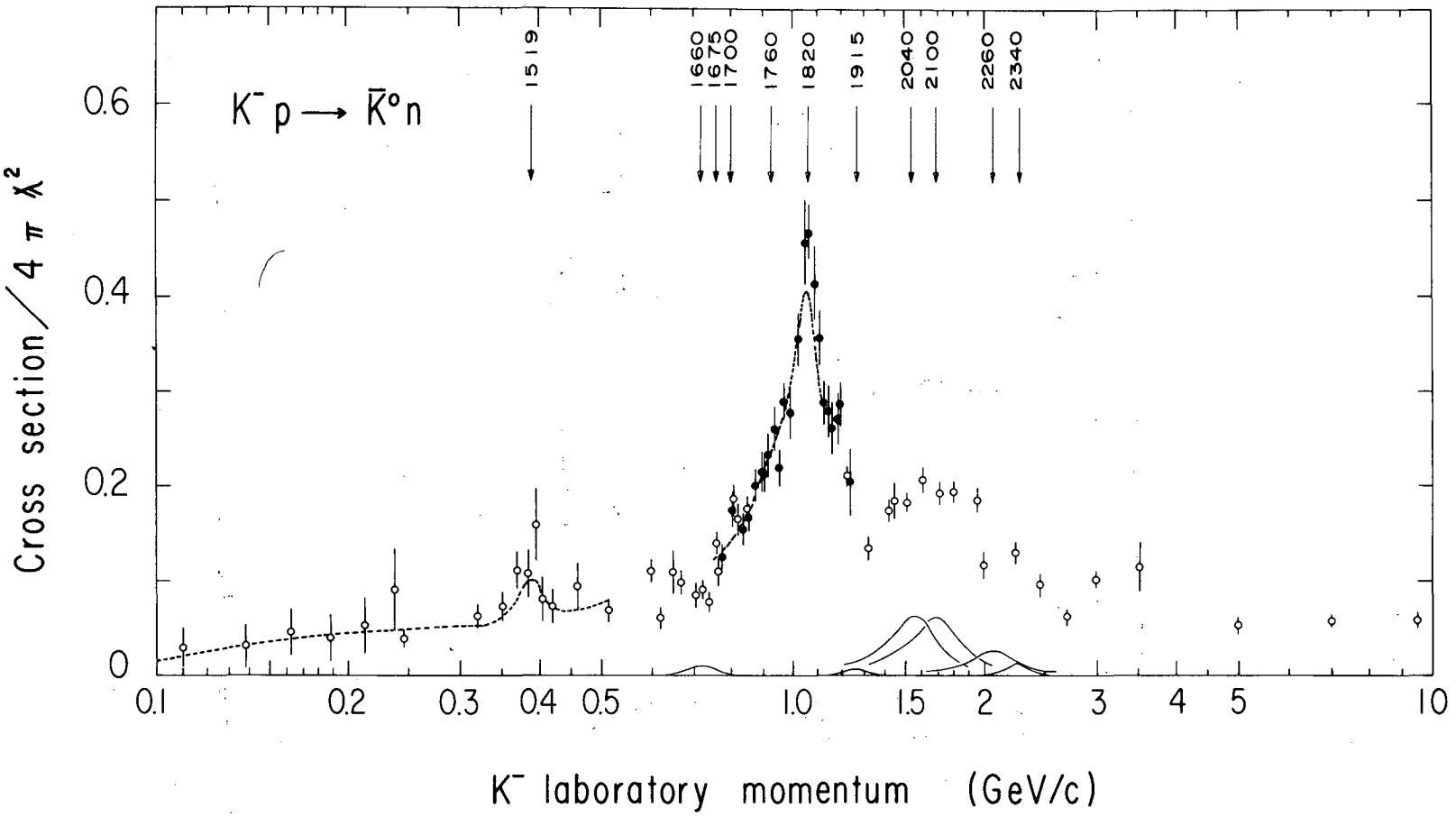

MUB-13313

Fig. 37. Cross section for $K^- p$ charge-exchange scattering as a function of incident K^- momentum.[41]

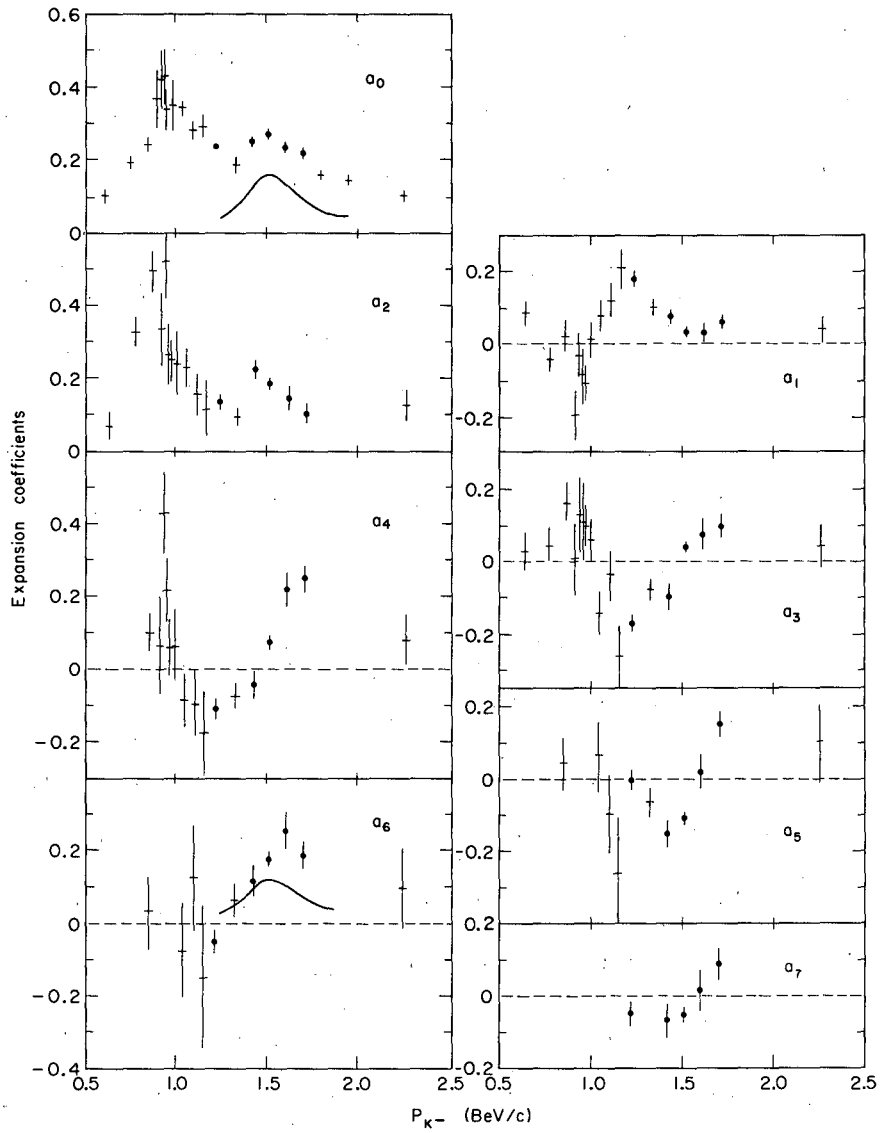

Fig. 38. The $\Lambda\pi^0$ data of Wohl et al.[52] in the region of $Y_1^*(2030)$ and $Y_0^*(2120)$.

$$a_6 = 18.18\,(D_5^* G_7 + F_5^* F_7) + 3.03\,(|F_7|^2 + |G_7|^2)$$

of IP(θ) are not shown, but the sign of the polarization gives the conclusive assignment $F_{7/2}$ to this resonance.

The $\bar{K}^0 n$ data are shown in Fig. 39. The presence of an a_7 coefficient, due to interference $F_7 G_7$, indicates that a second large G_7 amplitude is present. The curves in a_0, a_6, and a_7 are calculated with the assumption of two resonances with the following parameters:

Isospin	J^P	Mass (MeV)	Width (MeV)	Elasticity
1	$7/2^+$	2030	170	0.25
0	$7/2^-$	2120	145	0.25

These two resonances are also present in $\Sigma^{\pm}\pi^{\mp}$ channels with a non-negligible rate.[53]

9. Other Y^* Resonances

All the resonances with established quantum numbers are reported in Fig. 40 in a plot by Tripp.[2] There are 11 resonances whose quantum numbers have been measured. Their number is going to increase.

There are indications from Böck et al.[22] and Blanpied et al.[22] of the existence of other resonances at higher masses. In the first of these experiments, performed with a bubble chamber, final-state interactions of the type $p\bar{p} \rightarrow Y^* + n\pi$ were studied. There is an indication of new resonant states, mainly $Y_1^*(1940)$ and $Y_0^*(2300)$ (Fig. 41). Blanpied et al. studied the reaction $\gamma p \rightarrow K^+ Y^0$ in a photoproduction experiment. They have an indication of a new resonant state at 2245 MeV.

Cool et al.[28] measured the total cross sections of the $K^- p$ and $K^- d$ interaction; their results have already been shown in Figs. 23 and 24, respectively. Figure 42 shows the I = 0 and I = 1 parts of K^- nucleon interaction, extracted from the previous data, after appropriate corrections have

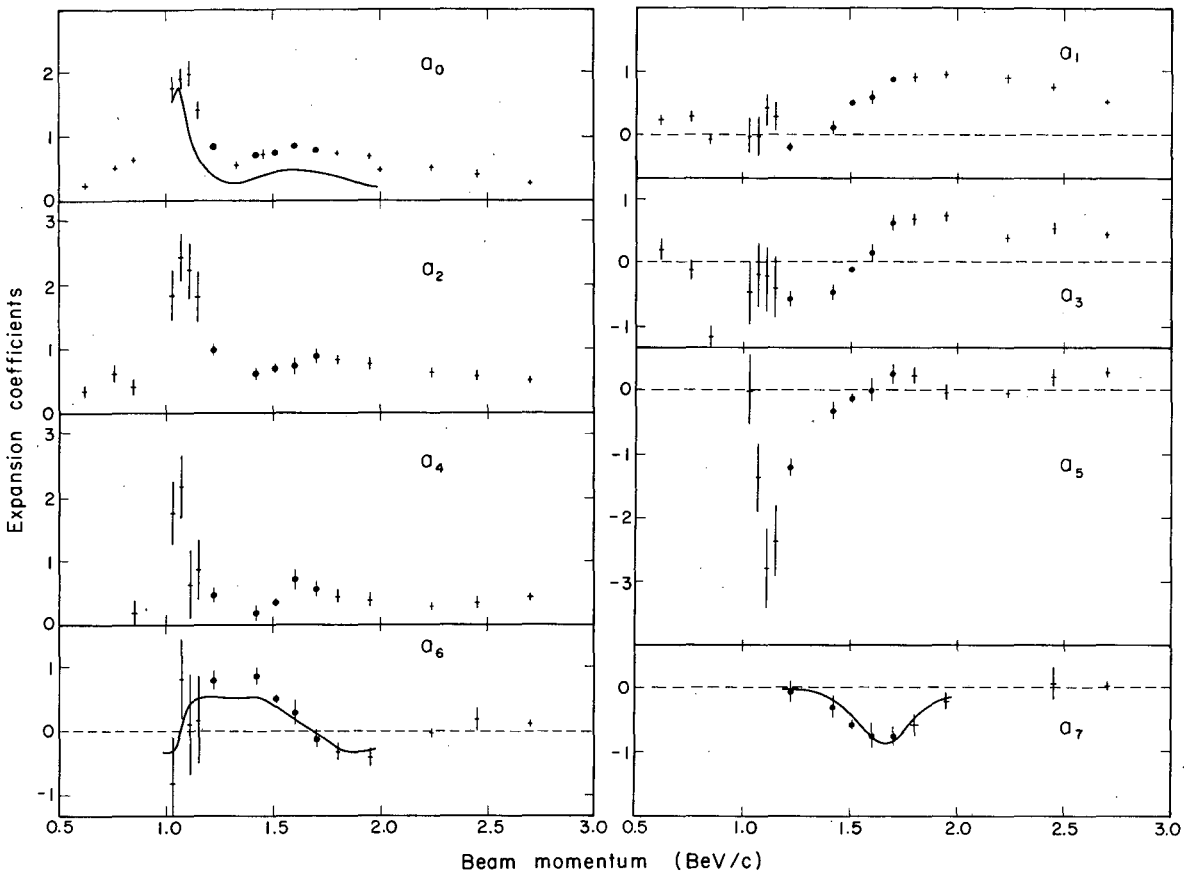

MUB-14085

Fig. 39. $\bar{K}^0N$ data of Wohl et al.[52] in the $Y_1^*(2030)$ and $Y_0^*(2120)$ region.

$$a_6 = 18.18\,(D_5^* G_7 + F_5^* F_7) + 3.03\,(|F_7|^2 + |G_7|^2)$$

$$a_7 = 22.84\,(F_7^* G_7)$$

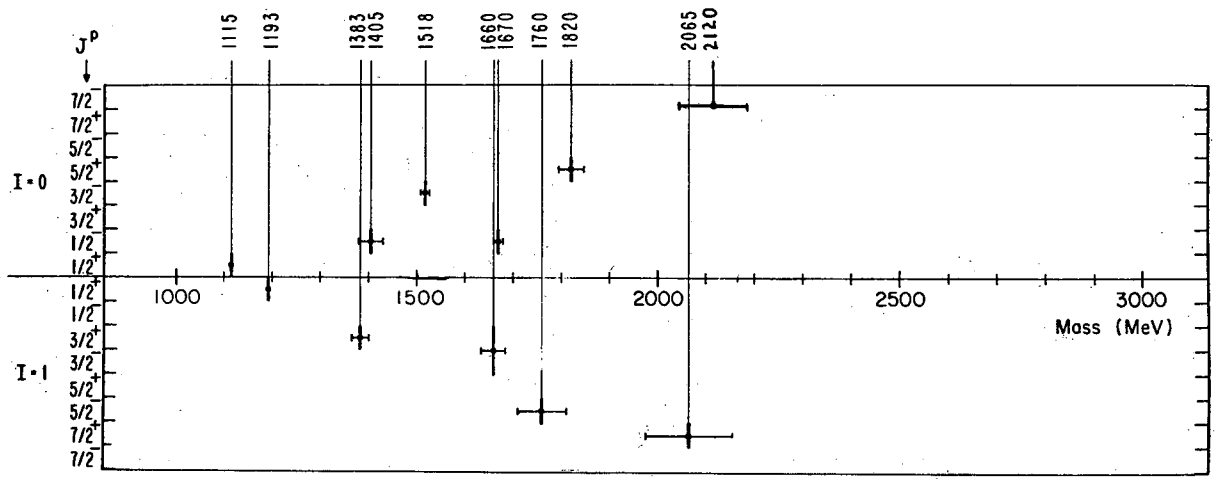

MUB-8799A

Fig. 40. Present strange-baryon spectroscopy. Taken from Ref. 2.

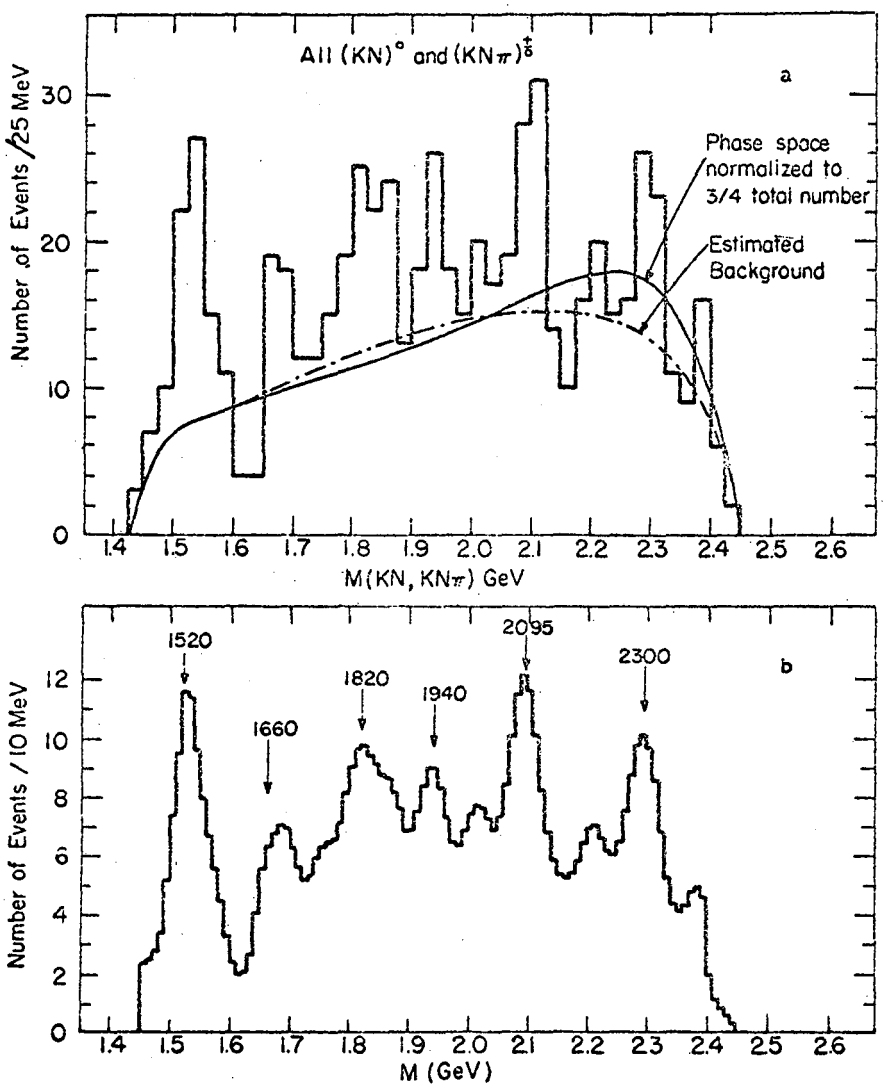

Fig. 41. Invariant-mass distribution of KN and KNπ final states. Data are from Böck et al.[22]

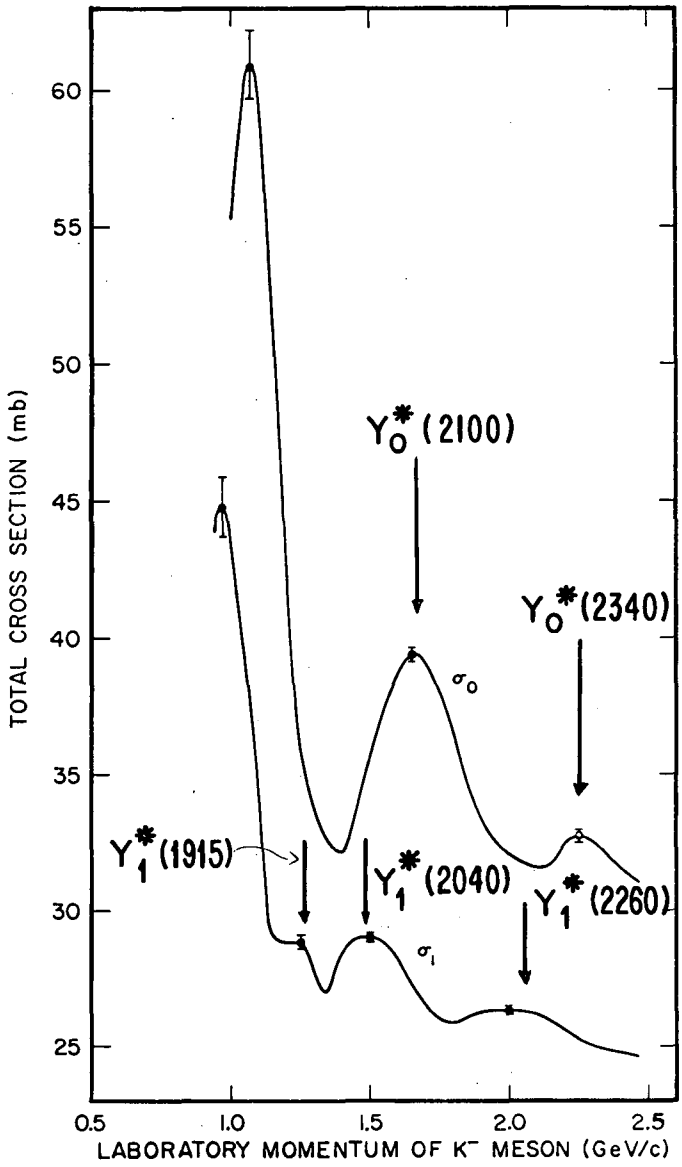

MUB-13301

Fig. 42. The KN total cross sections in the two isospin states. Plot from Cool et al.[28]

been made. Here, besides the known resonances, some new states appear in both isospin states. The following table summarizes the situation of the new resonances, for which the quantum numbers are not yet known.

Resonance	M (MeV)	Γ (MeV)
Y_0^*	2340 ± 20	105
Y_1^*	1915 ± 20	65
Y_1^*	2260 ± 20	180

For the $Y_1^*(1915)$, further experiments will be necessary in order to ascertain its position and quantum numbers. The data of the CERN-Heidelberg-Saclay collaboration[41] in the $\bar{K}N$ and $\Sigma^{\pm}\pi^{\mp}$ channels seem to require the existence of this resonance and an assignment of $J^P = 5/2^+$ is not in contradiction with the data.

10. Baryonic Resonances with S = -2

Since a year ago, no new data has become available concerning the Ξ^* production. At that time the situation was the one reported in Table 1. Only three states of this resonance are known--at 1530, 1816, and 1933 MeV. There is some indication of a new state at 1705 MeV, but the evidence is quite weak, and there is too little data for any conclusion to be reached on its existence. Figures 43 and 44 show the data of Smith et al.[54] Figure 43 shows the $\Xi\pi K$ final state; only $\Xi^*(1530)$ is present and some $\Xi^*(1933)$. The statistical significance of the enhancement at 1705 MeV is of the order of 2 standard deviations. Figure 44 shows the $\Lambda\bar{K}^0K^0$ final state; here again the evidence for its existence is not conclusive.

As far as the spin-parity determination of these Ξ^*'s is concerned, the $J^P = 3/2^+$ assignment for $\Xi^*(1530)$ is presently favored, the probability

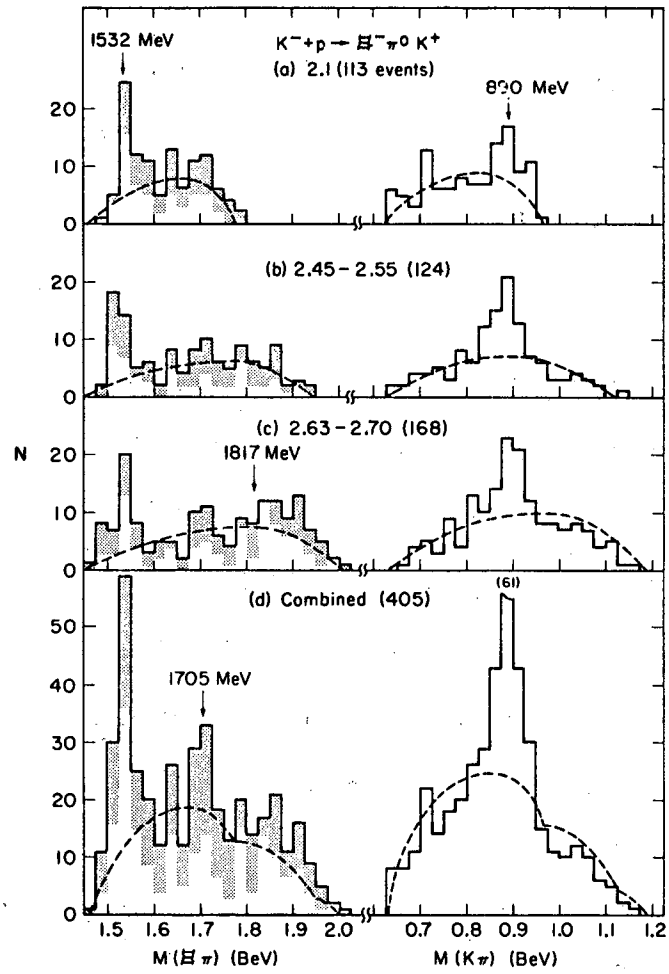

Fig. 43. Invariant mass of $\Xi\pi$ system from $\Xi^-\pi^0K^+$ final state. Data are from Smith and Lindsey.[54]

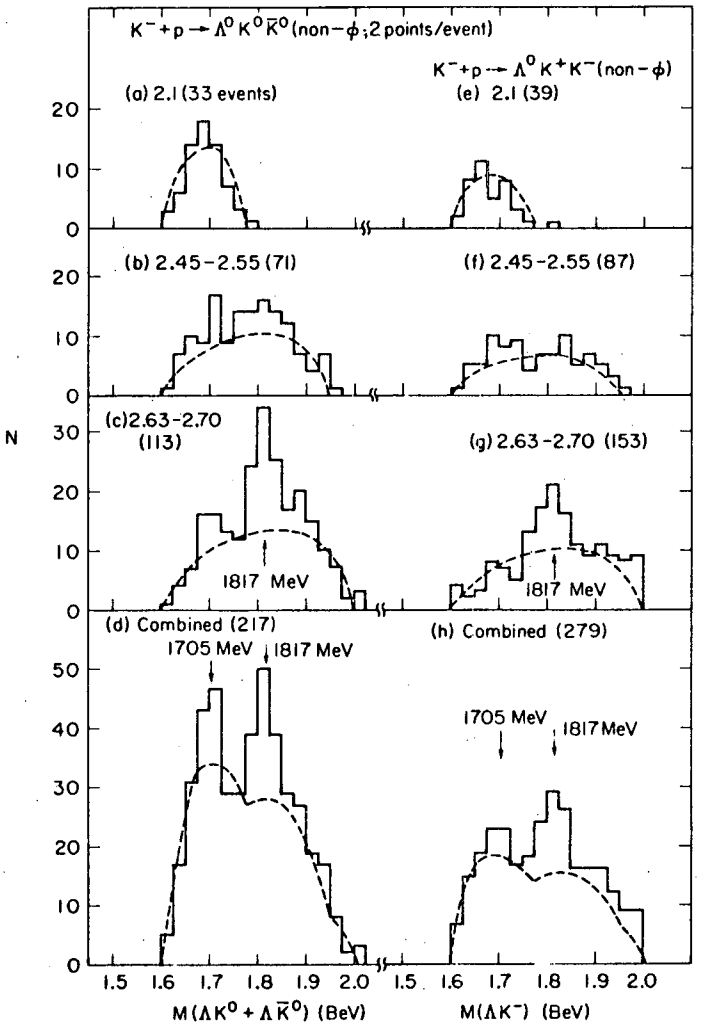

Fig. 44. Invariant mass of ΛK^0 system from $\Lambda K^0 \overline{K}^0$ final state. Data are from Smith and Lindsey.[54]

for the opposite parity being only ≈1%. For the $\Xi^*(1820)$, two assignments seem to be equally probable: $1/2^{\pm}$ or $3/2^-$. This result comes from the study of $\Xi^*(1820) \rightarrow \Xi^*(1530) + \pi$. The background present is quite large, and the statistics are small.[55]

11. Structure in the K^+N System (B = 1, S = +1)

Recently, very good measurements of the K^+p and K^+d total cross sections have been made by Cool et al.[56] in the 1.0- to 2.5-GeV/c region. Figure 45 shows the total cross section for K^+p up to 20 GeV/c. The 1.0- to 1.3-GeV/c region shows some unexpected structure--the elastic cross section plotted in the lower part of the graph starts falling rapidly after about 1 GeV/c.

The K^+d total cross sections are given in Fig. 46. Again some structure is evident around 1.2 GeV/c. By subtracting from K^+d, the K^+p cross section, with the appropriate screening corrections, the K^+n cross section is obtained. This is plotted in the lower part of Fig. 46.

Figure 47 shows the total cross section for the two isospin states I = 0 and I = 1. Both show the same structure and if interpreted as resonances, the two new states would have the following characteristics:

State	Mass (MeV)	Width (MeV)	Y	I	Multiplet	$\Delta\sigma_{max}$ (mb)
Z_0^*	1863 ± 20	150	2	0	$\overline{10}$	6 - 8
Z_1^*	1910 ± 20	180	2	1	27	1 - 2

Here $\Delta\sigma_{max}$ represents the estimated size of the bump in the total cross section.

As usual, we are reluctant to accept new resonances, especially if they are revolutionary--as these are. In fact, Z_1^* should be a member of the

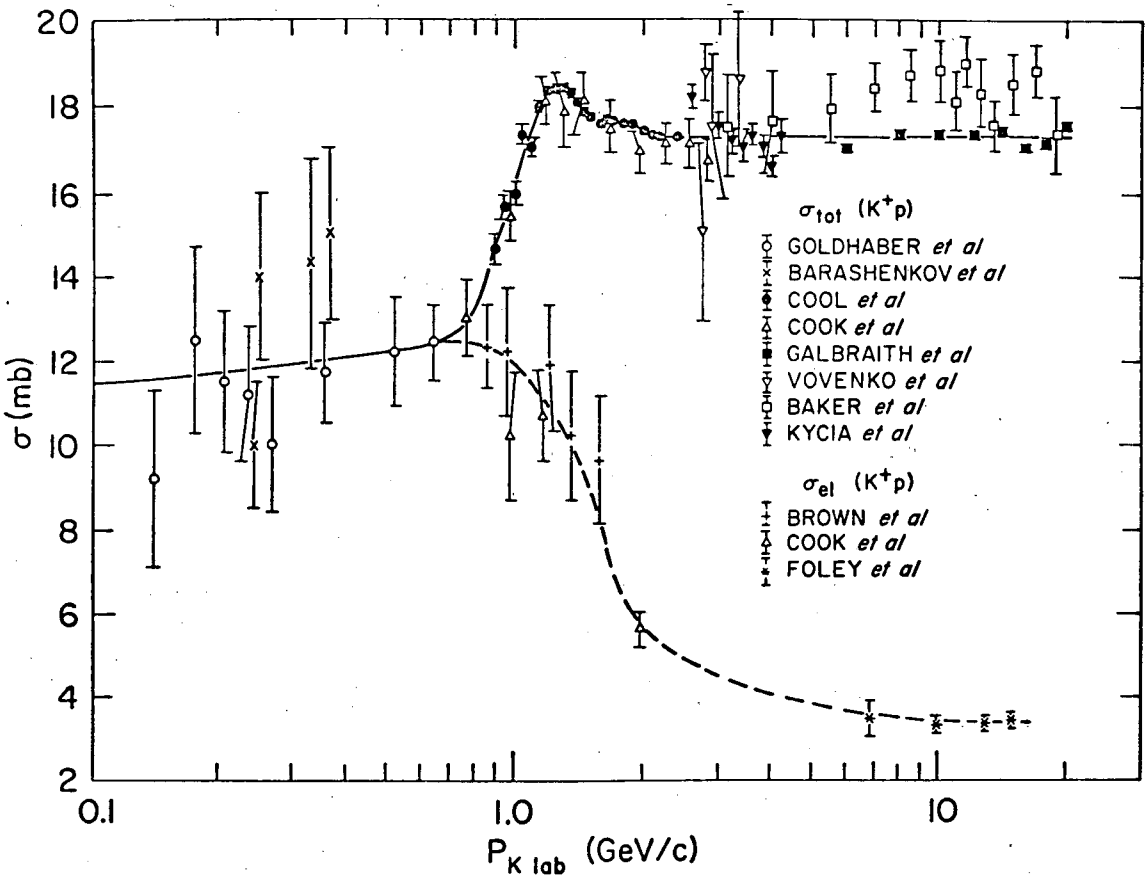

Fig. 45. K^+p total cross section up to 20 GeV/c.[56] The dashed curve represents the elastic cross section $K^+p \rightarrow K^+p$.

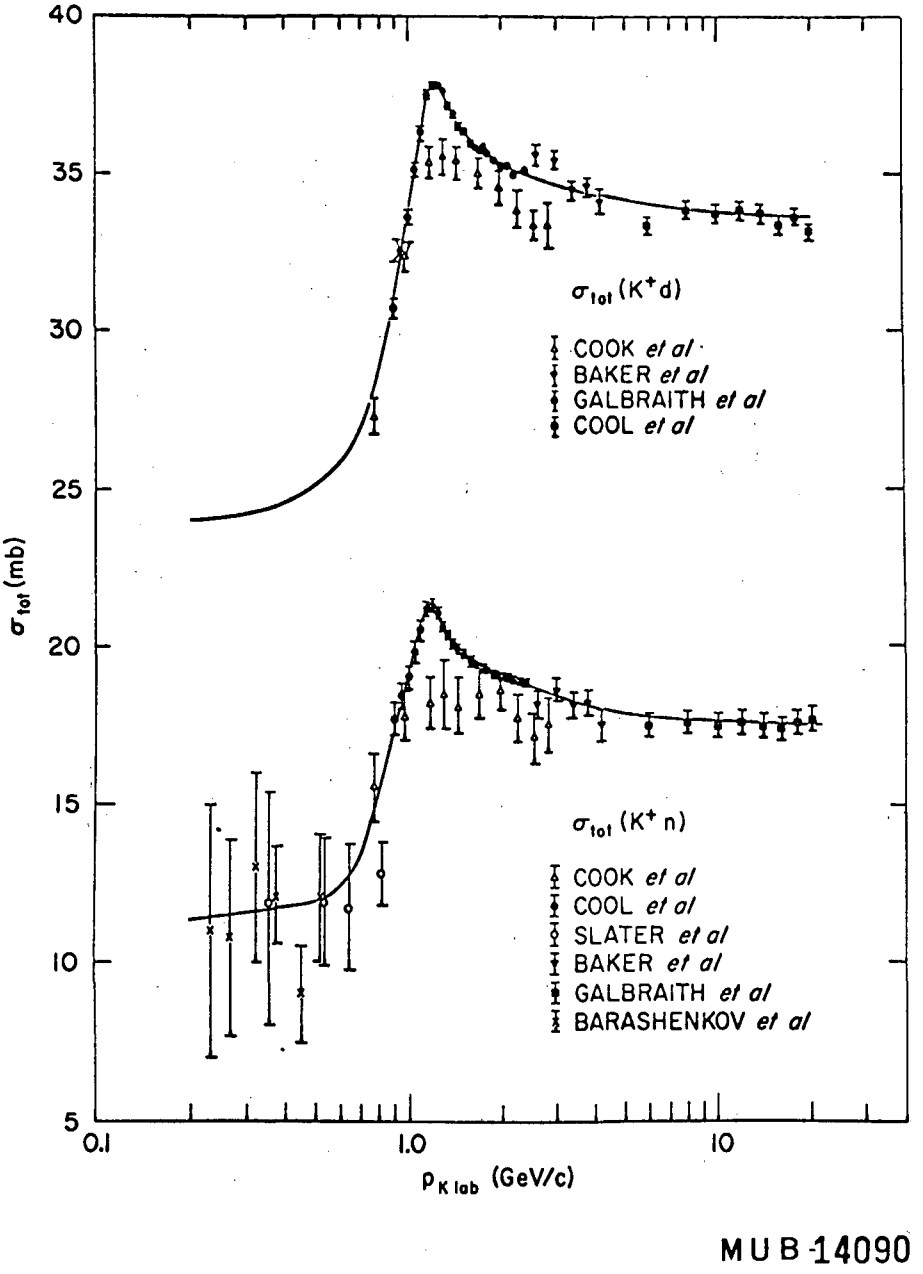

Fig. 46. Total cross section for K^+d and K^+n interaction. From Ref. 56.

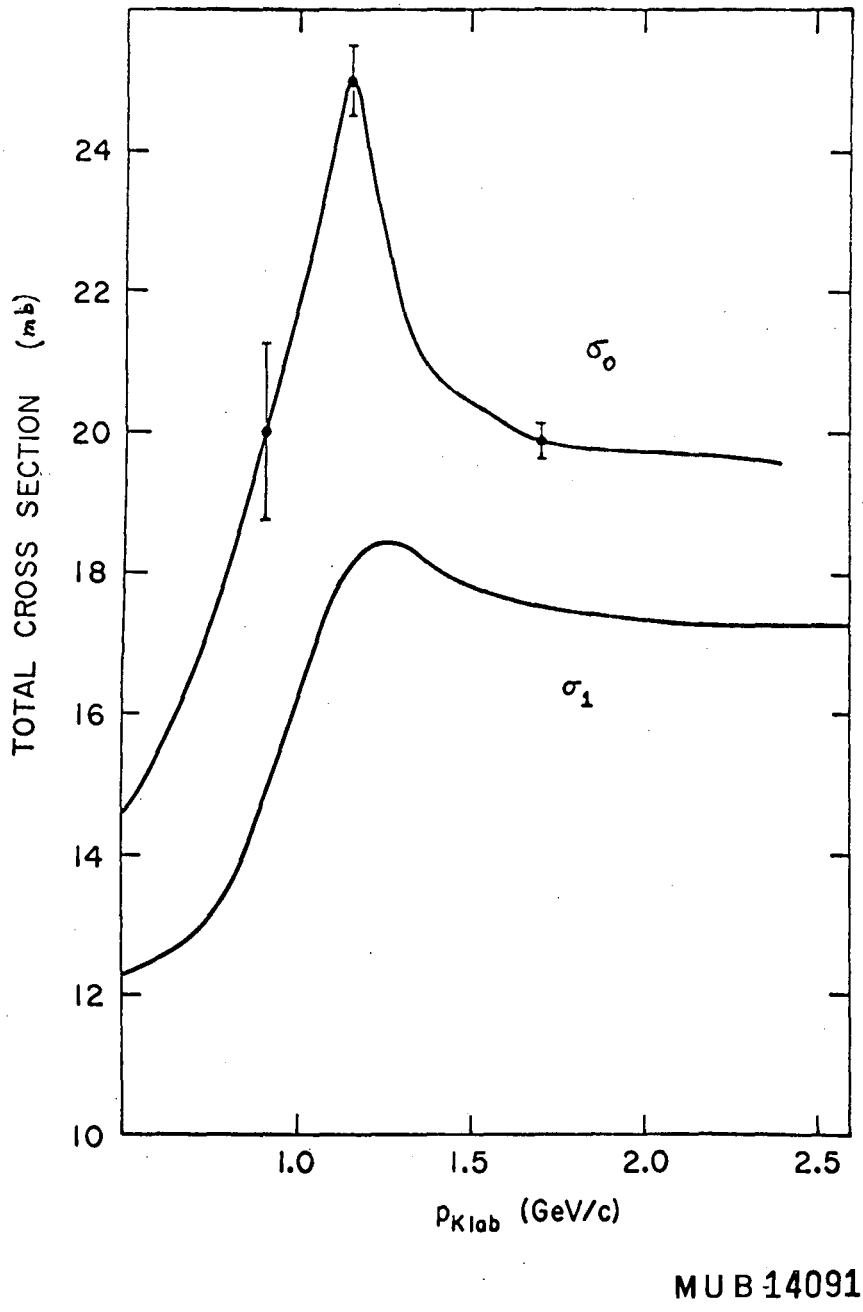

Fig. 47. The isotopic spin states, I = 1 and I = 0, for K^+N total cross section.[56]

27 representation and, if true, would be the first resonance to belong to it. The Z_0^* would be a member of a $\overline{10}$ representation.

For the I = 1 cross section, the rise at ≈1.2 GeV/c could be explained by the fact that inelastic processes start being important at that energy. In fact, the threshold for $K^+p \rightarrow \Delta(1238) + K$ is at this energy, and the cross section for this process has a sudden increase, shown in Fig. 48, which is taken from the paper of Ref. 57. The whole bump seems to be accounted for by the bump in the total cross section for $\Delta(1238) + K$. Whether this is an indication of a resonance (K^+p) decaying through the channel (ΔK), or an effect of a different type, is not clear at this time. The elastic cross section does not show any enhancement at this energy. Bland et al. are analyzing their data and increasing their statistics in order to clarify the situation.

It is at the present time more difficult to understand the large enhancement in the I = 0 state. In this state the ΔK channel cannot explain this behavior, since it cannot be in an I = 0 state. Preliminary data from Ref. 57 indicate that no inelastic channel shows such large enhancement.

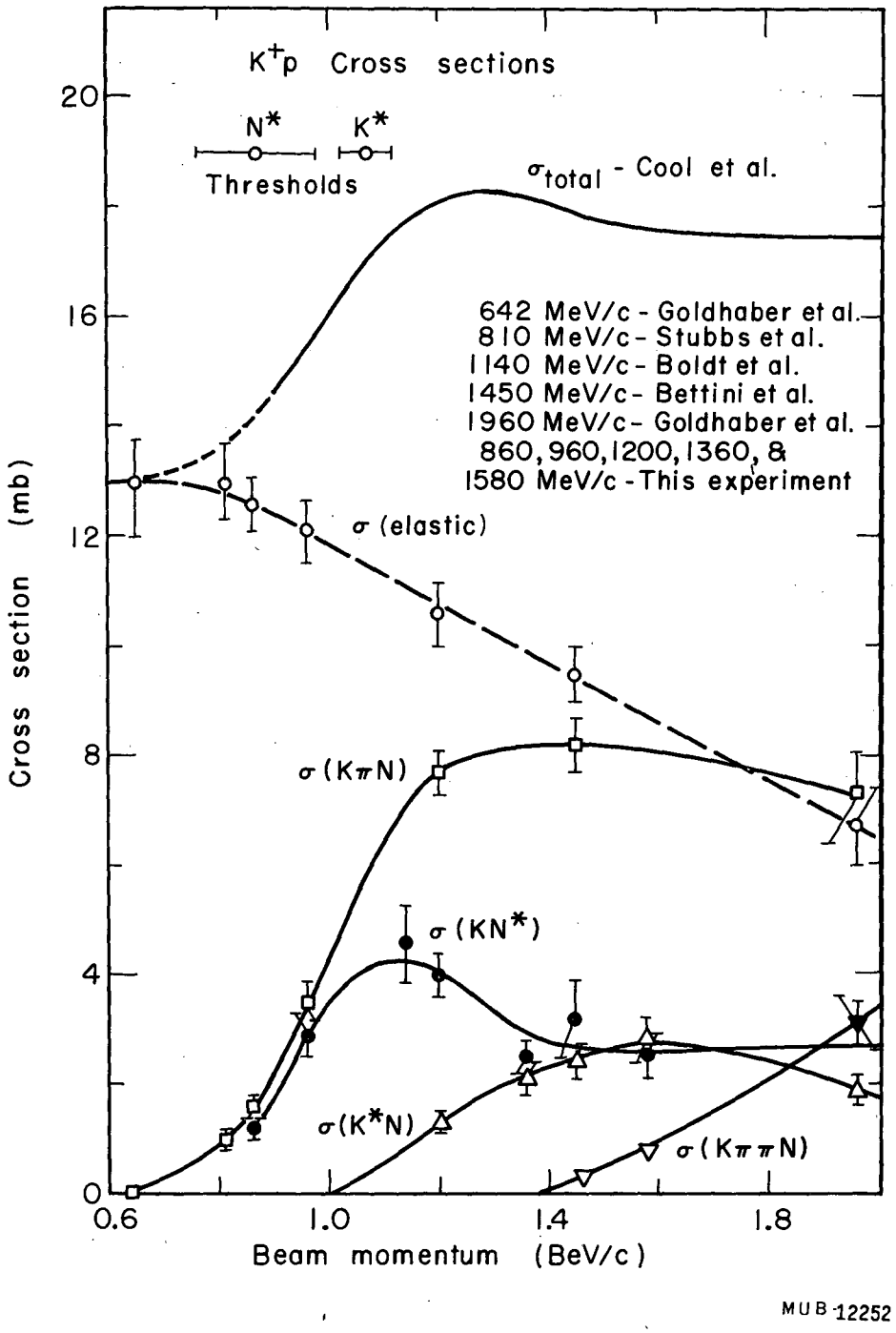

Fig. 48. Collection of K^+p cross sections made by Bland et al.[56] The upper curve is the total K^+p cross section. The other curves are labelled. The N^* here is the $\Delta(1238)$, the K^* is the $K^*(891)$.

III. PARTICLE SUPERMULTIPLETS

1. Introduction

In the preceding two sections we have reviewed the situation of baryon resonances: the established resonances and the uncertain ones. Professor Fiorini has reviewed the situation concerning the mesonic resonances.

Various authors have attempted to classify the known resonances in terms of SU(3) supermultiplets, and I will try to report the present situation.[58-60] I will not consider higher symmetry schemes: only "unbroken SU(3)" predictions are considered in this classification. The student is referred to Professor Coleman's lectures for discussions concerning the Gell-Mann/Okubo (GMO) mass formula and the decay rate calculations.[61]

As an experimentalist, I believe that at the present time we can classify mesons in nonets, and baryons in octets and decuplets, without the necessity of using higher representations.

2. Mesons

Almost all the mesons with established quantum numbers are now accommodated in SU(3) nonets. There are three established nonets and a possible one not completely established.

2.1 GMO Formula. Mixing

For the mesons the GMO formula is written in terms of mass squared instead of masses (see Ref. 61 for a discussion of this point). It has the form

$$4\hat{K} = 3\hat{\eta} + \hat{\pi}, \tag{15}$$

where $\hat{K}$ means m_K^2 (i.e., the mass squared of the I = 1/2 member of the octet), $\hat{\eta}$ ($= m_\eta^2$) indicates the isosinglet, and $\hat{\pi}$ ($= m_\pi^2$) is the isotriplet of the octet. [This notation has been introduced by Glashow and Socolow.[60]]

It turned out that this formula does not work for the 1^- octet [$K^*(891)$, $\rho(760)$, $\omega(783)$]. The derivation of the GMO formula neglects the possibility of mixing between different unitary multiplets of the same spin parity, mixing due to the symmetry-breaking interactions. If η' is a unitary singlet with the same J^P assignment as K, η, and π, the mixing of the two isosinglets η' and η is expressed in terms of an angle θ, defined as follows:

$$\begin{aligned} |8\rangle &= |\eta\rangle \cos\theta + |\eta'\rangle \sin\theta \\ |1\rangle &= -|\eta\rangle \sin\theta + |\eta'\rangle \cos\theta, \end{aligned} \tag{16}$$

where $|\eta\rangle$, $|\eta'\rangle$ represent the physical states, and $|8\rangle$, $|1\rangle$ represent the pure octet and singlet states.[62] The angle θ can be expressed as a function of measurable quantities, specifically masses, by applying the mass squared operator to the above Eqs. (16). One obtains

$$\sin^2\theta = \frac{\hat{\eta} - \hat{m}_8}{\hat{\eta} - \hat{\eta}'}, \tag{17a}$$

where $\hat{m}_8$ is the expectation value of the mass squared operator in the pure octet isosinglet state. It can be related to the physical masses of the I = 1/2 and I = 1 members of the octet through Eq. 15:

$$\hat{m}_8 = 1/3\,(4\hat{K} - \hat{\pi}). \tag{17b}$$

In conclusion for the mesons it turns out that it is necessary to talk about nonets instead of octets and singlets. The GMO formula is not a test any more, since there is a new parameter to calculate, i.e., the mixing angle.

So far, there is no reliable mass formula to test if nine states are members of a nonet,[63] but after the mixing angle is calculated from Eqs. (17) the comparison of the calculated and measured decay rates still offers a good test.

2.2 Established Nonets (0^-, 1^-, 2^+)

Glashow and Socolow, among others, have made extensive studies of these three nonets; their results are given in an article in which they discuss the existence of the 2^+ nonet.[60] Table 5 summarizes masses and mixing angles.[64] The predicted and measured decay rates are reported in

Table 5. Mass parameters of the established meson nonets.

Y	I	$J^P = 0^-$	$J^P = 1^-$	$J^P = 2^+$
0	1	$\pi(138)$	$\rho(760)$	$A_2(1300)$
-1	1/2	K(496)	$K^*(891)$	$K^*(1415)$
0	0	$\eta(549)$	$\Phi(1020)$	$f'(1500)$
0	0	$\eta'(959)$	$\omega(783)$	f(1254)
	m_8	596 MeV	930 MeV	1445 MeV
	θ	$\theta_0 = (11 \pm 2)°$	$\theta_1 = (39 \pm 1)°$	$\theta_2 = (29 \pm 9)°$

Table 6 for the vector mesons and the tensor nonet.[65] With the present experimental data, the agreement between predicted and measured decay rates is quite good.

A summary of the situation of these three vector nonets is shown in Fig. 49. This display, made by Rosenfeld,[66] has been suggested by Glashow and Socolow who notice certain remarkable similarities between the $J^P = 1^-$ nonet and the 2^+ nonet. I refer the reader to their paper, but I will summarize their remarks.

(i) The mass spectra of the two nonets are similar. In both nonets the $I = 1/2$ state is heavier than the $I = 1$ (the same is also true for the 0^- nonet). In both nonets there is a large mixing angle ($\theta_1 = 39°$ for the $J^P = 1^-$, $\theta_2 = 29°$ for the $J^P = 2^+$), and the heaviest state is the mostly octet $I = Y = 0$ member of the nonet.

(ii) The masses of the particles in each nonet satisfy the Schwinger mass formula,[63] which has been introduced for the vector nonet

$$(\hat{\phi} - \hat{m}_8)(\hat{\omega} - \hat{m}_8) = -8/9(\hat{K}^* - \hat{\rho})^2$$
$$\hat{m}_8 = 1/3(4\hat{K}^* - \hat{\rho}). \qquad (18)$$

For the 0^-, 1^-, 2^+ nonets, Eq. (18) gives

0^- $\quad 0.013 \pm 0.004 = 0.046 \pm 0.001$

1^- $\quad 0.044 \pm 0.001 = 0.040 \pm 0.002$

2^+ $\quad 0.09 \pm 0.05 = 0.05 \pm 0.03$

and it is not satisfied for the 0^- nonet.

(iii) The decay modes $\phi \to \rho\pi$ and $f' \to \pi\pi$ are analogous and both appear to be suppressed.

The preceding three points, and most of the features of the 1^- and 2^+ nonets, are in agreement with a nonet-coupling scheme first suggested by

Table 6. Decay rates of the established meson nonets.

	Decay mode	SU(3) factor	Predicted rate[a] (MeV)	Experimental rate (MeV)
$1^- \to 0^-0^-$	$K^* \to K\pi$	$1/4\ F^2$	Input	49 ± 3
	$\rho \to \pi\pi$	$1/3\ F^2$	171 ± 8	125 ± 25
	$\phi \to K\bar{K}$	$1/2 \cos^2\theta_1\ F^2$	3.1 ± 0.5	3.3 ± 0.6
$2^+ \to 0^-0^-$	$A_2 \to \pi\eta$	$8D^2$	8 ± 3	3 ± 2
	$A_2 \to K\bar{K}$	$12D^2$	Input	4.5 ± 1.5
	$f \to \pi\pi$	$3(2\ D \sin\theta_2 + G \cos\theta_2)^2$	Input	118 ± 20
	$f \to K\bar{K}$	$4(D \sin\theta_2 - G \cos\theta_2)^2$	6 ± 4	2 ± 2
	$f \to \eta\eta$	$(2\ D \sin\theta_2 - G \cos\theta_2)^2$	0.3 ± 0.3	small
	$K^* \to K\pi$	$18D^2$	30 ± 11	39 ± 20
	$K^* \to K\eta$	$2D^2$	0.9 ± 0.3	2 ± 2
	$f' \to \pi\pi$	$3(2\ D \cos\theta_2 - G \sin\theta_2)^2$	2 ± 4	0 ± 6
	$f' \to K\bar{K}$	$4(D \cos\theta_2 + G \sin\theta_2)^2$	33 ± 18	50 ± 25
	$f' \to \eta\eta$	$(2\ D \cos\theta_2 + G \sin\theta_2)^2$	9 ± 4	small
$2^+ \to 1^-0^-$	$A_2 \to \rho\pi$	$4\ H^2$	Input	80 ± 14
	$K^* \to K^*\pi$	$1.5\ H^2$	20 ± 4	43 ± 15
	$K^* \to \rho K$	$1.5\ H^2$	5.0 ± 1.4	14 ± 5
	$K^* \to \omega K$	$1.5 \sin^2\theta_1\ H^2$	1.5 ± 0.5	7 ± 4
	$f' \to K^*\bar{K}$	$6 \cos^2\theta_2\ H^2$	7 ± 4	34 ± 15

a. Predicted rates calculated by Goldberg et al. (Ref. 59).

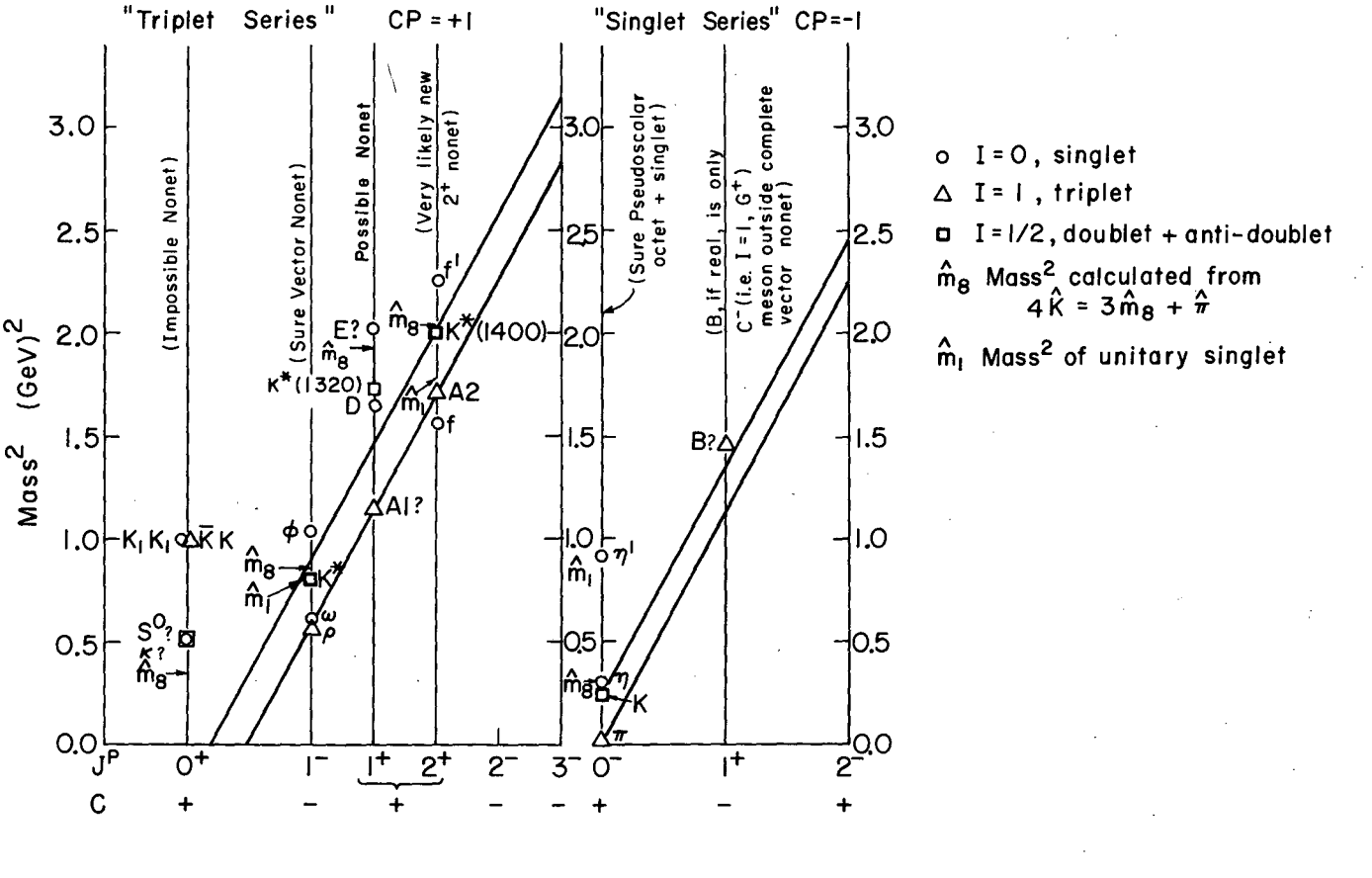

Fig. 49. Plot of known meson resonances.

Okubo[67] and by which the authors derive many other predictions, as yet to be checked, on electromagnetic decays of $J^P = 0^-$ and 1^- mesons.

2.3 Possible 1^+ Nonet

The possibility that A_1, K_c, D, and E mesons form a nonet has been analyzed by Flattè.[68] None of these mesons is yet well understood, as can be seen from Professor Fiorini's lectures. (The A_1 might still be a kinematical effect, but in this lecture it is appropriate to look into this possibility.)

The experimental data on A_1 and D mesons appear to be consistent with the assignment $J^P = 1^+$, and for K_c and E mesons this assignment is not excluded.

Another possibility is to substitute the $K^*(1320)$ for the K_c. This last state appears to be distinct from a kinematical enhancement produced in the same region by the Deck effect, as shown by Shen et al.[69] These authors discuss the possibility of the new 1^+ nonet: $[A_1, K^*(1320), D, E]$.

Tables 7 and 8 contain parameters and decay rates for both possible nonets. We note the following facts:

1. In version (a) the m_8 mass of 1260 ± 20 MeV is smaller than the D mass, but in one standard deviations can be identified with it. For version (b) the m_8 mass lies closer to the heaviest I = 0 state. This situation is similar to the one of the 1^- and 2^+ nonet.

2. For the Schwinger mass formula we have the following:

   a. $-0.02 \pm 0.03\ (\text{GeV})^4 = 0.09 \pm 0.03\ (\text{GeV})^4$

   b. $0.03 \pm 0.03\ (\text{GeV})^4 = 0.31 \pm 0.07\ (\text{GeV})^4$.

In either case it is not satisfied.

3. The decay-rate predictions for $1^+ \to 1^-0^-$ decays, reported in Table 8, present the following features:

Table 7. Parameters for possible 1^+ nonets.

		Version (a)		Version (b)	
Y	I		Mass (MeV)		Mass (MeV)
0	1	A_1	1080 ± 10	A_1	1080 ± 10
-1	1/2	K_c	1230 ± 15	K^{**}	1320 ± 10
0	0	D	1286 ± 6	E	1420 ± 10
0	0	E	1420 ± 10	D	1286 ± 6
m_8			1260 ± 20		1390 ± 21
$\sin^2\theta$			<0.025 ± 0.17		0.21 ± 0.11
θ			<9°		28° ± 8°

Table 8. Decay rates for possible 1^+ nonets.

	Decay mode	SU(3) factor	Version (a)				Version (b)			
				Phase space[a]	Predicted rate[a] (MeV)	Experimental rate (MeV)		Phase space[b]	Predicted rate[b] (MeV)	Experimental rate (MeV)
	$A_1 \to \rho\pi$	$4\,E^2$	A_1	0.200	Input	125	A_1	0.200	Input	125
	$K^{**} \to K^*\pi$	$1.5\,E^2$	K_c	0.181	42	60	$K^*(1320)$	0.194	44	80 ± 20[b]
	$\to \rho K$	$1.5\,E^2$		0.024	6			0.11	26	
$1^+ \to 1^-0^-$	$\to \omega K$	$1.5 \sin^2\theta_1\, E^2$		very		not		0.089	9	$6 \pm {}^{4}_{6}$[b]
	$\to K^*\eta$	$1.5 \sin^2\theta_0\, E^2$		small		seen				
	$D \to K^*\bar{K} + \bar{K}^*K$	$6 \sin^2\theta\, E^2$ [c]	D	0.001	1	40 ± 10	D	0.001	.2	40 ± 10
	$E \to K^*\bar{K} + \bar{K}^*K$	$6 \cos^2\theta\, E^2$ [c]	E	0.077	2	60 ± 10	E	0.076	56	60 ± 10

a. Calculations from Flatté (Ref. 68).
b. Shen et al. (Ref. 69).
c. For Version (a) this angle is $90° - \theta$, where θ is the angle of Table 7, because D and E are inverted.

a. For version (a), A_1 and K_c are consistent with their being members of the same nonet. The K_c is supposed to have a ratio $(K_c \to K^* \pi / K_c \to K\rho) = 42/6$. Baillon's[70] recent analysis agrees with this point. The predicted decay rates for the D and E mesons, however, are much too small.

b. For version (b), A_1 and $K^*(1320)$ are consistent with their being members of the same nonet. The calculated decay rate for the E meson is also in agreement with the observed rate, but the D-meson decay rate is still in disagreement with experiment.

In conclusion, version (b) seems to show better agreement with experimental data. However, the D meson, its mass being below the K^*K threshold, decays into $K\bar{K}\pi$ with $\Gamma = 40$ MeV, which implies that K_c and A_1 should also have analogous decay modes. Since they don't, this point strongly suggests that the D meson might not be part of this nonet. The decay rates of the E meson are not understood either, so it is better to wait before drawing any conclusions.

2.4 Other Representations

There is some evidence for the existence of a K^+K^+ meson[71] with a mass M = 1280 MeV, and Y = 2, I = 1. With this hypercharge-isospin assignment, the only representation it can belong to is a 27. However, contradictory evidence[72] has been presented lately, so it is better to wait for an experiment with larger statistics before accepting it.

3. Baryons

The largest success of SU(3) has been the discovery of the Ω^-, which completed the $J^P = 3/2^+$ decuplet.

The GMO formula for a decuplet predicts equal spacing between members of the decuplet

$$\Delta - Y_1^* = Y_1^* - \Xi^* = \Xi^* - \Omega^-, \qquad (19)$$

where the particle symbol indicates the corresponding particle mass. For the octet the GMO formula predicts

$$2(N + \Xi) = 3\Lambda + \Sigma. \qquad (20)$$

In addition, there is electromagnetic mass splitting within the isospin multiplets. The relation between the electromagnetic splittings for the members of the same octet has been obtained by Coleman and Glashow,[73]

$$m(\Xi^-) - m(\Xi^0) = m(\Sigma^-) - m(\Sigma^+) - [m(n) - m(p)], \qquad (21)$$

and it works very well.

3.1 Established Baryon Supermultiplets ($1/2^+$ Octet, $3/2^+$ Decimet)

There is one octet and one decuplet for which everything seems to work. The Gell-Mann/Okubo formula and the expected decay rates in the decuplet are in agreement with the calculations.

Table 9 shows the comparison of the GMO formula with the measured masses. There is only one prediction for the octet and two predictions for the decuplet. The agreement for the octet is at 1% in the Ξ mass, although for the decuplet it is much better.

Table 10 shows the second test of the predictions of "unbroken SU(3)." This is the comparison of predicted and observed rates of strong decays. Predicted values are taken from Ref. 59. Only the Ξ^* decay rate deviates significantly from the expected value, and the agreement for Y_1^* is quite good.[64]

3.2 Possible Baryon Octets: $3/2^-$, $5/2^+$

Of the many known resonances there are not enough states to complete octets with $J^P = 3/2^-$ and $5/2^+$, but many attempts have been made in this direction.

The study of the K^-p system is still quite incomplete from $P_K = 500$ MeV/c (total c.m. energy of the Kp system = 1560 MeV) on, and many more experiments are still needed before we can have a complete picture of the

Table 9. Established baryon supermultiplets.

(a) $1/2^+$ Octet

GMO formula: $2(N+\Xi) = 3\Lambda + \Sigma$

Y	I	Particle	Input (MeV)	Predicted (MeV)	Observed (MeV)
1	1/2	N	939		
0	0	Λ	1115		
0	1	Σ	1193		
-1	1/2	Ξ		1330 ± 1	1317 ± 1

(b) $3/2^+$ Decuplet

GMO formula: $\Delta - Y_1^* = Y_1^* - \Xi^* = \Xi^* - \Omega^-$

Y	I	Particle	Input (MeV)	Predicted (MeV)	Observed (MeV)
1	3/2	Δ	1236		
0	1	Y_1^*	1383		
-1	1/2	Ξ^*		1530	1530 ± 1
-2	0	Ω^-		1677	1675 ± 3

Table 10. Decay rates of the $3/2^+$ decuplet.
$J^P = 3/2^+ \rightarrow 1/2^+ + 0^-$

Decay mode	SU(3) factor	Predicted rate[a] (MeV)	Observed rate (MeV)
$\Delta(1236) \rightarrow N\pi$	1	Input	120 ± 5
$\Xi^*(1530) \rightarrow \Xi\pi$	1/2	14 ± 1	8 ± 2
$Y_1^*(1383) \rightarrow \Lambda\pi$	1/2	38 ± 3	40 ± 6
$Y_1^*(1383) \rightarrow \Sigma\pi$	1/3	5.2 ± 0.5	4 ± 1

a. Predicted rates as calculated by Goldberg et al. (Ref. 59).

existing resonant states with S = -1. The situation for S = -2 resonances is even worse.

Various attempts to form new octets have been made; we will consider the following four possibilities:[59]

$3/2^-$ { a: $N^*(1525)$, $Y_0^*(1519)$, $Y_1^*(1660)$, $\Xi^*(1815)$, and $Y_0^*(1700)$
b: $N^*(1525)$, $Y_0^*(1519)$, $Y_1^*(1660)$, $\Xi^*(1933)$, and $Y_0^*(1700)$

$5/2^+$ { a: $N^*(1688)$, $Y_0^*(1815)$, --- , $\Xi^*(1933)$
b: $N^*(1688)$, $Y_0^*(1815)$, --- , $\Xi^*(1815)$.

Let us examine the two tests separately: Gell-Mann/Okubo (GMO) mass formula and decay-rate predictions.

1. The GMO formula does not work for either of the $3/2^-$ proposed octets. For the $3/2^-$ (a) octet, the mass of the isosinglet should be $M_8 = 1673$ MeV; for the $3/2^-$ (b) it should be $M_8 = 1752$ MeV. This only means that there might be some mixing between $Y_0^*(1520)$ and another Y_0^* with $J^P = 3/2^-$.

Mixing between multiplets of the same spin and parity has been discussed up to now only for meson octets (see Par. 2.1). In the same way for baryon octets we would have:

$$\Lambda = |8\rangle \cos\theta + |1\rangle \sin\theta$$

$$\Lambda' = -|8\rangle \sin\theta + |1\rangle \cos\theta$$

or

$$\sin^2\theta = \frac{\Lambda - M_8}{\Lambda - \Lambda'} \qquad (22)$$

$$M_8 = \frac{2(N+\Xi) - \Sigma}{3}.$$

Recently a $Y_0^*(1700)$ has been detected (Par. 5, Part II), and there is some indication that it might have $J^P = 3/2^-$.[41] If this J^P assignment is confirmed, the mixing angle between $Y_0^*(1520)$ and $Y_0^*(1700)$ would be $\theta = 23°$ for octet (a).

Furthermore, the octet (b) would be excluded because $M_8 = 1752$ MeV and both physical states would have a lower mass.

For the two $5/2^+$ possibilities not much can be said because a Y_1^* is missing, and for the Y_0^* it is not possible to check the presence of mixing. If it were absent, the mass of Y_1^* would be $M_1 = 1575$ or 1800 MeV for case (a) or (b), respectively. The recently discovered $Y_1^*(1915)$ (see Par. 9, Part II) has a larger mass than either of the two possibilities.

2. Table 11 shows the calculated decay rates for all four possibilities. In view of mixing, the $Y_0^*(1520)$ decay rates have been disregarded in the calculations. Note in Table 11 that the agreement between calculated and experimental rates is quite bad, especially for Ξ^* decay rates.[59] If we exclude the Ξ^*, disagreement is not bad, and I personally think that the Ξ^* decay rates can radically change, since the experiments done until now have very small statistics.[64] As for the $Y_1^*(1660)$, the quoted branching ratios are also subject to change.

In conclusion, two more octets are suggested by the known resonances, but the experimental information is not sufficient to complete them nor to check the validity of the assumptions implicit in the GMO formula or the decay-rate calculations.

3.3 Other Baryon Resonances

Besides the possible $3/2^-$ and $5/2^+$ octets, there are many other states that do not complete octets and decimets. In Table 12 they are tabulated according to J^P, Y, and I quantum numbers.

The last entry in this table is an assignment to a certain representation, based only on the fact that the states on that line satisfy the isospin-hypercharge correlation expected for an eightfold or tenfold representation. Mass formula or decay rates are not introduced as tests at this stage.

Table 11. Decay rates for possible $3/2^-$, $5/2^+$ octets. †

J^P	Decay	SU(3) rate	Predicted rate (MeV) Version (a)	Experimental rate (MeV) Version (a)	Predicted rate (MeV) Version (b)	Experimental rate (MeV) Version (b)
$3/2^- \rightarrow 1/2^+ + 0^-$	$N^*(1518) \rightarrow N\pi$	3	Input	85 ± 11	Input	85 ± 11
	$Y_1^*(1660) \rightarrow \Sigma\pi$	$8a^2$	Input	12 ± 5	Input	12 ± 5
	$Y_1^*(1660) \rightarrow \Lambda\pi$	$4/3(1-a)^2$	12 ± 3	3 ± 10	12 ± 3	3 ± 10
	$Y_1^*(1660) \rightarrow \bar{K}N$	$2(1-2a)^2$	2 ± 3	5 ± 10	2 ± 3	5 ± 10
$a = 0.37 \pm 0.09$ ‡	$N^*(1518) \rightarrow N\eta$	$1/3(1-4a)^2$	0 ± 1	<10	0 ± 1	<10
	$\Xi^* \rightarrow \Lambda\bar{K}$	$1/3(1-4a)^2$	1 ± 1.5	20 ± 7	3 ± 5	~15
	$\Xi^* \rightarrow \Xi\pi$	$3(1-2a)^2$	3 ± 4	2 ± 2	8 ± 10	~135
	$\Xi^* \rightarrow \Sigma\bar{K}$	3	10 ± 2	0 ± 2	55 ± 13	small
$5/2^+ \rightarrow 1/2^+ + 0^-$	$N^*(1688) \rightarrow N\pi$	3	Input	90 ± 22	Input	90 ± 22
	$Y_0^*(1815) \rightarrow N\bar{K}$	$2/3(1+2a)^2$	Input	37 ± 17	Input	37 ± 17
	$Y_0^*(1815) \rightarrow \Sigma\pi$	$4(1-a)^2$	19 ± 15	4.5 ± 3	19 ± 15	4.5 ± 3
	$Y_0^*(1815) \rightarrow \Lambda\eta$	$4/3(1-a)^2$	0.4 ± 0.3	1 ± 2	0.4 ± 0.3	1 ± 2
$a = 0.35 \pm 0.25$ ‡	$N^*(1688) \rightarrow N\eta$	$1/3(1-4a)^2$	0 ± 1	2 ± 2	0 ± 1	2 ± 2
	$\Xi^* \rightarrow \Lambda\bar{K}$	$1/3(1-4a)^2$	1 ± 3	~15	0 ± 1	20 ± 7
	$\Xi^* \rightarrow \Xi\pi$	$3(1-2a)^2$	3 ± 10	~135	1 ± 3	2 ± 2
	$\Xi^* \rightarrow \Sigma\bar{K}$	3	12 ± 4	small	1.1 ± 0.4	0 ± 2

† Table reported from Ref. 59.
‡ $1-a/a$ is the D/F ratio, where D and F are the two possible types of couplings.

Table 12. Baryon resonances not yet classified.

J^P	$(Y)_I = (1)_{3/2}$	$(1)_{1/2}$	$(0)_0$	$(0)_1$	Representation
$1/2^-$			$Y_0^*(1405)$		①, ⑧
		$N^*(1512)$	$Y_0^*(1675)$?		⑧
		$N^*(1700)$			⑧
	$\Delta(1690)$				⑩
$1/2^+$		$N^*(1480)$			⑧
$5/2^-$		$N^*(1690)$		$Y_1^*(1765)$	⑧
$7/2^+$	$\Delta(1920)$			$Y_1^*(2040)$	⑩
$7/2^-$		$N^*(2190)$	$Y_0^*(2120)$		⑧

3.4 Other Representations

There has been some indication of an $I = 5/2$ resonance in the πp system, but with the present statistics it looks more like a kinematical effect.[74]

Also some dibaryon states have been mentioned in various cases, but they have been made in πd interactions and are very likely to be N^*N, where N is the remaining nucleon of the deuteron bound to the N^* system.[75]

The two recently discovered enhancements in a K^+p total cross section,[56] if proved to show a resonant behavior, would have the following properties:

Z_0^* $Y = 2$ $I = 0$ $\overline{10}$ representation

Z_1^* $Y = 2$ $I = 1$ 27 representation.

These last two states look very interesting and some experiments are under way to check their existence (see Par. 11, Part II).

3.5 Chew-Frautchi Plot for Baryon States

The summary of the actual situation in baryon resonances is shown in the Chew-Frautchi plot of Fig. 50. The lines connecting resonant states represent pure conjecture, since there is no single trajectory containing more than two resonances with established quantum numbers.

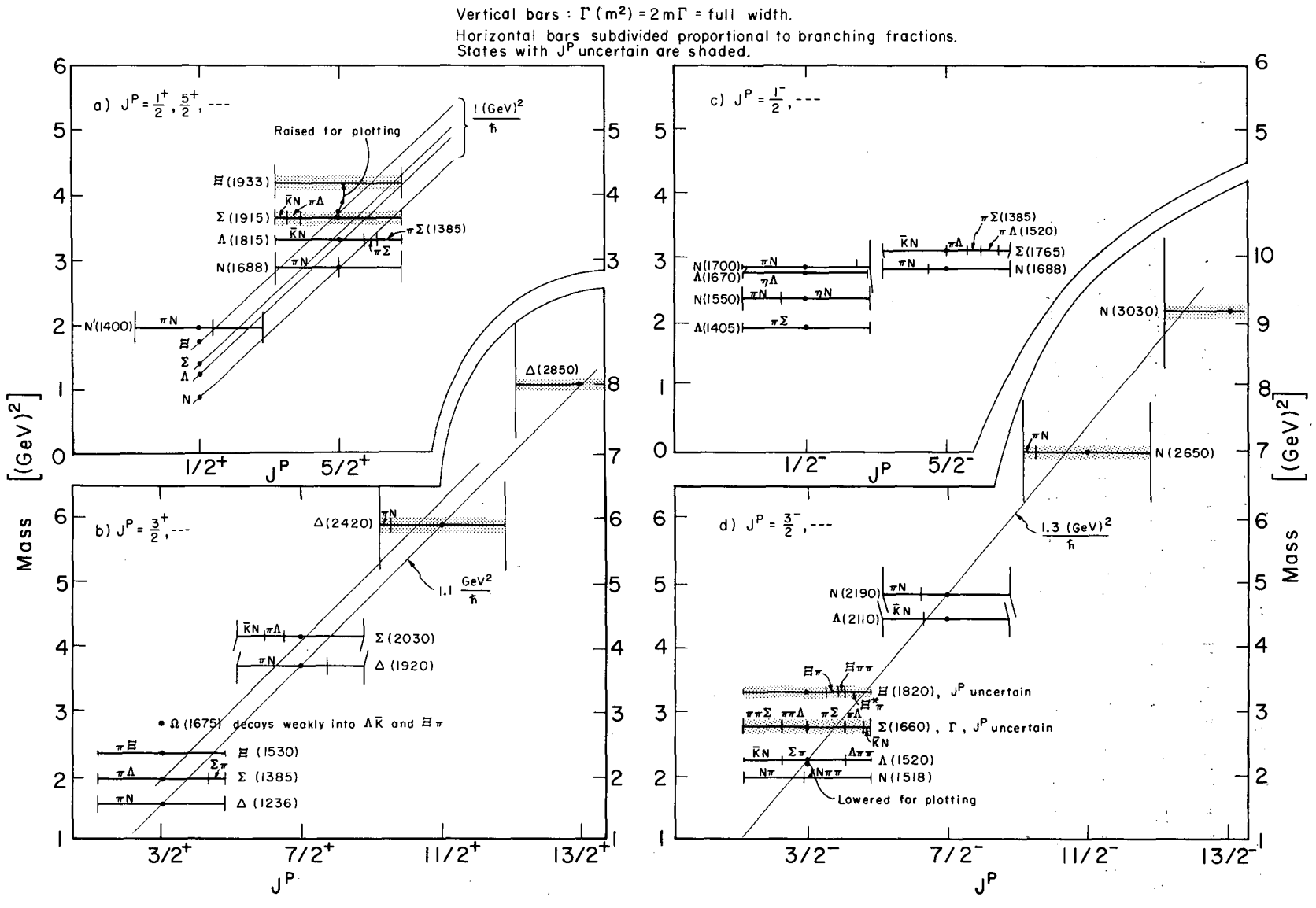

Fig. 50. Baryon states.[1]

ACKNOWLEDGMENTS

This work was done under the auspices of the U. S. Atomic Energy Commission.

FOOTNOTES AND REFERENCES

1. A. H. Rosenfeld, A. Barbaro-Galtieri, W. H. Barkas, P. L. Bastien, J. Kirz, and M. Roos, Rev. Mod. Phys. 37, 633 (1965), and UCRL-8030, Pt. I (1966).
2. We use the notation of R. D. Tripp in Baryon Resonances, CERN report 65-7 (Rev.), and International School of Physics, Enrico Fermi, XXXIII Course, Strong Interactions (Academic Press, N. Y., 1966), p. 70. The reader is referred to this article for further details and references.
3. R. H. Dalitz, Ann. Rev. Nucl. Sci. 13, 339 (1963).
4. C. Michael, Phys. Letters 21, 93 (1966).
5. A. N. Diddens, E. W. Jenkins, T. F. Kycia, and K. F. Riley, Phys. Rev. Letters 10, 262 (1963).
6. L. D. Roper, Phys. Rev. Letters 12, 340 (1964); L. D. Roper and R. W. Wright, Phys. Rev. 138, B921 (1965).
7. P. Auvil and C. Lovelace, Nuovo Cimento 33, 473 (1964); P. Auvil, C. Lovelace, A. Donnachie, and A. T. Lea, Phys. Letters 12, 76 (1964); A. Donnachie, A. T. Lea, and C. Lovelace, Phys. Letters 19, 146 (1965).
8. A. Donnachie and J. Hamilton, Phys. Rev. 138, B678 (1965).
9. B. H. Bransden, R. G. Moorhouse, and P. J. O'Donnell, Phys. Rev. 139, B1566 (1965); B. H. Bransden, R. G. Moorhouse, and P. J. O'Donnell, Phys. Letters 11, 339 (1964); B. H. Bransden and P. J. O'Donnell, Phys. Letters 19, 420 (1965).
10. P. Baryere, C. Brickman, A. V. Stirling, and G. Villet, Phys. Letters 18, 342 (1965).
11. A. H. Rosenfeld, Recent Progress in Meson and Baryon Spectroscopy, Lectures at Yalta International School on Symmetry of Elementary

Particles (to be published by Kiev Institute of Theoretical Physics, Kiev, Russia), and UCRL-16968, May 1966.

12. F. Bulos et al., Phys. Rev. Letters 13, 486 (1964).
13. A. W. Hendry and R. G. Moorhouse, Phys. Letters 18, 171 (1965).
14. C. Bacci, G. Penso, G. Salvini, C. Mencuccini, and V. Silvestrini, Phys. Rev. Letters 16, 157 (1966).
15. R. Prepost, D. Lundquist, and D. Quinn, Eta Photoproduction in the Region from Threshold to 900 MeV, Proc. of the Int. Symposium on Electron and Photon Interactions at High Energies, Hamburg (1965), published by Springer-Verlag, Berlin, Vol. II, p. 152.
16. C. A. Heusch, C. Y. Prescott, E. D. Bloom, and L. S. Rochester, Phys. Rev. Letters 17, 573 (1966).
17. R. Cence, Phys. Letters 20, 306 (1966).
18. K. Draxler and R. Hüper, Phys. Letters 20, 199 (1966).
19. G. Höhler, J. Baacke, and R. Strauss, Phys. Letters 21, 223 (1966), and references of this paper.
20. P. J. Duke, D. P. Jones, M. A. R. Kemp, P. G. Murphy, J. D. Prentice, J. J. Thresher, H. H. Atkinson, C. R. Cox, and K. S. Heard, Phys. Rev. Letters 15, 468 (1965).
21. A. Yokosawa, S. Suwa, R. E. Hill, R. J. Esterling, and N. E. Booth, Phys. Rev. Letters 16, 714 (1966).
22. See references listed in Ref. 1.
23. W. Galbraith, Proc. of Royal Society 289, 521 (1966).
24. R. M. Heinz and M. H. Ross, Phys. Rev. Letters 14, 1091 (1965).
25. S. W. Kormanyos, A. D. Krisch, J. R. O'Fallon, K. Ruddick, and L. G. Ratner, Phys. Rev. Letters 16, 709 (1966).
26. V. Barger and D. Cline, Phys. Rev. Letters 16, 913 (1966).

27. Figures 21 and 22 are from Charles Wohl, Scattering Amplitudes, Partial Waves, Resonant States, Alvarez Memo 584 (1966).

28. R. L. Cool, G. Giacomelli, T. F. Kycia, B. A. Leontic, K. K. Li, A. Lundby, and J. Teiger, Phys. Rev. Letters 16, 1228 (1966).

29. J. K. Kim, Phys. Rev. Letters 14, 29 (1965).

30. M. Sakitt, T. B. Day, R. G. Glasser, N. Seeman, J. Friedman, W. E. Humphrey, and R. R. Ross, Phys. Rev. 139, B719 (1965).

31. M. Watson, M. Ferro-Luzzi, and R. D. Tripp, Phys. Rev. 131, 2248 (1963).

32. J. D. Davies, J. D. Dowell, P. M. Hattersley, R. J. Homer, A. W. O'Dell, A. A. Carter, K. F. Riley, R. J. Tapper, D. V. Bugg, R. S. Gilmore, K. M. Knight, D. C. Salter, G. H. Stafford, and E. J. N. Wilson, presented to the XIIIth High Energy Conference at Berkeley and reported by M. Ferro-Luzzi (rapporteur's talk on Strange Resonances) in Proceedings of the XIIIth High Energy Symposium, Berkeley, Calif., Aug. 31-Sept. 7, 1966.

33. Gerald Lynch, $\bar{K}N$ Total Cross Sections from .65 to 2.48 BeV/c, Alvarez Memo 600 (1966). I apologize with the authors of Ref. 31 for not showing their own graphs, but they are not available to me. The magnitude of the bumps in the cross sections of the two isospin states is similar to the one obtained by Lynch.

34. D. Berley, P. L. Connolly, E. L. Hart, D. C. Rahm, D. L. Stonehill, B. Thevenet, W. J. Willis, and S. S. Yamamoto, Phys. Rev. Letters 15, 641 (1965).

35. R. H. Dalitz, Ann. Rev. Nucl. Sci. 13, 339 (1963).

36. Experiment in progress. W. J. Willis, Yale University, priv. com. (1966).

37. D. Berley, P. L. Connolly, E. L. Hart, D. C. Rahm, D. L. Stonehill,

B. Thevenet, W. J. Willis, and S. S. Yamamoto, Quantum Numbers of the $Y_1^*(1660)$, Proceedings of the XIIth High Energy Physics Conference at Dubna, 1964 (published by Atomizdat, Moscow, 1966), Vol. I, p. 565.

38. M. Taher-Zadeh, D. J. Prowse, P. E. Schlein, W. E. Slater, D. H. Stork, and H. K. Ticho, Phys. Rev. Letters 11, 470 (1963).

39. P. E. Schlein and P. G. Trippe, UCLA Memo 1016.

40. D. Rahm et al., Σ Production in K^-p Interactions from 600 to 820 MeV/c, presented orally at the XIIIth International Conference on High Energy Physics at Berkeley, Calif., Aug. 30-Sept. 7, 1966. (See M. Ferro-Luzzi rapporteur's talk.)

41. R. Armenteros, M. Ferro-Luzzi, D. W. G. Leith, R. Levi-Setti, A. Minten, R. D. Tripp, H. Filthuth, V. Hepp, E. Klüge, H. Schneider, R. Barloutaud, P. Granet, J. Meyer, and J. P. Porte, Particle Wave Analysis in K^-p Interactions from 700 to 1220 MeV/c, presented orally at the XIIIth International Conference on High Energy Physics at Berkeley, Calif., Aug. 31-Sept. 7, 1966. (See M. Ferro-Luzzi rapporteur's talk.)

42. A. Barbaro-Galtieri, M. H. Alston, A. H. Rosenfeld, unpublished data.

43. G. W. London, R. R. Rau, N. P. Samios, S. S. Yamamoto, M. Goldberg, S. Lichtman, M. Primer, and J. Leitner, Phys. Rev. 143, 1034 (1966).

44. A. Leveque et al., French-British collaboration, Phys. Letters 18, 69 (1965).

45. P. Eberhard, F. T. Shively, R. R. Ross, D. M. Siegel, J. R. Ficenec, R. I. Hulsizer, D. W. Mortara, M. Pripstein, and W. P. Swanson, Phys. Rev. Letters 14, 466 (1965), and P. Eberhard, private communication.

46. W. E. Slater, P. M. Dauber, P. E. Schlein, D. H. Stork, and H. K. Ticho, Bull. Am. Phys. Soc. 10, 1196 (1965).

47. A. Barbaro-Galtieri, A. Husein, and R. D. Tripp, Phys. Letters 6, 296 (1963).

48. R. Armenteros, M. Ferro-Luzzi, D. W. G. Leith, R. Levi-Setti, A. Minten, R. D. Tripp, H. Filthuth, V. Hepp, E. Kluge, H. Schneider, R. Barloutaud, P. Granet, J. Meyer, and J. P. Porte, Phys. Letters 19, 338 (1965).

49. R. W. Berge, R. P. Ely, G. E. Kalmus, A. Kernan, J. Louie, J. S. Sahouria, and W. M. Smart, Spin and Parity of the $Y_0^*(1815)$ and $Y_1^*(1765)$, Proceedings of Athens Conference on Resonant Particles (1965), p. 296 (published by Ohio University, 1965).

50. W. M. Smart, A. Kernan, G. E. Kalmus, and R. P. Ely, Phys. Rev. Letters 17, 556 (1966).

51. V. Cook, B. Cork, T. F. Hoang, D. Keefe, L. T. Kerth, W. A. Wenzel, and T. F. Zipf, Phys. Rev. 123, 320 (1961).

52. C. W. Wohl, F. T. Solmitz, and M. L. Stevenson, Phys. Rev. Letters 17, 107 (1966).

53. Analysis in progress at Berkeley by A. Barbaro-Galtieri.

54. G. A. Smith and J. S. Lindsey, Final-State Interaction Involving Hyperons, Proceedings of Athens Conference on Resonant Particles (1965), p. 251 (published by Ohio University, 1965).

55. D. Merrill, Decay Properties of the Ξ Hyperon (Ph. D. Thesis), UCRL-16455 (to be issued).

56. R. L. Cool, G. Giacomelli, T. F. Kycia, B. A. Leontic, K. K. Li, A. Lundby, and J. G. Teiger, Phys. Rev. Letters 17, 102 (1966).

57. R. G. Bland, M. G. Bowler, J. L. Brown, G. Goldhaber, S. Goldhaber, J. A. Kadyk, V. H. Seeger, and G. H. Trilling, Inelastic K^+p Interactions between 860 and 1580 MeV/c, presented at Session 9b.8 of the

XIIIth International Conference on High Energy Physics at Berkeley, Calif., Aug. 31-Sept. 7, 1966. See M. Ferro-Luzzi rapporteur's talk.

58. J. Leitner, An Experimentalist's View of SU(3), ONR Report 66-1, Syracuse University (1966).

59. M. Goldberg, J. Leitner, R. Musto, and L. O'Raifeartaigh, Nuovo Cimento 45, 169 (1966). This paper contains an extensive list of references.

60. S. L. Glashow and R. H. Socolow, Phys. Rev. Letters 15, 329 (1966).

61. S. Coleman, Inside SU(3). Lectures given at the Ettore Maiorana Summer School, Erice, Italy.

62. J. J. Sakurai, Phys. Rev. Letters 9, 472 (1962).

63. The Schwinger mass formula [J. Schwinger, Phys. Rev. 135, B816 (1966)] has been derived only for vector mesons; it has not been proved to be valid in general. See following paragraphs for tests on this formula.

64. Parameters taken from Tables 1 and 2 revised form of A. H. Rosenfeld, A. Barbaro-Galtieri, W. H. Barkas, P. L. Bastien, J. Kirz, and M. Roos, Rev. Mod. Phys. 37, 633 (1965). Where an x scale factor is present, the quoted error has been increased by that factor.

65. Calculated rates from Goldberg et al.,[59] since they have used as input more recent experimental data than any previous calculations.

66. A. H. Rosenfeld, Mesons, in Proceedings of the Oxford Conference on High-Energy Physics (1965) (Rutherford High Energy Laboratory, England, 1966), Vol. II, p. 5, and UCRL-16462.

67. S. Okubo, Phys. Letters 5, 165 (1963).

68. S. M. Flatté, Can the A_1, K_c, D and E form a 1^+ Nonet? Lawrence Radiation Laboratory, Alvarez Memo 579 (1966).

69. B. C. Shen, I. Butterworth, C. Fu, G. Goldhaber, S. Goldhaber, and

G. H. Trilling, Phys. Rev. Letters 17, 726 (1966); and UCRL-16930.

70. P. Baillon, Ph. D. Thesis (French), University of Paris (1965).

71. M. Ferro-Luzzi, R. George, Y. Goldschmidt-Clermont, V. P. Henri, B. Jongejans, D. W. G. Leith, G. R. Lynch, F. Muller, and J. M. Perreau, Phys. Letters 17, 155 (1966).

72. A. R. Erwin, W. D. Walker, and A. Weinberg, Phys. Rev. Letters 16, 1063 (1966).

73. S. Coleman and S. L. Glashow, Phys. Rev. Letters 6, 423 (1961).

74. G. Goldhaber, S. Goldhaber, T. O'Halloran and B. C. Shen, referred by G. Goldhaber in "Experimental Study of Multiparticle Resonance Decays," Proceedings of the Second Coral Gables Conference on Symmetry Principles, University of Miami (1965) (Freeman and Company, San Francisco and London), p. 34; G. Alexander, C. Benary, R. Reuter, A. Shapira, E. Simopoulou and G. Yecutieli, Phys. Rev. Letters 15, 207 (1965).

75. See, for example, I. Butterworth, J. L. Brown, G. Goldhaber, S. Goldhaber, A. H. Hirata, J. A. Kadyk, and G. H. Trilling, Phys. Rev. Letters 15, 500 (1966).